

Distinct Tau Prion Strains Propagate in Cells and Mice and Define Different Tauopathies

David W. Sanders,^{1,4} Sarah K. Kaufman,^{1,4} Sarah L. DeVos,¹ Apurwa M. Sharma,¹ Hilda Mirbaha,¹ Aimin Li,¹ Scarlett J. Barker,¹ Alex C. Foley,³ Julian R. Thorpe,³ Louise C. Serpell,³ Timothy M. Miller,¹ Lea T. Grinberg,² William W. Seeley,² and Marc I. Diamond^{1,*}

¹Department of Neurology, Washington University in St. Louis, St. Louis, MO 63105, USA

²Department of Neurology and Pathology, University of California, San Francisco, San Francisco, CA 94143, USA

³School of Life Sciences, University of Sussex, Falmer BN1 9QG, UK

⁴Co-first author

*Correspondence: diamondm@neuro.wustl.edu

<http://dx.doi.org/10.1016/j.neuron.2014.04.047>

SUMMARY

Prion-like propagation of tau aggregation might underlie the stereotyped progression of neurodegenerative tauopathies. True prions stably maintain unique conformations (“strains”) in vivo that link structure to patterns of pathology. We now find that tau meets this criterion. Stably expressed tau repeat domain indefinitely propagates distinct amyloid conformations in a clonal fashion in culture. Reintroduction of tau from these lines into naive cells reestablishes identical clones. We produced two strains in vitro that induce distinct pathologies in vivo as determined by successive inoculations into three generations of transgenic mice. Immunopurified tau from these mice recreates the original strains in culture. We used the cell system to isolate tau strains from 29 patients with 5 different tauopathies, finding that different diseases are associated with different sets of strains. Tau thus demonstrates essential characteristics of a prion. This might explain the phenotypic diversity of tauopathies and could enable more effective diagnosis and therapy.

INTRODUCTION

Tauopathies are a diverse group of neurodegenerative diseases defined by accumulation of fibrillar deposits of the microtubule-associated protein tau (MAPT) (Lee et al., 2001). Alzheimer’s disease (AD), the most common tauopathy, affects >30 million people worldwide and will afflict >120 million by 2050 (Holtzman et al., 2011). MAPT mutations cause dominantly inherited tauopathies (Hutton et al., 1998) and most increase the propensity of tau to form amyloids (Barghorn et al., 2000), which are paracrystalline protein assemblies rich in beta-sheet structure (Bonar et al., 1969). Most tauopathy cases are sporadic, with variable clinical and pathological presentation (Lee et al., 2001).

The prion hypothesis posits that pathological aggregates of the mammalian prion protein (PrP) cause infectious, sporadic,

and familial neurodegenerative diseases (Prusiner, 1998). In contrast, yeast prions are adaptive and confer phenotypic diversity and rapid evolution of new traits in times of stress (True and Lindquist, 2000). Both yeast and mammalian prions form strains, which are encoded by distinct fibrillar structures (Safar et al., 1998; Toyama et al., 2007). Prion strains determine the incubation periods of disease in humans (Kim et al., 2012) and mice (Legname et al., 2006). In addition, human prion strains are thought to underlie clinical symptoms and pathological presentation (Collinge and Clarke, 2007).

The hypothesis that common neurodegenerative diseases such as AD could be caused by a prion-like mechanism was suggested three decades ago (Prusiner, 1984). Recently, however, experimental work on diverse amyloids has generated new interest (Frost and Diamond, 2010; Guo and Lee, 2014). Human neurodegenerative diseases target unique neural networks (Braak and Braak, 1995; Seeley et al., 2009), an observation most parsimoniously explained by the network-based spread of a toxic agent (Raj et al., 2012; Zhou et al., 2012). Prior studies suggest that tau aggregates spread among cells via templated conformational change (Frost et al., 2009a; Holmes et al., 2013). In vivo work supports this model (Clavaguera et al., 2009; de Calignon et al., 2012; Iba et al., 2013; Kim et al., 2010; Liu et al., 2012) as has similar work with other intracellular amyloids such as α -synuclein (Desplats et al., 2009; Luk et al., 2012) and extracellular amyloids including amyloid β (Meyer-Luehmann et al., 2006).

Bona fide prions are defined by propagation of distinct conformational strains in vivo, and prior studies have hinted at prion-like strain properties of non-PrP human amyloids. For example, amyloid β protein forms at least two distinct, self-propagating fibrillar conformations in vitro (Petkova et al., 2005) and in vivo (Lu et al., 2013). Others have demonstrated propagation in vitro of distinct tau (Frost et al., 2009b; Siddiqua and Margittai, 2010) and α -synuclein conformers (Bousset et al., 2013; Guo et al., 2013; Sacino et al., 2013). While provocative, these prior studies have not demonstrated that noninfectious proteopathic seeds act as true prions. Specifically, it has not been shown that distinct conformations or “strains” are capable of transmission into a living cell or organism, propagation through multiple generations, extraction, and reintroduction to naive cells or organisms to replicate the same structural phenotype (Collinge

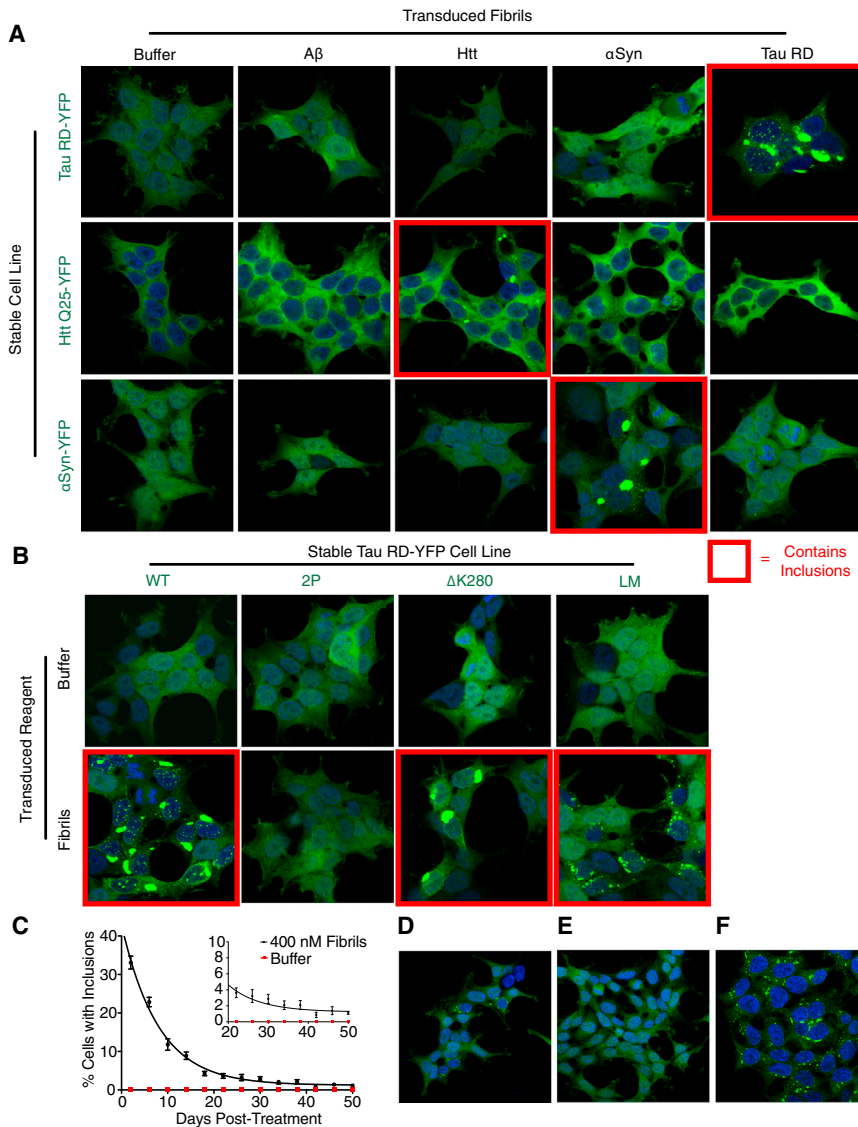


Figure 1. Homotypic Seeding Produces Stably Propagated Tau RD Inclusions

(A) Polyclonal HEK293 lines stably expressing YFP-tagged tau RD, α -synuclein, or htt exon1(Q25) were transduced with buffer, or fibrils of A β , Htt, α -syn, or tau RD. Cells were DAPI-stained on day 6. Only homotypic seeding occurred. See Figure S1A for construct diagrams, Figure S1B for quantification, and Figures S1C and S1D for similar homotypic seeding with full-length (FL) 4R1N tau P301S.

(B) Polyclonal HEK293 lines stably expressing tau RD-YFP with no mutations (WT), Δ K280 (proaggregation), Δ K280/I277P/I308P (2P; anti-aggregation), or P301L/V337M (LM; proaggregation) were transduced with either buffer or tau RD fibrils. Upon fibril transduction, all form inclusions, except for 2P.

(C) Tau RD(LM)-YFP cells transduced with either buffer or tau RD fibrils were passaged every two days. On every other passage, the percentage of cells with inclusions was quantified (n = 10 fields, each with 150+ cells per condition). Inset highlights inclusion-positive cells at later time points. Error bars represent SEM.

(D) At day 50 following exposure to fibrils, inclusion-positive cells were visible.

(E and F) At day 3 following exposure to fibrils, tau RD(LM)-YFP cells were diluted sparsely on coverslips and grown for 8 days. Colonies were either 100% inclusion-negative (E) or 100% inclusion-positive (F).

and Clarke, 2007). This is important not for semantic reasons, but because if prion mechanisms underlie human disease, only stably propagating strains can account for stereotyped clinical presentation and network spread. In this study, we have found that tau acts as a prion by these criteria, and, further, that individual human tauopathies are associated with unique strains.

RESULTS

Homotypic Seeding of Tau Depends on Beta-Sheet Structure

Amino acid sequence disparities impair cross-seeding between PrP moieties from different species, leading to “seeding barriers” (Collinge and Clarke, 2007). To test the fidelity of hetero- versus homotypic seeding for tau, we expressed several amyloidogenic proteins and exposed them to a variety of fibrillar seeds. Prolonged expression of full-length (FL) tau can be toxic to dividing cells. Thus for tau, we expressed the aggregation-

competent core, termed the repeat domain (tau RD; aa 244–372 of the 441 aa FL tau 4R2N) (Wischik et al., 1988). We generated polyclonal HEK293 cell lines stably expressing tau RD-YFP, α -synuclein-YFP, or huntingtin (htt) exon 1(Q25)-YFP (see Figure S1A for construct diagrams). Inclusions did not occur in any line without exposure to exogenous fibrils. However, upon transduction of fibrils (A β [1–42], htt exon 1 N17[Q35], α -synuclein, tau RD) with liposomes, we observed homotypic but not heterotypic seeding for each amyloidogenic protein (Figure 1A; Figure S1B for quantification), consistent with sequence-specific templating. Prior reports have indicated that in certain cases, α -synuclein aggregates can cross-seed FL tau (Giasson et al., 2003; Guo et al., 2013; Waxman and Giasson, 2011). Thus, we tested this for both YFP-tagged and untagged versions of FL tau 4R1N P301S. We observed only homotypic seeding and no cross-seeding of tau by α -synuclein or any other amyloid (Figures S1C and S1D). This is consistent with sequence-specific templating, although we cannot rule out the possibility that different amyloid conformers are capable of heterologous seeding, as has previously been reported (Guo et al., 2013).

Amyloids typically feature a cross beta-sheet conformation (Bonar et al., 1969). We exploited two proline substitutions (I277P/I308P) in tau that block its ability to enter into this

quaternary form (von Bergen et al., 2001) to test whether inclusion formation requires this property. Polyclonal HEK293 cell lines stably expressing tau RD-YFP with no mutations (wild-type, WT), P301L/V337M (LM: proaggregation), Δ K280 (proaggregation), or Δ K280/I277P/I308P (2P: antiaggregation) were transduced with tau RD fibrils. All formed inclusions except tau RD(2P)-YFP, confirming that beta-sheet structure is required for tau RD inclusion formation in our model system (Figure 1B).

Stable Inheritance of Tau RD Aggregates

Seeded htt exon 1 (Ren et al., 2009), Sup35NM (Krammer et al., 2009), SOD1 (Münch et al., 2011), and α -synuclein (Bousset et al., 2013) form persistent intracellular inclusions in cultured cells. We tested this for tau RD. We transduced tau RD fibrils or buffer into polyclonal tau RD(LM)-YFP (hereafter, referred to as tau RD) cells, chosen for their superior ability to be seeded relative to tau RD(WT)-YFP, and quantified the percentage of cells with inclusions on every other passage. Transduced fibrils induced tau RD inclusions that persisted >50 days postexposure (Figure 1C). We hypothesized that the aggregated state was stably inherited because inclusion-containing cells formed local clusters (Figure 1D). To test this, we sparsely diluted fibril-transduced tau RD cells to isolate individual colonies. These were composed of either 100% inclusion-negative (Figure 1E) or 100% inclusion-positive (Figure 1F) cells, indicating stable inheritance of the aggregated state.

Tau RD Propagates Conformationally Distinct Strains

Only prion protein (PrP) (Birkett et al., 2001) and certain fungal prions (e.g., Sup35 [PSI⁺]) (Derkatch et al., 1996) unequivocally propagate distinct conformational states, or strains, in cell culture. To test the ability of tau RD to propagate distinct conformers, we diluted fibril-transduced monoclonal tau RD cells and isolated individual clones that stably propagated inclusions (Figure 2A). Previous work with the Sup35 protein has indicated that inclusion morphology is a proxy for biochemically distinct yeast prion strains in dividing mammalian cells (Krammer et al., 2009). We thus characterized 20 tau RD clones based on inclusion morphology, numbered in order of isolation. Most (Figure S2A) featured small juxtanuclear inclusions with many nuclear speckles, exemplified by clone 9 (Figure 2B). Clone 10 alone propagated a single, large juxtanuclear inclusion (Figure 2B). We confirmed that stably propagated tau RD inclusions were amyloids as clones 9 and 10, but not inclusion-negative clone 1, bound X-34, a Congo red derivative that stains beta-sheet structures (Figure 2C).

To characterize the clones biochemically, we first used semi-denaturing detergent agarose gel electrophoresis (SDD-AGE), a method that differentiates strains based on aggregate size (Kryndushkin et al., 2003). Tau RD species from clone 10 were larger than those propagated by clone 9 (Figure 2D). Thus, the clone 10 fibrils might not be as readily fragmented into smaller species (Tanaka et al., 2006). Next, we used sedimentation analysis to differentiate the strains (Tanaka et al., 2006). Clone 1 had entirely soluble tau RD, whereas clones 9 and 10 had insoluble tau RD (Figure 2E). Clone 10 featured more soluble tau RD than clone 9. To probe for structural differences, we used limited proteolysis as has been used previously for differentiating PrP conformers

(Bessen and Marsh, 1994). Cell lines propagating aggregates (clones 9, 10) featured pronase-resistant species between 10 and 13 kDa, as well as between 20 and 25 kDa in size (Figure 2F). Clone 9 produced a smear between 10 and 13 kDa, whereas clone 10 produced a clear doublet. These studies indicated clear differences in biochemical characteristics of the clones, consistent with distinct strain conformations.

Prion strains often have different seeding efficiencies, which can result in variable incubation times in vivo (Legname et al., 2006). Thus we compared the clones, modifying a preexisting split-luciferase complementation assay (Naik and Piwnicka-Worms, 2007) for use as a tau aggregation sensor (Figure S1A). Clone 1 contained no seeding activity. However, inclusion-containing lines seeded robustly, especially clone 9, which seeded more than clone 10 (Figure 2G). Differences in seeding were not an artifact of cell confluency, as determined by normalizing to cell number in seeding experiments (Figure S2B).

Next, we compared the toxicities of clones 9 and 10. Although clone 9 lysate initially seeded a greater number of cells, these were rapidly eliminated relative to those induced by clone 10 (Figure 2H). Furthermore, cells containing clone 9-derived inclusions grew more slowly than those derived from clone 10 (Figure 2I). Whereas growth rate of nontransfected HEK293 cells was not affected by inoculation with clone 9 lysate, growth of tau RD cells was impaired following the same treatment (Figure S2C). This was not seen for clone 10. Finally, an LDH assay suggested that clone 9 lysate is toxic to tau RD cells relative to a sham treatment (Figure S2D).

A previous study reported that tau from human brain can induce aggresome structures in vitro (Santa-Maria et al., 2012). Thus, we examined the subcellular localization of inclusions associated with clones 9 and 10. Based on antivimentin stains (Figure S2E), electron microscopy (Figure S2F), and anti- γ -tubulin stains (Figure S2G), we conclude that juxtanuclear clone 10 inclusions are canonical aggresomes, unlike the inclusions of clone 9. Intracellular clone 9 inclusions did not colocalize with PML bodies (Figure S2H). Thus, clones 9 and 10 propagate conformationally distinct tau prion strains, with different consequences for the cell. To test the fidelity of strain inheritance, we passaged them continuously for 6 months. Inclusion morphologies (Figure 2J) and limited proteolysis patterns (Figure 2K) associated with clones 9 and 10 were unaltered. Thus, tau RD prion strains are robust, maintaining their phenotypes indefinitely in cell culture.

Transfer of Strain Phenotype to Naive Cells

To rule out an effect of cell background on strain formation, we transduced clone 9 and 10 lysates into naive monoclonal tau RD cells, isolating 6 colonies (A–F) for each (Figure 3A). We evaluated derivative clones (9C was lost in passage) by inclusion morphology (Figure 3B), SDD-AGE (Figure 3C), sedimentation analyses (Figure 3D; Figure S3B), seeding activity (Figure 3E), and limited proteolysis (Figure 3F). In all cases, derivative clones matched their associated progenitors, indicating that tau RD prion strains are encoded by conformation, independent of cell background. Faithful templating into naive cells also occurred after passive addition of lysates to media (Figure S3A), thus indicating that bypassing physiological uptake is not necessary for

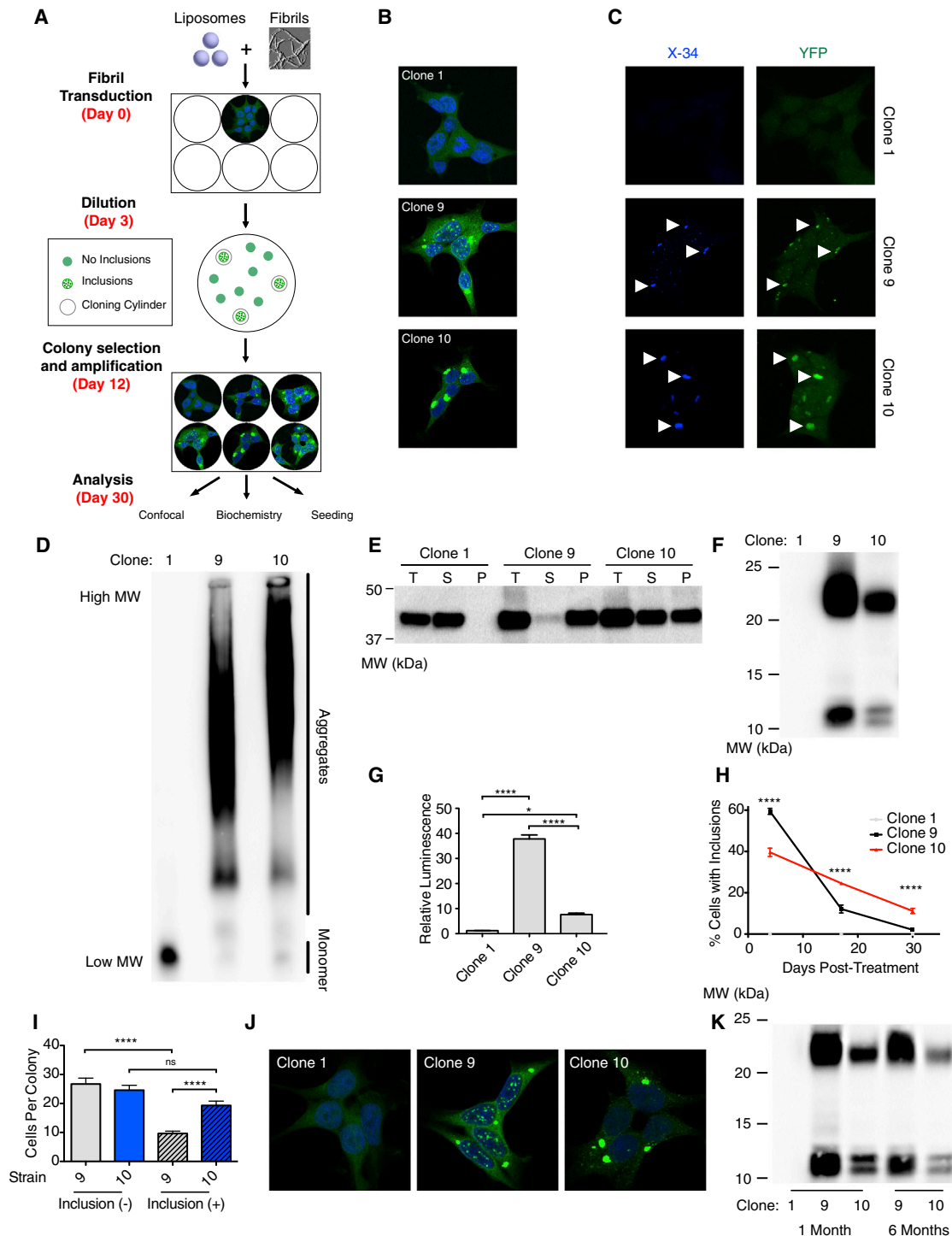


Figure 2. Generation of Stably Inherited Tau RD Prion Strains

(A) A monoclonal HEK293 line stably expressing tau RD(LM)-YFP (hereafter referred to as tau RD) was transduced with tau RD fibrils. At day 3, cells were diluted sparsely in a 10 cm dish. At day 12, inclusion-positive colonies were identified and picked, amplifying to confluency in separate 10 cm dishes. At day 30, cells were replated for confocal analysis or harvested for subsequent experiments.

(B) Confocal analysis of morphologically distinct tau RD prion strains. Clone 1 does not contain inclusions. Clone 9 contains nuclear speckles and a small juxtannuclear inclusion. Clone 10 features one very large juxtannuclear inclusion and no nuclear speckles. See Figure S2A for other clones.

(C) Clones 1, 9, and 10 were stained with X-34, an amyloid dye. X-34 staining is only observed in clone 9 and clone 10, indicating that the propagated aggregates are amyloids.

(legend continued on next page)

templating. With a Tet Off line to control tau RD expression, we demonstrated that the aggregate-positive phenotype can be cured by stopping expression for 7 days and then restarting it (Figures S3C and S3D).

To rule out an artifact of using artificial truncated tau RD and dividing cell model systems, we examined FL tau inclusion formation in primary cortical neurons. Neurons expressing FL tau P301S-YFP formed detergent-resistant inclusions following treatment with clone 9 or 10, but not clone 1 or PBS (Figure 3G). Clone 9 seeded very robustly relative to clone 10 (Figure S3E). Clone 9 lysate created inclusions throughout the soma and processes of neurons with untagged and YFP-tagged FL P301S tau, whereas clone 10 lysate primarily seeded inclusion bodies confined to the soma (Figure 3G; Figures S3F and S3G). Corroborating prior studies (Aoyagi et al., 2007; Miyasaka et al., 2001), we observed a seeding barrier between WT tau and P301 mutants (P301L, P301S). Specifically, aggregates from clones 9 and 10, which feature both the P301L and V337M mutations, never seeded aggregation in neurons expressing FL tau WT-YFP (Figure 3H) and FL tau WT (no tag) (data not shown). This seeding barrier was confirmed to be asymmetric by using a panel of split-luciferase tau RD mutant pairs (Figure S3H), which demonstrated that WT tau RD can seed all forms of RD (WT, P301L, P301S, P301L/V337M), whereas P301 mutants cannot seed WT.

Tau Strains Induce Unique Pathologies in Transgenic Tau P301S Mice

Inoculation of recombinant fibrils into transgenic P301S mice (Yoshiyama et al., 2007), which express a form of mutant tau associated with dominantly inherited tauopathy, rapidly induces pathology within weeks (Iba et al., 2013). Thus, we tested whether tau strains formed in cell culture would have similar effects. We inoculated equivalent amounts of lysate from clones 1, 9, and 10, as well as recombinant tau RD fibrils (RF), bilaterally into the hippocampi of 3-month-old mice (Figure 4A). For all experiments, conditions were gender matched (Table S1). After 3 weeks, RFs induced tangle-like pathology when assessed by AT8 (Figures 4B and 4C), an antibody against FL phospho-tau, as previously reported (Iba et al., 2013). Clones 9 and 10 induced

unique pathologies, whereas clone 1 did not cause any detectable abnormality (Figures 4C and 4D). Whereas clone 9 induced tangle-like inclusions throughout CA1 and CA3, clone 10 induced AT8-positive puncta in mossy fiber tracts (Figure 4D). Staining with MC1, an antibody against conformationally-altered tau (Jicha et al., 1997), confirmed these differences (Figure S4A). X-34, an amyloid dye, primarily recognized clone 9 pathology (Figure S4A), although light staining was observed in CA1 of clone 10-inoculated mice. Pathological differences could not be explained by differences in the amount of total or insoluble tau RD inoculated (Figures S4E and S4F). Injected WT mice never developed pathology (Figure S4B), possibly due to a seeding barrier between inoculated tau RD and WT murine tau (Figure 3H; Figures S3E and S3H).

P301S mice inoculated with clone 10 uniquely accumulated elongated Iba1-positive rod microglia (Figure 4E), which aligned end-to-end parallel to CA1 pyramidal axons (Figure S4C). Such unique coupling of rod microglia has been observed in a rodent traumatic-brain-injury model and might be protective for injured axons (Ziebell et al., 2012). WT mice inoculated with clones 9 and 10 did not feature this pathology, indicating that endogenous human P301S tau is required for this induced microglial phenotype (Figure S4D).

Tau Strains Are Stably Propagated through Multiple Generations in Mice

Prions can be stably passaged in vivo (Bruce et al., 1994). Thus, we performed serial inoculation of brain homogenates into naive P301S mice (Figure 5A). Brain homogenate from WT or P301S mice inoculated with clones 1, 9, or 10 (termed generation G0) was inoculated into naive P301S mice (generation G1). After 28 days, brains were collected for histology and biochemistry, and the process was repeated in a second round of P301S mice (generation G2). Immunohistochemistry demonstrated identical pathology for each generation of mice: clone 9 serial propagation induced AT8-positive, tangle-like pathology in CA1 and CA3 regions, whereas clone 10 serial propagation induced AT8-positive puncta in the mossy fiber tracts of the hippocampus (Figures 5B and 5C; Figure S5A). Clone 1 induced no pathology in any generation (Figure 5B; Figure S5B).

(D) SDD-AGE demonstrates that clone 10 features larger aggregates than clone 9.

(E) Sedimentation analysis was performed on clones 1, 9, and 10. Pellet (P) was isolated from supernatant (S) by ultracentrifugation. For clones 9 and 10, supernatant was loaded at a 3:1 ratio to pellet and total (T) to allow clear detection; clone 1, a 1:1 ratio. Clone 1 has all tau RD in the supernatant, whereas clone 9 has almost all tau RD in the pellet. Clone 10 has mixed solubility.

(F) Limited proteolysis (pronase) digests all tau RD in clone 1 but reveals protease-resistant tau RD peptides between 10 and 13 kDa, as well as between 20 and 25 kDa in clone 9 and 10. Unlike clone 9, clone 10 digestion produces a doublet, consistent with a distinct conformation.

(G) A split-luciferase assay reports differential seeding efficiency of tau RD prion strains. A polyclonal HEK293 line expressing both tau RD-CLuc and tau RD-Nluc was transduced with lysate from the three clones. Clone 1 does not seed aggregation. Clone 9 seeds robustly, whereas clone 10 seeds significantly less. Averages of four separate experiments are shown, each read in quadruplicate 48 hr posttransduction (error bars = S.E.M, * = $p < 0.05$, **** = $p < 0.0001$). See Figure S2B for evidence that differences in cell confluency do not account for differences in luminescence.

(H) Inclusion elimination rates differ between clones. After transduction with lysate from clone 9 or 10, the percentage of cells containing inclusions was quantified on days 4, 17, and 30 ($n = 10$ fields, each with 150+ cells per condition). Cells with inclusions derived from clone 9 are eliminated more rapidly from the population. Error bars represent SEM, **** = $p < 0.0001$.

(I) Clone 9-transduced cells grow more slowly. After transduction of stable cells, colonies with inclusions derived from clone 9 have fewer cells than colonies with inclusions derived from clone 10. Colonies without inclusions have identical cell numbers (error bars represent SEM, **** = $p < 0.0001$). See Figure S2C for differences in cell growth rate in tau RD(LM)-HA cells and Figure S2D for LDH toxicity assay in tau RD(LM)-HA background.

(J) Clones 1, 9, and 10 maintain distinctive morphologies after 6 months in culture. See also Figure S2E–S2H for data indicating that juxtannuclear clone 10, but not clone 9, inclusions are aggregates.

(K) Structural characteristics (limited proteolysis digestion patterns) of strains are propagated with high fidelity over 6 months.

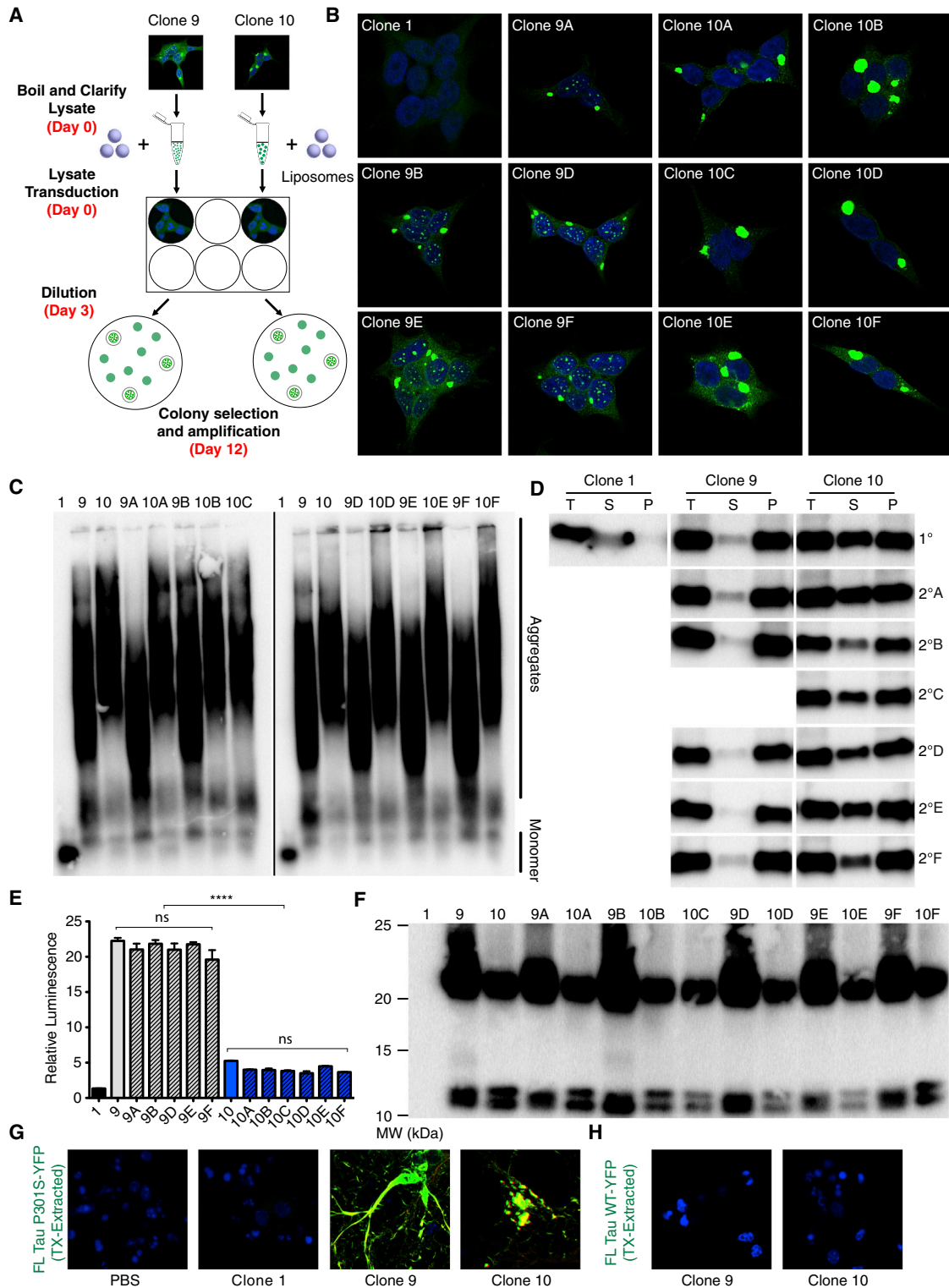


Figure 3. Tau RD Aggregates Transfer Strain Conformations into Naive Cells

(A) Lysates from clones 9 and 10 were transduced into naive tau RD-YFP cells and monoclonal inclusion-containing cells were isolated and amplified. Six secondary clones were generated for each condition, but one (clone 9C) failed to amplify.

(B) Morphologies of primary clones are maintained in secondary cell lines. See also Figure S3A, which demonstrates that this templating of morphology is not dependent on liposome-mediated transduction of lysate.

(legend continued on next page)

Homogenate from WT mice inoculated with the original cell tau strains (G0) did not produce pathology upon passage into P301S mice (Figure S5C). Therefore, pathology observed in G1 and G2 cannot be due to residual tau RD seeds from the original inoculum, and tau prions propagate unique phenotypes for multiple passages *in vivo*.

In Vivo Tau Strains Maintain Phenotypes upon Passage back into Cells

To conclusively test whether tau strains are biochemically stable after passage *in vivo*, we isolated FL P301S tau from microdissected hippocampi of injected mice (G0) by using a monoclonal antibody (HJ8.5) that binds an epitope present in FL tau, but not tau RD (Yanamandra et al., 2013). We assessed seeding activity in G0 samples by split-luciferase complementation and inclusion counts. Only hippocampi from P301S mice (G0) injected with tau RD aggregates contained seeding activity (Figure 6A; Figure S6A). This did not correlate with the amount of immunoprecipitated tau (Figure S6D). WT mouse hippocampi never seeded, regardless of the inoculum. We next tested whether the strains introduced into G0 mice could be reisolated in tau RD cells. Scoring of single colonies based on morphology (containing or lacking nuclear speckles) suggested that strains were unaltered following a single passage through mice (Figures S6B and S6C). To further confirm this, we blindly selected and amplified a single representative colony associated with each mouse. All G0-clone 9 and G0-clone 10 samples recapitulated the morphologies of the original clones 9 and 10 (Figure 6B). Limited proteolysis patterns (Figure 6C) and seeding propensities were also identical (Figure 6D).

Similar experiments were performed following the third passage (G2). Immunoprecipitated (IP) tau from pooled G2-clone 9 and G2-clone 10 homogenates seeded far more strongly than G2-clone 1 homogenates (Figure 6E). Immunoglobulin G (IgG)-precipitated material did not seed (Figure 6E; Figure S6E), and IP tau seeded as strongly as crude homogenate in a split-luciferase assay (Figure S6E). Tau alone thus accounts for the seeding activity reported in these assays.

Next, we introduced IP material from G2 mice into tau RD reporter cells and scored colonies based on morphology prior to isolation of monoclonal lines. G2-clone 9 colonies almost exclusively featured nuclear inclusions, whereas virtually all G2-clone 10 colonies lacked them (Figure S6F). The rare inclusion-positive colonies associated with G2-clone 1 also featured nuclear inclu-

sions, which suggested that some of the G2-clone 10 colonies containing nuclear inclusions could arise from an intrinsic P301S-derived strain. Monoclonal strains ($n = 12$) were blindly selected for each G2 cohort. In all but one case (G2-clone 10D), inclusion morphologies matched that of the original inoculate (Figure 6F; Figure S6G). For both clone 9 and 10 cohorts, 11 of 12 clones matched their parental counterpart based on both limited proteolysis (Figure 6G) and seeding activity (Figure 6H). Intriguingly, the two outliers (G2-clone 9G, G2-clone 10D) had identical proteolysis patterns and seeding ratios, which were unique from those of all other clones. We speculate that these clones result from an intrinsic strain within 4-month-old P301S mice. We conclude that tau prion strains are stable across numerous passages through cells and animals.

Spread of Tau Pathology to Distant, Synaptically Connected Regions

After inoculation with recombinant tau fibrils, pathology can develop in synaptically connected regions (Iba et al., 2013). Our preliminary observations indicated that serial inoculations with clone 9 induced pathology in the ipsilateral entorhinal cortex (EC) (data not shown). To test for spread, we performed a final inoculation (G3) into the left hippocampus of P301S mice. After five weeks, G3-clone 9 mice had AT8-positive pathology in regions that project to or from the hippocampus (Figure 7A) including ipsilateral and contralateral EC, retrosplenial cortex (RSp), and contralateral hippocampus (Figure 7B–7D; Figure S7A) (Andersen, 2007; van Groen et al., 2003). Ipsilateral EC had robust pathology in layers II/III, whereas contralateral EC pathology occurred in deeper cortical layers, suggesting spread along defined anatomical connections (van Groen et al., 2003). Furthermore, pathology was observed in ipsilateral subiculum and dentate gyrus (Figure S7B). In contrast, G3-clone 1 brain did not show AT8-positivity above baseline (Figures 7B and 7D). Overt spread was not observed in G3-clone 10 mice (data not shown), perhaps due to its decreased seeding ability (Figure 2G; Figure S3E). A heatmap summarizes the brain regions with enhanced AT8-positive pathology in G3-clone 9 mice (Figure 7C). These results agree with previous work suggesting that seeded intracellular amyloids spread along discrete neural networks (de Calignon et al., 2012; Iba et al., 2013; Liu et al., 2012; Luk et al., 2012; Zhou et al., 2012). We cannot completely exclude the possibility that this was due to *trans*-synaptic spread of inoculum.

(C) SDD-AGE of lysates from both primary and secondary clones demonstrates similar aggregate sizes in secondary clones relative to the primary ones. A line separates gels run separately.

(D) Sedimentation analysis was performed as described in Figure 2E. Secondary clones feature similar sedimentation patterns to the clones from which they were derived. For original blots, see Figure S3B.

(E) Split-luciferase complementation demonstrates similar seeding efficiencies in secondary lines versus parental lines. Averages of four separate experiments are shown, each read in quadruplicate 48 hr posttransduction of lysate (error bars represent SEM, **** = $p < 0.0001$).

(F) Limited proteolysis shows that all clone 10 derivatives feature a doublet whereas clone 9 derivatives are associated with an unresolvable band between 10 and 13 kDa. Clone 9 derivatives feature a more resistant band between 20 and 25 kDa. See Figures S3C and S3D for reversibility of aggregated state.

(G) Lysates from clones 9 and 10, but not clone 1, induce detergent-resistant FL tau P301S-YFP species, which colocalize with AT8 (red) in primary cortical neurons. Clone 9 induces tangle-like structures throughout the soma and neuritic processes. Clone 10 primarily seeds punctate-like structures in the soma. See Figure S3E for data showing that clone 9 seeds more widespread inclusion formation, Figure S3F for similar results in neurons expressing untagged FL tau P301S, and Figure S3G for images of tangles throughout processes of clone 9-inoculated neurons.

(H) Clone 9 and clone 10 lysates containing tau RD(P301L/V337M)-YFP, do not seed inclusion formation in neurons expressing WT FL tau. For evidence that this is due to an asymmetric seeding barrier between FL tau with and without P301 mutations, see Figure S3H.

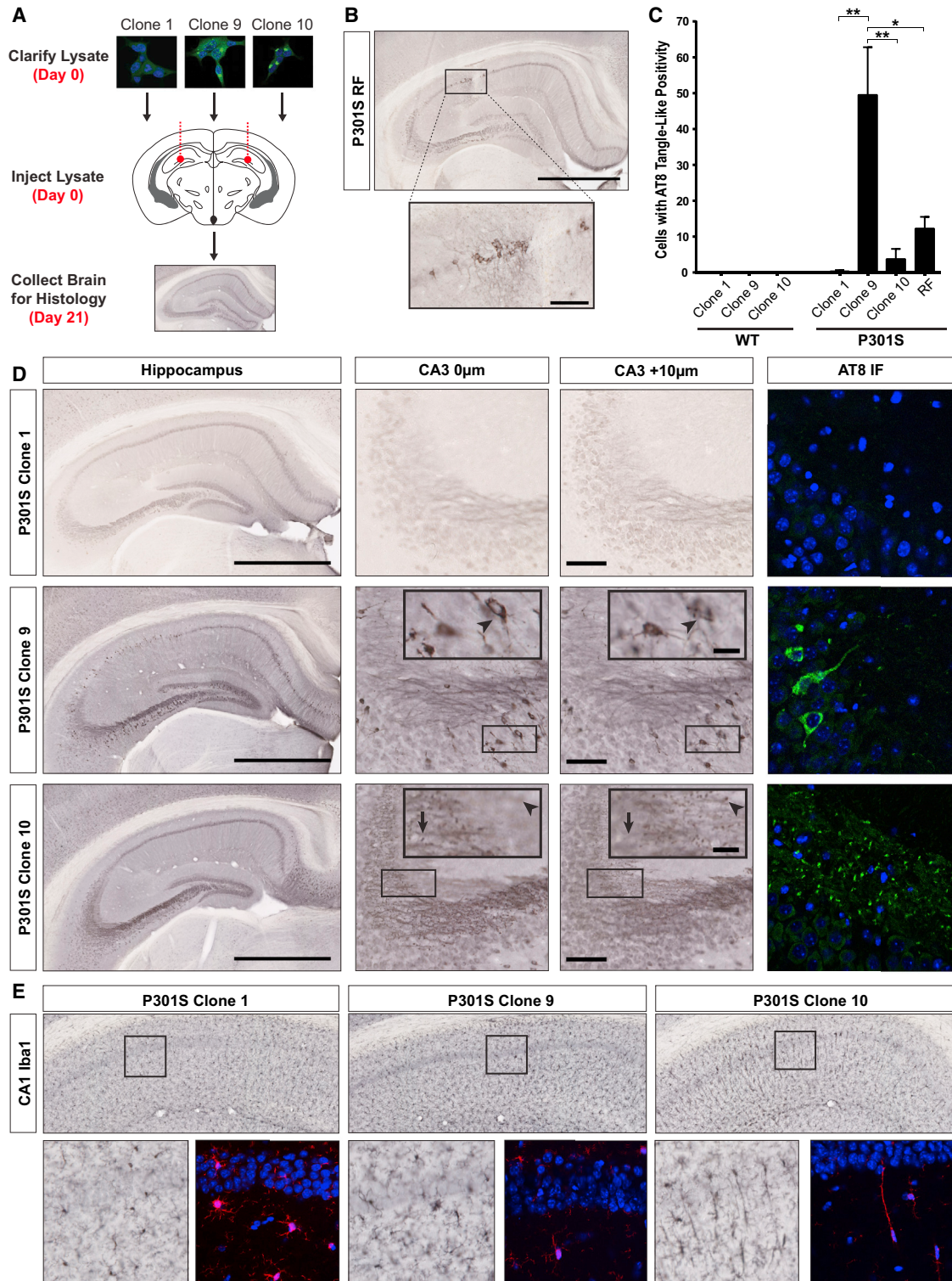


Figure 4. Clone 9 and 10 Induce Unique Tau and Microglia Pathology in P301S Mice

(A) Lysates (10 µg total protein) were injected bilaterally into the hippocampi of 3 month P301S and WT mice. At 21 days postinjection, left hemispheres were collected for histology and right hemispheres for homogenization. See Table S1 for description of mice used in all experiments.

(B) Recombinant tau RD fibrils (RF) induce tangle-like, AT8-positive tau pathology near the injection site in CA1 (scale bars represent hippocampus – 1 mm and inset – 100 µm).

(legend continued on next page)

Intrapatient and Interdisease Phenotypic Diversity in the Tauopathies

It has been hypothesized that conformationally distinct tau prion strains might be associated with individual tauopathies (Clavaguera et al., 2013b; Frost and Diamond, 2010), and a recent study found that inoculation of transgenic human tau mice with brain homogenates from patients with different tauopathies recapitulates certain pathological features of the diseases (Clavaguera et al., 2013a). To examine whether inclusion morphology is a reasonable indicator of distinct strains, we first used our cell model to examine brain homogenates from three individuals with clinically distinct, pathologically verified tauopathies (all patient samples obtained from the Neurodegenerative Disease Brain Bank at UCSF): Alzheimer's disease (AD), corticobasal degeneration (CBD), and argyrophilic grain disease (AGD). We transduced IP or crude (CR) homogenate into the monoclonal Tet Off HEK293 cell line (Figure 8A), used for its relatively high tau RD expression and greater seeding efficacy, and characterized resulting colonies morphologically and biochemically (Figures S8A–S8I). Each brain induced a unique inclusion morphology, independent of the transduction method (IP versus CR) (Figures S8A–S8D). By analyzing three representative clones derived from each brain by sedimentation analysis (Figure S8E), seeding (Figures S8F and S8G), and limited proteolysis (Figures S8H and S8I), we concluded that morphology reliably differentiates biochemically distinct strains. Next, we expanded our analysis to include IP tau from patients with AD (n = 6), AGD (n = 6), CBD (n = 6), Pick's disease (PiD, n = 5), and progressive supranuclear palsy (PSP; n = 6) (Table S2). Excepting PiD, a three-repeat tauopathy, these are predominantly four-repeat (AGD, CBD, PSP) or mixed-repeat (AD) tauopathies that differ in the morphology and distribution of neuronal and glial tau inclusions (Lee et al., 2001). We transduced IP tau from each sample into the monoclonal Tet Off cell line and isolated clones with inclusions (Figure 8A). We identified six morphological phenotypes as follows: (1) no seeding, (2) toxic (all cells with inclusions died and clones could not be isolated), (3) mosaic (unstable prion strain), (4) ordered, (5) disordered, and (6) speckles (Figure 8B). We blindly scored all clones based on tau RD inclusion morphology. This revealed distinct strain compositions across the diseases (Figure 8C). AD patient samples revealed remarkable homogeneity, suggesting a predominant strain. Other disorders revealed interpatient variation. Some patients featured homogeneous strain composition (e.g., certain patients with AGD, PSP), whereas others exhibited considerable heterogeneity. With few exceptions (e.g., AD1–AD4, AGD2, CBD5, PiD3), most patient samples produced two or more strains. The range

of phenotypes associated with single patients suggests a diversity of patient-derived tau prion strains. Because the cell-based strain isolation system can likely amplify only a subset of strains, these data suggest that a disease-associated ensemble or “cloud” of conformations exists within individual patients. Nevertheless, certain tauopathies can be differentiated by their strain composition.

DISCUSSION

Many papers describing “prion-like” behavior of proteins associated with neurodegenerative diseases have been published in the last several years. In the case of tau, fibrils transmit its aggregated state from the outside to the inside of a cell (Frost et al., 2009a; Holmes et al., 2013), suggesting that this mechanism could account for the stereotyped progression of tauopathies. This model of disease was subsequently supported in vivo with reports of *trans*-synaptic spread of pathology (de Calignon et al., 2012; Kim et al., 2010; Liu et al., 2012) and protein-only induction of tau inclusions (Iba et al., 2013). Work with other intracellular amyloids (Desplats et al., 2009; Holmes and Diamond, 2012; Münch et al., 2011; Ren et al., 2009) has suggested that prion-like transmission can explain the progression of many neurodegenerative diseases.

Whether or not various noninfectious amyloids are “true” prions has become a contentious subject of debate. Some define prions as being capable of interorganism transmission of pathology and by the ability to survive freely in the environment (Aguzzi and Rajendran, 2009). To date, there exists no evidence that this definition can be applied to proteins other than PrP. This restrictive definition, based on early research into prion diseases such as kuru and scrapie, potentially ignores a rich biology that mechanistically unites many common diseases. Importantly, we now know that the vast majority of human prion diseases have noninfectious etiology, and that their great phenotypic heterogeneity can be attributed to strains (Collinge and Clarke, 2007). With respect to prion-like intracellular amyloids in humans, recent data indicate that homogenates from distinct tauopathies might reproduce certain pathological features of the diseases in transgenic mice, which is consistent with strain behavior (Clavaguera et al., 2013a). Other studies explicitly suggest the existence of α -synuclein strains, based on the production of different α -synuclein conformers in vitro (Bousset et al., 2013; Guo et al., 2013; Sacino et al., 2013). However, to account for phenotypic diversity at a systems level, a prion strain must replicate with remarkable reliability for extended periods of time. A stringent test of this is to ensure that the strain is stable,

(C) Quantification of tangle-like, AT8-positive cell bodies within the hippocampus (CA1 and CA3) of WT and P301S mice. P301S mice injected with clone 9 lysate have significantly more AT8-positive cell bodies than those injected with clone 1, clone 10, or RF (error bars represent SEM, * = $p < 0.05$, ** = $p < 0.01$). WT mice do not develop pathology after injection.

(D) P301S mice were inoculated with clone 1, clone 9, or clone 10 lysate. Representative whole hippocampus images are shown with the corresponding CA3 z stacks. Arrowheads in clone 9 CA3 insets highlight an AT8-positive cell body that can be seen throughout both z stack images. The arrow and arrowhead in clone 10 CA3 insets each represent a different AT8-positive puncta that is visible in only one z stack plane (scale bars represent hippocampus – 1 mm; CA3 – 100 μ m; CA3 inset and AT8 IF – 25 μ m; n = 3–4 per clone). See Figure S4A for MC1 and X-34 staining, Figure S4B for lack of pathology in inoculated WT mice.

(E) Iba1 staining of microglia in CA1 of inoculated P301S mice indicates that only clone 10 induces the formation of rod microglia, which extend highly polarized processes into CA1. See Figure S4C for columns of rod microglia in these animals and Figure S4D for absence of these microglia in clone 10-inoculated WT animals. See Figure S4E and Figure S4F for data indicating that identical amounts of total and insoluble tau were used in inoculations.

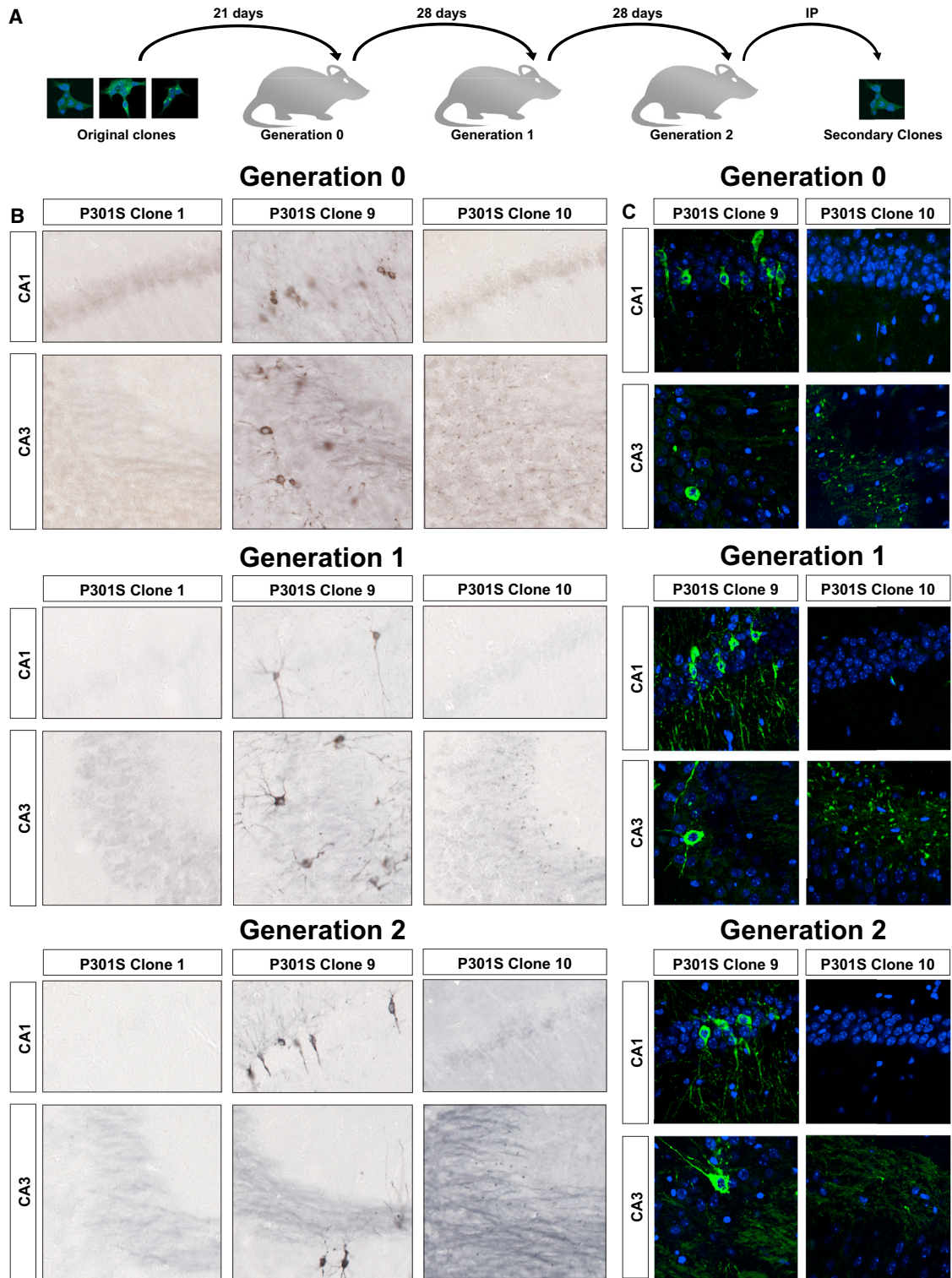


Figure 5. Tau Strains Passage Stably through Multiple Generations of P301S Mice

(A) Lysates (10 μ g protein) were injected bilaterally into the hippocampi of 3-month-old P301S mice (Generation 0/G0). At 21 days postinjection, brains were collected for histology and homogenization. Hippocampal homogenate (10 μ g) was then bilaterally inoculated into a new round of 3-month-old P301S mice (Generation 1/G1) followed by a 28-day incubation before the process was repeated for a new cohort of 3-month-old P301S mice (Generation 2/G2). At G0 and

(legend continued on next page)

isolatable, and replicates its phenotype through living systems with high fidelity (Bruce et al., 1994; Prusiner, 1998). Until now, these characteristics have not been linked to a mammalian protein other than PrP. Based on these criteria, our data strongly suggest that tau should be considered a bona fide prion. Fittingly, we also find that different tauopathies are associated with different strains. This has direct implications for understanding the phenotypic diversity of tauopathies.

Tau as a Prion in Cell Culture and Mice

We began this work by establishing a monoclonal HEK293 cell line that stably expresses the tau repeat domain fused to YFP. In the absence of tau aggregate exposure, these cells propagate only tau RD monomer (“naïve” cells). Induction of aggregation with recombinant fibrils, however, created clonal lines (clone 9 and clone 10) that indefinitely propagate unique aggregate structures, or strains, from mother to daughter cells. These strains differ with respect to inclusion morphology, aggregate size, sedimentation profile, seeding capacity, protease digestion patterns, toxicity, and subcellular localization. Importantly, these properties are cell-independent, because we recreated the strains by protein transfer into naive cells. Furthermore, the distinct inclusion morphologies we observed might represent specific cellular responses to different aggregate conformations, consistent with their unique patterns of compartmentalization. The cell-culture system established here might thus prove useful to detect, propagate, and characterize additional tau prion strains, as well as to understand the cellular mechanisms that govern strain replication, subcellular localization, degradation, and toxicity.

In vivo, we found that strains 9 and 10 induce unique pathological phenotypes in transgenic P301S mice. Moreover, clone 10 lysate uniquely results in the formation of rod-shaped microglia, which indicates that distinct tau conformers initiate different physiological responses in vivo. More remarkably, we report that the morphological phenotypes breed true through multiple generations of mice, a property that is shared with PrP. We recognize that pathological phenotypes can be prone to bias in detection. Thus, we passaged strains back to naive tau RD-YFP cells, conclusively demonstrating the robust inheritance of tau conformations. This data also indicates that the repeat domain is sufficient to encode strains that are unaltered by templating of their structure to FL tau. Therefore, the reported cell model is useful for detecting and propagating physiologically relevant tau prion strains. Finally, using unilateral inoculation of clone 9 lysate, we show that tau aggregation propagates along known anatomical connections, supporting conclusions of previous studies (de Calignon et al., 2012; Iba et al., 2013; Liu et al., 2012). More importantly, however, these cellular and in vivo studies indicate that a mammalian protein amyloid other than PrP templates itself with high fidelity through living systems.

Tau Prion Strains in Human Tauopathy Brains

Knowing that tau acts as a prion in experimental models, we examined whether this concept could explain phenotypic diversity observed in tauopathies. Brain samples from three patients with distinctive tauopathies induced diverse self-propagating tau prion strains in culture. Our initial work with these strains indicated that inclusion morphology is a reliable surrogate for more labor-intensive biochemical characterization. This led us to assess the morphological phenotypes of tau strains derived from numerous patients (n = 29) across a spectrum of tauopathies (AD, AGD, CBD, PiD, PSP). Each of the diseases was associated with several cellular inclusion morphologies, although certain diseases (AD, CBD, PiD) are more homogeneous than others (PSP, AGD). It is noteworthy that AD pathology is characteristically more uniform than other tauopathies (Duyckaerts et al., 2009; Feany et al., 1996), and the tau strains isolated from AD brains were by far the most homogeneous. The isolation of multiple conformers from individuals suggests that a tau aggregate ensemble exists within each person, and that standard methodologies (e.g., histopathology, inoculation into mice, protease digestion) will be insufficient for a nuanced understanding of this conformational complexity. Similar to what has been reported for PrP amyloids (Collinge and Clarke, 2007; Li et al., 2010), we speculate that these clouds of tau conformers are prone to selective pressures at the cellular level, which might have implications for therapies that target extracellular tau (Holmes et al., 2013; Yanamandra et al., 2013).

Although we have now succeeded in categorizing multiple distinct strains, the cell-based isolation method can only detect those that successfully template to tau RD-YFP and propagate without overt cellular toxicity. The inability to reselect clone 9 derivatives in the Tet Off background illustrates this problem. On the other extreme, strains that do not propagate with high fidelity might be lost prior to clonal selection. For example, the strains present in several AGD and PiD samples were not stable in cell culture, making detailed characterization of these strains difficult with our model system. Furthermore, it is likely that seeding barriers between tau from patient brain (consisting of various tau isoforms and posttranslationally modified species) and tau RD in cell-culture limits the strains we can detect. Our observation of an asymmetric seeding barrier between P301 mutants and WT tau underscores this limitation, as does recent work indicating similar barriers between three-repeat (3R) and four-repeat (4R) tau (Dinkel et al., 2011). Despite some limitations, the model system presented here has many advantages over standard animal inoculations, because it is less resource-intensive and can parse multiple conformations from a single isolate. Finally, knowledge of the existence of multiple strains in vivo might allow us to characterize them on molecular terms and diagnose patients with much greater precision, possibly by determining structures and conformational

G2, hippocampal homogenates were IP (anti-tau 8.5; epitope = aa 25–30; outside RD region) and inoculated into the original tau RD-YFP line to test the fidelity of strain inheritance (G0 and G2 clones). For each cohort, n = 3–4 animals.

(B and C) AT8 staining (DAB = B and immunofluorescence = C) reveals that the morphological phenotypes of phosphorylated tau inclusions breed true through multiple generations of tau P301S mice. See Figure S5A for images of whole hippocampi, Figure S5B for images of clone 1 AT8 immunofluorescence, and Figure S5C for data indicating that strain passage is not due to residual tau RD seeds remaining in diluted inoculate.

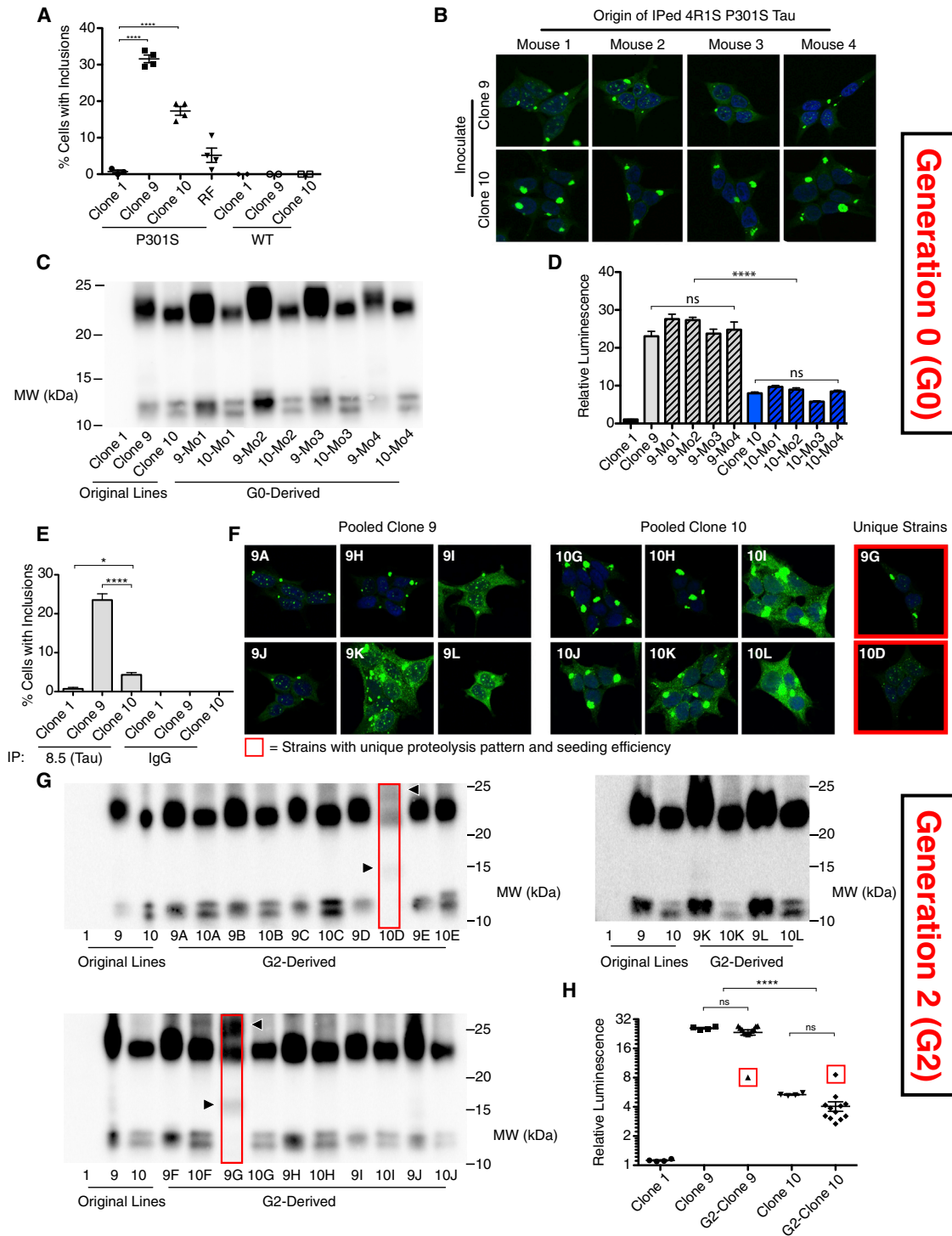


Figure 6. Strains Transfer Faithfully to Cell Culture after Passage through Generation 0 and Generation 2 Mice

(A) IP material was transduced into tau RD-YFP cells prior to passage onto coverslips. At 96 hr, cells were fixed. Only clone 9-, clone 10-, and RF-inoculated mice seed inclusions robustly. WT mouse homogenates never seed aggregation. Ten fields, each with 100+ cells, were analyzed per brain, and averages were collapsed within cohorts (error bars represent SEM, **** = $p < 0.0001$). See also Figure S6A for split-luciferase complementation data. (B) Inclusion morphologies are maintained following passage through P301S mice (G0). IP FL tau from individual P301S mice inoculated with clone 9 or clone 10 was transduced into tau RD-YFP cells, and a single representative clone per mouse was isolated and amplified. All G0-derived clones continue to propagate the original phenotypes. See also Figures S6B and S6C for quantification of colony morphologies prior to monoclonal cell line isolation and Figure S6D for quantification of total IP tau used in G0 experiments.

(legend continued on next page)

epitopes specific to individual diseases. This could help facilitate therapeutic strategies tailored toward the underlying protein pathology.

Expanding the Spectrum of Prion Diseases

Our data, along with cell-culture (Holmes and Diamond, 2012), pathological (Clavaguera et al., 2013b), and imaging (Greicius and Kimmel, 2012) studies are consistent with the model of cell-cell “transmission” of neurodegenerative diseases throughout the nervous system. Our finding of multiple self-propagating conformations in experimental and patient-derived tau preparations suggests that tau should be defined as a prion, because it encodes self-catalyzing conformational information that it propagates indefinitely with high fidelity. Importantly, however, there is no evidence to suggest that AD or other tauopathies are infectious in the classical sense, as they are not known to be communicable between individuals. The infectious property of PrP^{Sc} might reflect its anomalous biochemical stability or expression profile, whereas a host of other cell biological and biophysical properties, especially the ability to encode self-propagating conformers, will more appropriately unify the growing family of “prion-like” proteins. Indeed, the vast majority (>95%) of human prion disease cases appear to be genetic or sporadic, indicating that infectivity should not be a restrictive criterion. We predict that strains associated with distinct clinical phenotypes will also be identified for synucleinopathies and ALS/FTLD spectrum disorders, both of which feature diversity in pathological presentation (Halliday et al., 2011; Van Langenhove et al., 2012). Understanding disparate amyloid neurodegenerative diseases in light of this model should create new possibilities for common diagnostic and therapeutic approaches.

EXPERIMENTAL PROCEDURES

Statistical Analysis

Unless explicitly stated, all statistical analyses used one-way analysis of variance with Bonferroni's multiple comparison test.

Liposome-Mediated Transduction of Fibrils, Lysate, Brain Homogenate

Cell lines were plated at 250,000 cells per well in 12-well plates. Twenty-four hr later, fibrils or lysate were combined with OptiMEM (GIBCO) to a final volume

of 100 μ L. 96 μ L OptiMEM and 4 μ L lipofectamine-2000 (Invitrogen) was then added to a final volume of 200 μ L. After 20 min, liposome preparations were added to cells. Eighteen hr later, cells were replated in wells of a 6-well plate. For more details, see [Supplemental Experimental Procedures](#).

Semidenaturing Detergent Agarose Gel Electrophoresis

SDD-AGE was performed as previously described (Kryndushkin et al., 2003) with minor modifications. Cell pellets lysed in 0.05% Triton X were clarified by sequential centrifugations (500 \times g, 1000 \times g). Low-SDS 1.5% agarose gels were prepared by dissolving agarose in buffer G (20 mM Tris-Base, 200 mM glycine, in ddH₂O) with 0.02% SDS. For each condition, 5 μ g of clarified cell lysate was incubated with 0.02% SDS sample buffer for 7 min prior to loading. SDD-AGE was run in Laemmli buffer (Buffer G with 0.1% SDS). Protein was transferred to Immobilon P (Millipore). Membranes were probed for tau with rabbit polyclonal anti-tau ab64193 (1:4000, AbCam) and counter-probed with goat anti-rabbit HRP (1:4,000, Jackson ImmunoTherapy). For more details, see [Supplemental Experimental Procedures](#).

Sedimentation Analysis

Clarified cell lysate was centrifuged at 100,000 \times g for 1 hr. Supernatant was placed aside and the pellet was washed with 1.5 ml PBS prior to ultracentrifugation at 100,000 \times g for 30 min. The supernatant was aspirated and the pellet was resuspended by boiling in RIPA buffer with 4% SDS and 100 mM DTT. Bradford assay (Bio-Rad) with BSA standard curve was used to normalize all protein concentrations. Samples were run on 4%–15% SDS-PAGE gels (Bio-Rad) and protein was transferred to Immobilon P (Millipore). Membranes were probed for tau as described above. For more details, see [Supplemental Experimental Procedures](#).

Split-Luciferase Complementation Assay

Polyclonal HEK293 cells stably expressing tau RD-Cluc and tau RD-Nluc were plated at 240,000 cells per well in 12-well plates 24 hr prior to cell lysate transduction. Clarified cell lysate was prepared as described above. Cell lysate (20 μ g in 10 μ L volume) was diluted with 90 μ L OptiMEM (GIBCO) and incubated with 96 μ L OptiMEM and 4 μ L lipofectamine-2000 (Invitrogen) for 20 min. Liposome preparations were then added to cells and 18 hr later, cells were replated in quadruplicate in a 96-well plate. Twenty-four hr later, media was aspirated from wells and replaced with luciferin solution (150 μ g/mL D-luciferin potassium salt, Gold Biosciences, in Dulbecco's phosphate-buffered saline, GIBCO). Cells were incubated with luciferin solution for 3 min at 37°C prior to reading luminescence with a Tecan M1000 fluorescence plate reader. For more details, see [Supplemental Experimental Procedures](#).

Protease Digestion

Pronase (Roche) was diluted in PBS to a final concentration of 1 mg/mL and single-use aliquots were stored at -80° C. Clarified cell lysate was prepared

(C) Limited proteolysis reveals that G0 clones feature similar banding patterns to the original parental lines, with G0-clone 10 featuring a doublet between 10–13 kDa (versus smear for G0-clone 9) and a band between 20 and 25 kDa that is slightly smaller than G0-clone 9 bands.

(D) Split-luciferase complementation demonstrates similar seeding efficiencies in G0 clones relative to original parental lines. Averages of four separate experiments are shown, each read in quadruplicate at 48 hr posttransduction of lysate (error bars represent SEM, **** = $p < 0.0001$).

(E) IP material from pooled G2 mice was transduced into naive tau RD-YFP cells prior to passage onto coverslips. At 96 hr, cells were fixed. Seeding of inclusion formation is significantly greater for G2-clone 9 and G2-clone 10 mice than G2-clone 1 mice. G2-clone 1 tau induces inclusions on rare occasions (~1% of cells). Seeding is specific to tau because IgG-precipitated material never seeds. Ten fields, each with 150+ cells, were analyzed per condition (error bars represent SEM, * = $p < 0.05$, **** = $p < 0.0001$). See also [Figure S6E](#) for split-luciferase complementation data.

(F) Inclusion morphologies are maintained following passage through three generations of mice. IP full-length tau from pooled G2 homogenates was transduced into tau RD-YFP cells, and 12 clones per cohort were isolated. Representative examples are shown. The two clones boxed in red feature similar limited proteolysis digestion patterns and seeding ratios to each other, which are unique from all 22 other clones. See [Figure S6F](#) for quantification of colony morphologies prior to monoclonal cell line isolation and [Figure S6G](#) for images of all 24 clones.

(G) Limited proteolysis reveals that G2 clones feature similar banding patterns to their parental lines, with G2-clone 10 featuring a doublet between 10–13 kDa (versus smear for G2-clone 9) and a band between 20 and 25 kDa that is slightly smaller than G2-clone 9 digests. Two clones (boxed in red), one for each cohort, are unique in featuring bands at 15 and 25 kDa.

(H) Split-luciferase complementation demonstrates similar seeding efficiencies in G2 clones relative to original parental lines. Seeding ratios were averaged across clones, each of which was read in quadruplicate at 48 hr posttransduction of lysate (error bars represent SEM, **** = $p < 0.0001$). Boxed in red are two outlier clones (9G and 10D), which also feature unique inclusion morphologies and limited proteolysis digestion patterns.

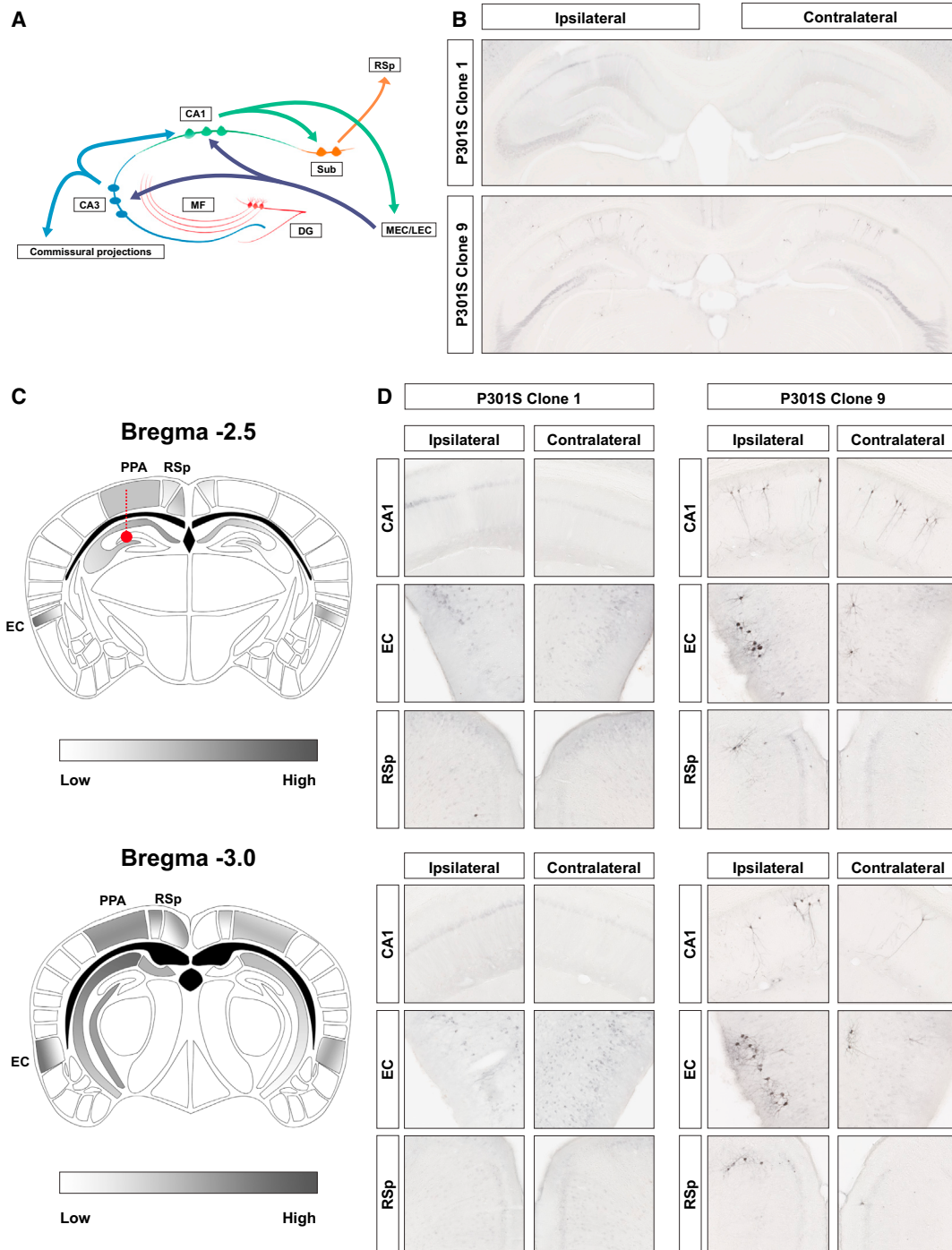


Figure 7. Anterograde and Retrograde Spread of Pathology to Synaptically Connected Regions in Generation 3-clone 9 Mice

(A) Schematic of known projections to and from the hippocampus (DG, dentate gyrus; MEC/LEC, medial and lateral entorhinal cortices; MF, mossy fibers; RSp, retrosplenial cortex; Sub, subiculum).

(B) Representative images of AT8 staining in the hippocampi of G3 mice inoculated with 10 μ g of G2 brain homogenate. Spread of clone 9 pathology to the contralateral hippocampus is evident. See Figure S7A for whole brain slices.

(C) Summary of pathology present in G3-clone 9 mice. Gradient represents semiquantitative analysis of neurofibrillary tangle-like AT8 cell body positivity observed in each region (PPA, posterior parietal association area) both 2.5 and 3.0 mm posterior to bregma.

(D) AT8 histopathology observed in brain regions with known projections to and from the hippocampus. Ipsilateral AT8 pathology is observed in the EC and appears in cortical layers II-III, whereas contralateral pathology is observed in deeper layers of the EC. Pathology is also observed in the retrosplenial cortex, especially ipsilateral to the injection site. See Figure S7B for subiculum and dentate gyrus images.

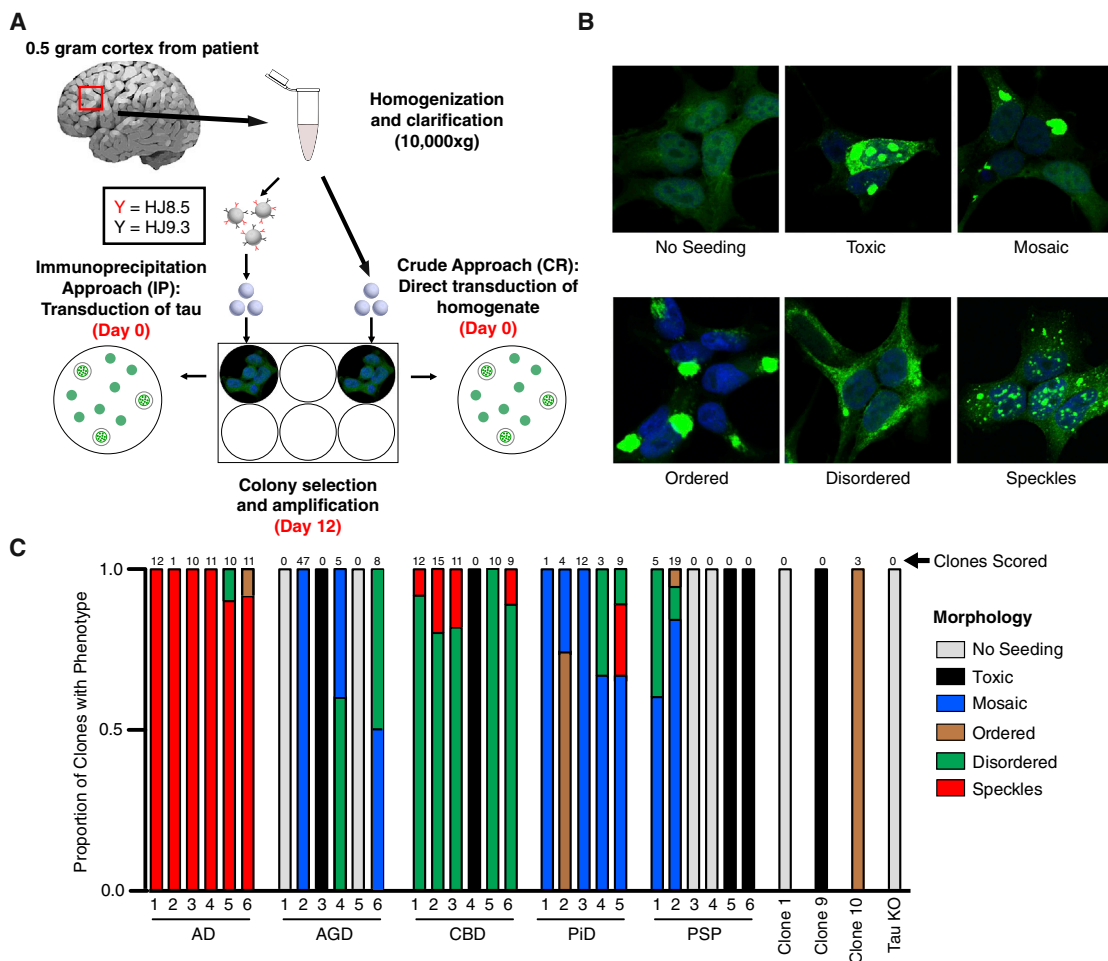


Figure 8. Diverse Tau Prion Strains within Patients and across Diseases

(A) Schematic illustrating methods used to generate patient-derived tau RD prion strains in a monoclonal Tet Off-tau RD-YFP line. See Figure S8 for data indicating that different inclusion morphologies are associated with different biochemical and seeding properties.

(B) Morphological phenotypes associated with tau RD prion strains induced by patient material: no seeding, toxic, mosaic, ordered, disordered, speckles. Representative examples are shown.

(C) IP tau from 29 patient samples (AD, Alzheimer's disease; AGD, argyrophilic grain disease; CBD, corticobasal degeneration; PiD, Pick's disease; PSP, progressive supranuclear palsy) was transduced into tau RD-YFP cells (Tet Off) and as many inclusion-positive clones as could be identified for each patient sample were blindly picked and amplified. Once confluent in 10 cm dishes, morphological phenotypes were scored by a separate blinded experimenter. See Table S2 for numerical values, patient-related information, and tissue origin.

as previously described (see SDD-AGE) and protein concentrations were normalized to 1.7 $\mu\text{g}/\mu\text{L}$. 17 μg (10 μL) of cell lysate was added to 10 μL of pronase at a concentration of 100 $\mu\text{g}/\text{mL}$ (diluted in PBS) for a final volume of 20 μL . Cell lysates were digested at 37°C for one hour. Reactions were quenched by addition of 20 μL 2 \times sample buffer (final SDS concentration of 1%) and boiling for 5 min. Each sample (15 μL) was run on a 10% Bis-Tris NuPAGE gel (Novex by Life Technologies) and protein was transferred to Immobilon P (Millipore). Membranes were probed for tau as described above. For more details, see Supplemental Experimental Procedures.

Animals and Hippocampal Injections

Transgenic mice expressing FL human tau 4R1N P301S under the murine prion promoter (Yoshiyama et al., 2007) were maintained on a B6C3 background. P301S and nontransgenic littermates were anesthetized with isoflurane and were bilaterally injected into the hippocampus (from bregma: -2.5 mm posterior, ± 2 mm lateral, -1.8 mm ventral) with either 2 μL of

5 $\mu\text{g}/\mu\text{L}$ clarified lysate/homogenate or 2 μL of 2.5 $\mu\text{g}/\mu\text{L}$ recombinant tau RD fibrils as previously described (DeVos and Miller, 2013). For all experiments, conditions were gender-matched (Table S1). Unilateral injections were used for G3 spread experiments. All protocols involving animal use were approved by the institutional animal care and use committee at Washington University in St. Louis. For more details, see Supplemental Experimental Procedures.

Histology and Immunohistochemistry

Sections (50 μm) were taken through the entire left hemisphere with a freezing microtome. For DAB stains, brain slices were incubated with indicated antibodies overnight at 4°C. Slices were then counter-stained with the appropriate secondary. Slices were then incubated at room temperature for 30 min with the VECTASTAIN Elite ABC Kit (Vector Labs), followed by DAB development with the DAB Peroxidase Substrate Kit with the optional nickel addition (Vector Labs). Histological images and z stacks were captured with the Olympus Nanozoomer 2.0-HT (Hamamatsu) and analyzed with the NDP viewer software

(Hamamatsu). For immunofluorescence stains, slices were incubated in blocking solution with indicated primary antibody overnight at 4°C, followed by appropriate secondary labeling. For more details, see [Supplemental Experimental Procedures](#).

SUPPLEMENTAL INFORMATION

Supplemental Information includes eight figures, two tables, and Supplemental Experimental Procedures and can be found with this article online at <http://dx.doi.org/10.1016/j.neuron.2014.04.047>.

AUTHOR CONTRIBUTIONS

D.W.S. and S.K.K. contributed equally to this work. D.W.S. performed all cell culture and biochemistry experiments. S.K.K. performed all animal experiments. S.L.D. provided technical assistance and guidance for animal inoculations. A.M.S. aided with biochemistry. H.M. and A.L. contributed unpublished reagents. S.J.B. helped with cell-culture experiments and performed blind scoring. A.C.F., J.R.T., and L.C.S. performed electron microscopy. L.T.G. and W.W.S. analysed and selected human samples. D.W.S., S.K.K., S.L.D., T.M.M., and M.I.D. designed experiments. D.W.S., S.K.K., and M.I.D. analysed results and wrote the manuscript.

ACKNOWLEDGMENTS

We thank John Cirrito, Peter Davies, David Holtzman, Paul Kotzbauer, Jeffrey Milbrandt, and David Piwnica-Worms for reagents. We thank Dorrie Young for help with figures and Jan Bieschke, William Dauer, Jen Dulle, Bess Frost, Brandon Holmes, Suzanne Schindler, Kevin Stein, and Heather True for critiques. Our work was funded by the Tau Consortium, Muscular Dystrophy Association, American Health Assistance Foundation, Ruth K. Broad Foundation, Harrington Discovery Institute, and the NIH (1F31NS086251, D.W.S.; 1R01NS071835, M.I.D.; 1R01NS078398, T.M.M.). This work was supported by the Hope Center Alafi Neuroimaging Lab and a P30 Neuroscience Blueprint Interdisciplinary Center Core award to Washington University (P30NS057105). Human tissue samples were provided by the Neurodegenerative Disease Brain Bank at the University of California, San Francisco, which receives funding support from NIH grants P01AG019724 and P50AG023501, the Consortium for Frontotemporal Dementia Research, and the Tau Consortium. M.I.D. acknowledges a potential conflict of interest in that he is a coinventor of antibodies used in this study (HJ9.3 and HJ8.5) that have been licensed by C2N Diagnostics through an agreement with Washington University in St. Louis.

Accepted: April 15, 2014

Published: May 22, 2014

REFERENCES

- Aguzzi, A., and Rajendran, L. (2009). The transcellular spread of cytosolic amyloids, prions, and prionoids. *Neuron* *64*, 783–790.
- Andersen, P. (2007). *The Hippocampus Book*. (Oxford: Oxford University Press).
- Aoyagi, H., Hasegawa, M., and Tamaoka, A. (2007). Fibrillogenic nuclei composed of P301L mutant tau induce elongation of P301L tau but not wild-type tau. *J. Biol. Chem.* *282*, 20309–20318.
- Barghorn, S., Zheng-Fischhöfer, Q., Ackmann, M., Biernat, J., von Bergen, M., Mandelkow, E.M., and Mandelkow, E. (2000). Structure, microtubule interactions, and paired helical filament aggregation by tau mutants of frontotemporal dementias. *Biochemistry* *39*, 11714–11721.
- Bessen, R.A., and Marsh, R.F. (1994). Distinct PrP properties suggest the molecular basis of strain variation in transmissible mink encephalopathy. *J. Virol.* *68*, 7859–7868.
- Birkett, C.R., Hennion, R.M., Bembridge, D.A., Clarke, M.C., Chree, A., Bruce, M.E., and Bostock, C.J. (2001). Scrapie strains maintain biological phenotypes on propagation in a cell line in culture. *EMBO J.* *20*, 3351–3358.
- Bonar, L., Cohen, A.S., and Skinner, M.M. (1969). Characterization of the amyloid fibril as a cross-beta protein. *Proc. Soc. Exp. Biol. Med.* *131*, 1373–1375.
- Bousset, L., Pieri, L., Ruiz-Arlandis, G., Gath, J., Jensen, P.H., Habenstein, B., Madiona, K., Olieric, V., Böckmann, A., Meier, B.H., and Melki, R. (2013). Structural and functional characterization of two alpha-synuclein strains. *Nat Commun* *4*, 2575.
- Braak, H., and Braak, E. (1995). Staging of Alzheimer's disease-related neurofibrillary changes. *Neurobiol. Aging* *16*, 271–8–discussion278–84.
- Bruce, M., Chree, A., McConnell, I., Foster, J., Pearson, G., and Fraser, H. (1994). Transmission of bovine spongiform encephalopathy and scrapie to mice: strain variation and the species barrier. *Philos. Trans. R. Soc. Lond. B Biol. Sci.* *343*, 405–411.
- Clavaguera, F., Bolmont, T., Crowther, R.A., Abramowski, D., Frank, S., Probst, A., Fraser, G., Stalder, A.K., Beibel, M., Staufienbiel, M., et al. (2009). Transmission and spreading of tauopathy in transgenic mouse brain. *Nat. Cell Biol.* *11*, 909–913.
- Clavaguera, F., Akatsu, H., Fraser, G., Crowther, R.A., Frank, S., Hench, J., Probst, A., Winkler, D.T., Reichwald, J., Staufienbiel, M., et al. (2013a). Brain homogenates from human tauopathies induce tau inclusions in mouse brain. *Proc. Natl. Acad. Sci. USA* *110*, 9535–9540.
- Clavaguera, F., Lavenir, I., Falcon, B., Frank, S., Goedert, M., and Tolnay, M. (2013b). "Prion-like" templated misfolding in tauopathies. *Brain Pathol.* *23*, 342–349.
- Collinge, J., and Clarke, A.R. (2007). A general model of prion strains and their pathogenicity. *Science* *318*, 930–936.
- de Calignon, A., Polydoro, M., Suárez-Calvet, M., William, C., Adamowicz, D.H., Kopeikina, K.J., Pittstick, R., Sahara, N., Ashe, K.H., Carlson, G.A., et al. (2012). Propagation of tau pathology in a model of early Alzheimer's disease. *Neuron* *73*, 685–697.
- Derkatch, I.L., Chernoff, Y.O., Kushnirov, V.V., Inge-Vechtomov, S.G., and Liebman, S.W. (1996). Genesis and variability of [PSI] prion factors in *Saccharomyces cerevisiae*. *Genetics* *144*, 1375–1386.
- Desplats, P., Lee, H.-J., Bae, E.-J., Patrick, C., Rockenstein, E., Crews, L., Spencer, B., Masliah, E., and Lee, S.-J. (2009). Inclusion formation and neuronal cell death through neuron-to-neuron transmission of alpha-synuclein. *Proc. Natl. Acad. Sci. USA* *106*, 13010–13015.
- DeVos, S.L., and Miller, T.M. (2013). Direct intraventricular delivery of drugs to the rodent central nervous system. *J. Vis. Exp.* *12*, e50326.
- Dinkel, P.D., Siddiqua, A., Huynh, H., Shah, M., and Margittai, M. (2011). Variations in filament conformation dictate seeding barrier between three- and four-repeat tau. *Biochemistry* *50*, 4330–4336.
- Duyckaerts, C., Delatour, B., and Potier, M.-C. (2009). Classification and basic pathology of Alzheimer disease. *Acta Neuropathol.* *118*, 5–36.
- Feany, M.B., Mattiace, L.A., and Dickson, D.W. (1996). Neuropathologic overlap of progressive supranuclear palsy, Pick's disease and corticobasal degeneration. *J. Neuropathol. Exp. Neurol.* *55*, 53–67.
- Frost, B., and Diamond, M.I. (2010). Prion-like mechanisms in neurodegenerative diseases. *Nat. Rev. Neurosci.* *11*, 155–159.
- Frost, B., Jacks, R.L., and Diamond, M.I. (2009a). Propagation of tau misfolding from the outside to the inside of a cell. *J. Biol. Chem.* *284*, 12845–12852.
- Frost, B., Ollesch, J., Wille, H., and Diamond, M.I. (2009b). Conformational diversity of wild-type Tau fibrils specified by templated conformation change. *J. Biol. Chem.* *284*, 3546–3551.
- Giasson, B.I., Forman, M.S., Higuchi, M., Golbe, L.I., Graves, C.L., Kotzbauer, P.T., Trojanowski, J.Q., and Lee, V.M.-Y. (2003). Initiation and synergistic fibrillization of tau and alpha-synuclein. *Science* *300*, 636–640.
- Greicius, M.D., and Kimmel, D.L. (2012). Neuroimaging insights into network-based neurodegeneration. *Curr. Opin. Neurol.* *25*, 727–734.

- Guo, J.L., Covell, D.J., Daniels, J.P., Iba, M., Stieber, A., Zhang, B., Riddle, D.M., Kwong, L.K., Xu, Y., Trojanowski, J.Q., and Lee, V.M. (2013). Distinct α -synuclein strains differentially promote tau inclusions in neurons. *Cell* **154**, 103–117.
- Guo, J.L., and Lee, V.M. (2014). Cell-to-cell transmission of pathogenic proteins in neurodegenerative diseases. *Nat. Med.* **20**, 130–138.
- Halliday, G.M., Holton, J.L., Revesz, T., and Dickson, D.W. (2011). Neuropathology underlying clinical variability in patients with synucleinopathies. *Acta Neuropathol.* **122**, 187–204.
- Holmes, B.B., and Diamond, M.I. (2012). Cellular mechanisms of protein aggregate propagation. *Curr. Opin. Neurol.* **25**, 721–726.
- Holmes, B.B., DeVos, S.L., Kfoury, N., Li, M., Jacks, R., Yanamandra, K., Ouidja, M.O., Brodsky, F.M., Marasa, J., Bagchi, D.P., et al. (2013). Heparan sulfate proteoglycans mediate internalization and propagation of specific proteopathic seeds. *Proc. Natl. Acad. Sci. USA* **110**, E3138–E3147.
- Holtzman, D.M., Morris, J.C., and Goate, A.M. (2011). Alzheimer's disease: the challenge of the second century. *Sci Transl Med* **3**, 77sr1.
- Hutton, M., Lendon, C.L., Rizzu, P., Baker, M., Froelich, S., Houlden, H., Pickering-Brown, S., Chakraverty, S., Isaacs, A., Grover, A., et al. (1998). Association of missense and 5'-splice-site mutations in tau with the inherited dementia FTDP-17. *Nature* **393**, 702–705.
- Iba, M., Guo, J.L., McBride, J.D., Zhang, B., Trojanowski, J.Q., and Lee, V.M.-Y. (2013). Synthetic tau fibrils mediate transmission of neurofibrillary tangles in a transgenic mouse model of Alzheimer's-like tauopathy. *J. Neurosci.* **33**, 1024–1037.
- Jicha, G.A., Bowser, R., Kazam, I.G., and Davies, P. (1997). Alz-50 and MC-1, a new monoclonal antibody raised to paired helical filaments, recognize conformational epitopes on recombinant tau. *J. Neurosci. Res.* **48**, 128–132.
- Kim, W., Lee, S., Jung, C., Ahmed, A., Lee, G., and Hall, G.F. (2010). Interneuron transfer of human tau between Lamprey central neurons in situ. *J. Alzheimers Dis.* **19**, 647–664.
- Kim, C., Haldiman, T., Surewicz, K., Cohen, Y., Chen, W., Blevins, J., Sy, M.-S., Cohen, M., Kong, Q., Telling, G.C., et al. (2012). Small protease sensitive oligomers of PrP^{Sc} in distinct human prions determine conversion rate of PrP(C). *PLoS Pathog.* **8**, e1002835.
- Krammer, C., Kryndushkin, D., Suhre, M.H., Kremmer, E., Hofmann, A., Pfeifer, A., Scheibel, T., Wickner, R.B., Schätzl, H.M., and Vorberg, I. (2009). The yeast Sup35NM domain propagates as a prion in mammalian cells. *Proc. Natl. Acad. Sci. USA* **106**, 462–467.
- Kryndushkin, D.S., Alexandrov, I.M., Ter-Avanesyan, M.D., and Kushnirov, V.V. (2003). Yeast [PSI⁺] prion aggregates are formed by small Sup35 polymers fragmented by Hsp104. *J. Biol. Chem.* **278**, 49636–49643.
- Lee, V.M., Goedert, M., and Trojanowski, J.Q. (2001). Neurodegenerative tauopathies. *Annu. Rev. Neurosci.* **24**, 1121–1159.
- Legname, G., Nguyen, H.-O.B., Peretz, D., Cohen, F.E., DeArmond, S.J., and Prusiner, S.B. (2006). Continuum of prion protein structures enciphers a multitude of prion isolate-specified phenotypes. *Proc. Natl. Acad. Sci. USA* **103**, 19105–19110.
- Li, J., Browning, S., Mahal, S.P., Oelschlegel, A.M., and Weissmann, C. (2010). Darwinian evolution of prions in cell culture. *Science* **327**, 869–872.
- Liu, L., Drouet, V., Wu, J.W., Witter, M.P., Small, S.A., Clelland, C., and Duff, K. (2012). Trans-synaptic spread of tau pathology in vivo. *PLoS ONE* **7**, e31302.
- Lu, J.-X., Qiang, W., Yau, W.-M., Schwieters, C.D., Meredith, S.C., and Tycko, R. (2013). Molecular structure of β -amyloid fibrils in Alzheimer's disease brain tissue. *Cell* **154**, 1257–1268.
- Luk, K.C., Kehm, V.M., Zhang, B., O'Brien, P., Trojanowski, J.Q., and Lee, V.M.-Y. (2012). Intracerebral inoculation of pathological α -synuclein initiates a rapidly progressive neurodegenerative α -synucleinopathy in mice. *J. Exp. Med.* **209**, 975–986.
- Meyer-Luehmann, M., Coomaraswamy, J., Bolmont, T., Kaeser, S., Schaefer, C., Kilger, E., Neuenschwander, A., Abramowski, D., Frey, P., Jaton, A.L., et al. (2006). Exogenous induction of cerebral beta-amyloidogenesis is governed by agent and host. *Science* **313**, 1781–1784.
- Miyasaka, T., Morishima-Kawashima, M., Ravid, R., Kamphorst, W., Nagashima, K., and Ihara, Y. (2001). Selective deposition of mutant tau in the FTDP-17 brain affected by the P301L mutation. *J. Neuropathol. Exp. Neurol.* **60**, 872–884.
- Münch, C., O'Brien, J., and Bertolotti, A. (2011). Prion-like propagation of mutant superoxide dismutase-1 misfolding in neuronal cells. *Proc. Natl. Acad. Sci. USA* **108**, 3548–3553.
- Naik, S., and Piwnica-Worms, D. (2007). Real-time imaging of beta-catenin dynamics in cells and living mice. *Proc. Natl. Acad. Sci. USA* **104**, 17465–17470.
- Petkova, A.T., Leapman, R.D., Guo, Z., Yau, W.-M., Mattson, M.P., and Tycko, R. (2005). Self-propagating, molecular-level polymorphism in Alzheimer's beta-amyloid fibrils. *Science* **307**, 262–265.
- Prusiner, S.B. (1984). Some speculations about prions, amyloid, and Alzheimer's disease. *N. Engl. J. Med.* **310**, 661–663.
- Prusiner, S.B. (1998). Prions. *Proc. Natl. Acad. Sci. USA* **95**, 13363–13383.
- Raj, A., Kuceyeski, A., and Weiner, M. (2012). A network diffusion model of disease progression in dementia. *Neuron* **73**, 1204–1215.
- Ren, P.-H., Lauckner, J.E., Kachirskaja, I., Heuser, J.E., Melki, R., and Kopito, R.R. (2009). Cytoplasmic penetration and persistent infection of mammalian cells by polyglutamine aggregates. *Nat. Cell Biol.* **11**, 219–225.
- Sacino, A.N., Thomas, M.A., Ceballos-Diaz, C., Cruz, P.E., Rosario, A.M., Lewis, J., Giasson, B.I., and Golde, T.E. (2013). Conformational templating of α -synuclein aggregates in neuronal-glia cultures. *Mol. Neurodegener.* **8**, 17.
- Safar, J., Wille, H., Itri, V., Groth, D., Serban, H., Torchia, M., Cohen, F.E., and Prusiner, S.B. (1998). Eight prion strains have PrP(Sc) molecules with different conformations. *Nat. Med.* **4**, 1157–1165.
- Santa-Maria, I., Varghese, M., Ksiezak-Reding, H., Dzhun, A., Wang, J., and Pasinetti, G.M. (2012). Paired helical filaments from Alzheimer disease brain induce intracellular accumulation of Tau protein in aggresomes. *J. Biol. Chem.* **287**, 20522–20533.
- Seeley, W.W., Crawford, R.K., Zhou, J., Miller, B.L., and Greicius, M.D. (2009). Neurodegenerative diseases target large-scale human brain networks. *Neuron* **62**, 42–52.
- Siddiqua, A., and Margittai, M. (2010). Three- and four-repeat Tau coassemble into heterogeneous filaments: an implication for Alzheimer disease. *J. Biol. Chem.* **285**, 37920–37926.
- Tanaka, M., Collins, S.R., Toyama, B.H., and Weissman, J.S. (2006). The physical basis of how prion conformations determine strain phenotypes. *Nature* **442**, 585–589.
- Toyama, B.H., Kelly, M.J.S., Gross, J.D., and Weissman, J.S. (2007). The structural basis of yeast prion strain variants. *Nature* **449**, 233–237.
- True, H.L., and Lindquist, S.L. (2000). A yeast prion provides a mechanism for genetic variation and phenotypic diversity. *Nature* **407**, 477–483.
- van Groen, T., Miettinen, P., and Kadish, I. (2003). The entorhinal cortex of the mouse: organization of the projection to the hippocampal formation. *Hippocampus* **13**, 133–149.
- Van Langenhove, T., van der Zee, J., and Van Broeckhoven, C. (2012). The molecular basis of the frontotemporal lobar degeneration-amyotrophic lateral sclerosis spectrum. *Ann. Med.* **44**, 817–828.
- von Bergen, M., Barghorn, S., Li, L., Marx, A., Biernat, J., Mandelkow, E.M., and Mandelkow, E. (2001). Mutations of tau protein in frontotemporal dementia promote aggregation of paired helical filaments by enhancing local beta-structure. *J. Biol. Chem.* **276**, 48165–48174.
- Waxman, E.A., and Giasson, B.I. (2011). Induction of intracellular tau aggregation is promoted by α -synuclein seeds and provides novel insights into the hyperphosphorylation of tau. *J. Neurosci.* **31**, 7604–7618.
- Wischik, C.M., Novak, M., Thøgersen, H.C., Edwards, P.C., Runswick, M.J., Jakes, R., Walker, J.E., Milstein, C., Roth, M., and Klug, A. (1988). Isolation

- of a fragment of tau derived from the core of the paired helical filament of Alzheimer disease. *Proc. Natl. Acad. Sci. USA* 85, 4506–4510.
- Yanamandra, K., Kfoury, N., Jiang, H., Mahan, T.E., Ma, S., Maloney, S.E., Wozniak, D.F., Diamond, M.I., and Holtzman, D.M. (2013). Anti-tau antibodies that block tau aggregate seeding in vitro markedly decrease pathology and improve cognition in vivo. *Neuron* 80, 402–414.
- Yoshiyama, Y., Higuchi, M., Zhang, B., Huang, S.-M., Iwata, N., Saido, T.C., Maeda, J., Suhara, T., Trojanowski, J.Q., and Lee, V.M.-Y. (2007). Synapse loss and microglial activation precede tangles in a P301S tauopathy mouse model. *Neuron* 53, 337–351.
- Zhou, J., Gennatas, E.D., Kramer, J.H., Miller, B.L., and Seeley, W.W. (2012). Predicting regional neurodegeneration from the healthy brain functional connectome. *Neuron* 73, 1216–1227.
- Ziebell, J.M., Taylor, S.E., Cao, T., Harrison, J.L., and Lifshitz, J. (2012). Rod microglia: elongation, alignment, and coupling to form trains across the somatosensory cortex after experimental diffuse brain injury. *J. Neuroinflammation* 9, 247.

Neuron, Volume 82

Supplemental Information

**Distinct Tau Prion Strains Propagate in Cells
and Mice and Define Different Tauopathies**

**David W. Sanders, Sarah K. Kaufman, Sarah L. DeVos, Apurwa M. Sharma, Hilda
Mirbaha, Aimin Li, Scarlett J. Barker, Alex C. Foley, Julian R. Thorpe, Louise C. Serpell,
Timothy M. Miller, Lea T. Grinberg, William W. Seeley, and Marc I. Diamond**

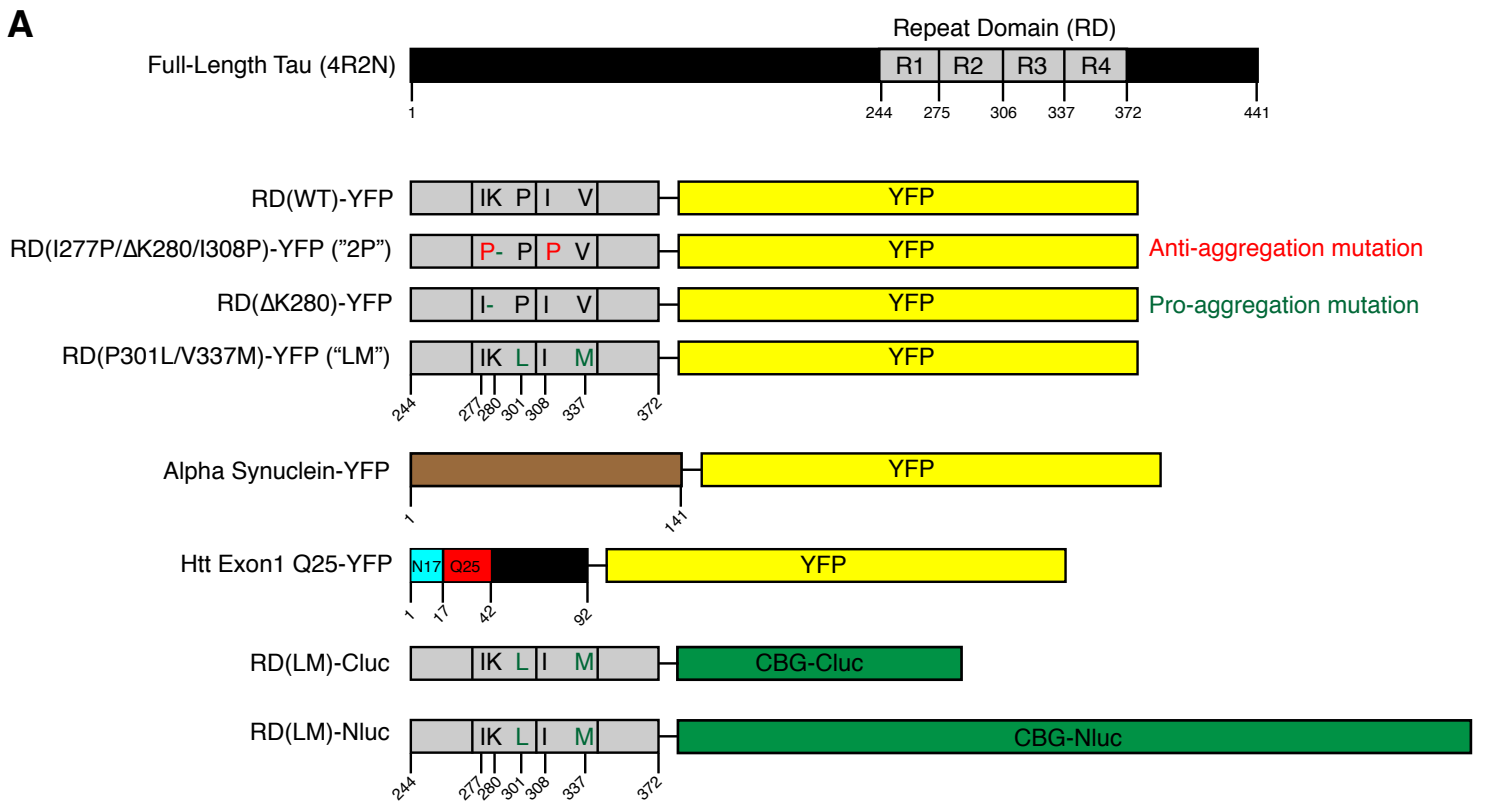
Figure S1, related to Figure 1. – Constructs and lack of cross-seeding

(A) Diagrams illustrating constructs used in this study.

(B) Quantification of seeding efficiency of fibril and cell line pairs. Ten fields, each with 150+ cells, were quantified per condition. Percent positive averages are followed by the S.E.M.

(C) Polyclonal HEK293 lines stably expressing FL tau 4R1N P301S (with or without YFP tag) were transduced with buffer, A β , Htt, α -syn, or tau RD fibrils. Cells were stained for phospho-tau (AT8) on Day 6. Only homotypic seeding was observed.

(D) Quantification of seeding efficiency of fibrils transduced into FL tau P301S cell lines. Ten fields, each with 150+ cells, were quantified. Percent positive averages are plotted. Error bars represent S.E.M.



B

HEK293 Cell Line	Buffer	Alpha Synuclein	Tau RD	Htt N17-Q35	Amyloid Beta
Alpha Synuclein	0	3.2±0.5	0	0	0
Tau RD	0	0	36.6±1.8	0	0
Htt Exon1-Q25	0	0	0	24.7±1.7	0

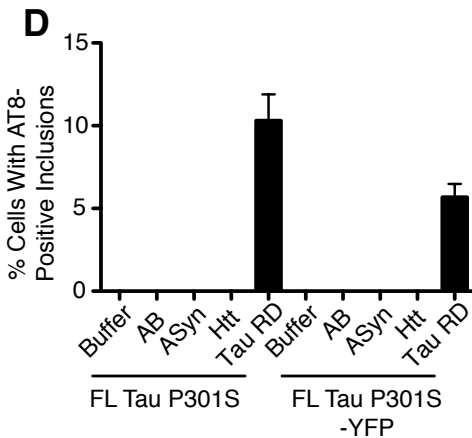
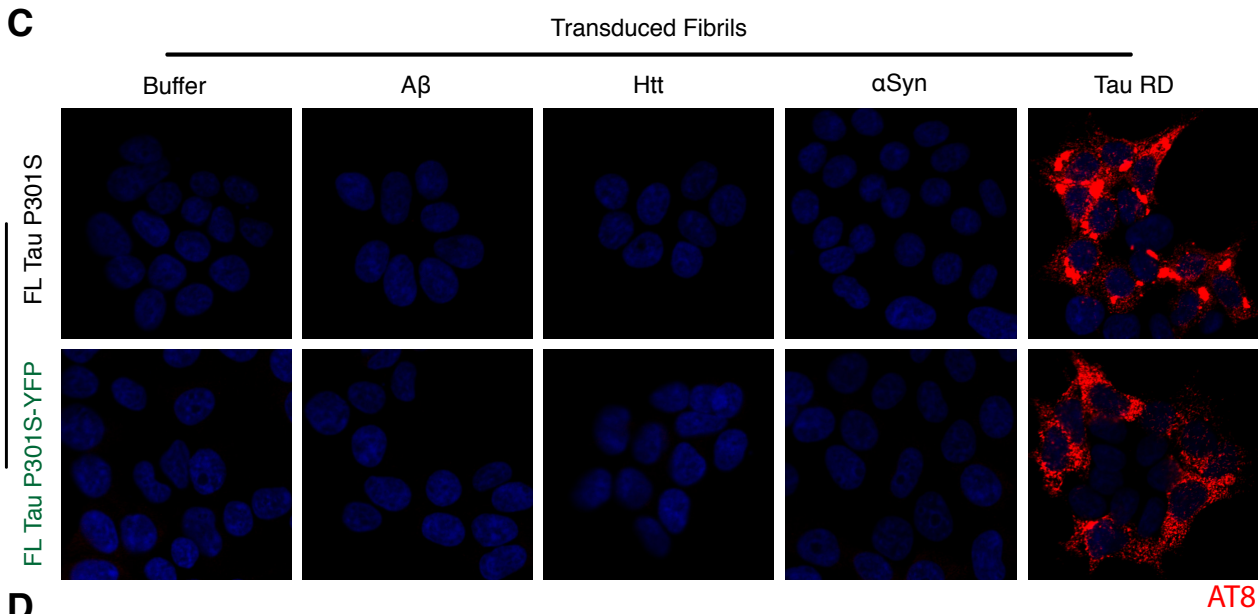


Figure S2, related to Figure 2. – Morphologies of all clones and strain-specific properties of Clones 9 and 10

(A) Confocal images of representative cells from all 20 clones. Nuclear aggregates are present in all clones except Clone 1 (no inclusions) and Clone 10 (one large juxtannuclear inclusion with no nuclear inclusions).

(B) Normalization of luminescence based on Hoechst stain reveals that differences in seeding ratios between Clones 9 and 10 are not due to differences in cell confluency (error bars = S.E.M).

(C) Lysates were transduced into either non-transfected (NT) cells or those stably expressing tau RD(LM)-HA. Clone 1 and 10 lysate do not affect cell numbers as measured by Hoechst stain at Day 4. However, Clone 9 lysate significantly reduces the number of cells in the tau RD(LM)-HA background, revealing that Clone 9's toxicity is dependent on expression of tau RD(LM) (error bars = S.E.M, **** = $p < 0.0001$).

(D) Tau RD(LM)-HA cells were transduced with lysates from Clones 1, 9, and 10. LDH levels in the media were measured at Day 4 and compared to those of lysed cells (toxic control). Clone 9 is especially toxic relative to sham-treated cells (error bars = S.E.M, ** = $p < 0.01$).

(E) Clones 9 and 10 were stained for vimentin, which forms a cage around aggresomes. Vimentin cages are observed around the large juxtannuclear inclusion of Clone 10 cells but not around the inclusion of Clone 9, indicating the Clone 10 aggregates form canonical aggresomes, whereas Clone 9 inclusions do not.

(F) Transmission electron microscopic analysis of Clone 10 cells reveals large aggresome structures indenting the nuclear envelope. Clone 9 cells feature small, round, nuclear inclusions. Immuno-EM confirms that both types of inclusions contain tau RD.

(G) Co-localization of juxtannuclear Clone 10 but not Clone 9 inclusions with γ -tubulin, a marker of the microtubule-organizing center (MTOC), suggests that only the former are true aggresomes. Arrowheads point to juxtannuclear tau RD inclusions, whereas arrows point to MTOCs.

(H) Staining of nuclear PML bodies, organizing centers for degradation of nuclear aggregates, demonstrates that Clone 9 nuclear inclusions are in a unique compartment.

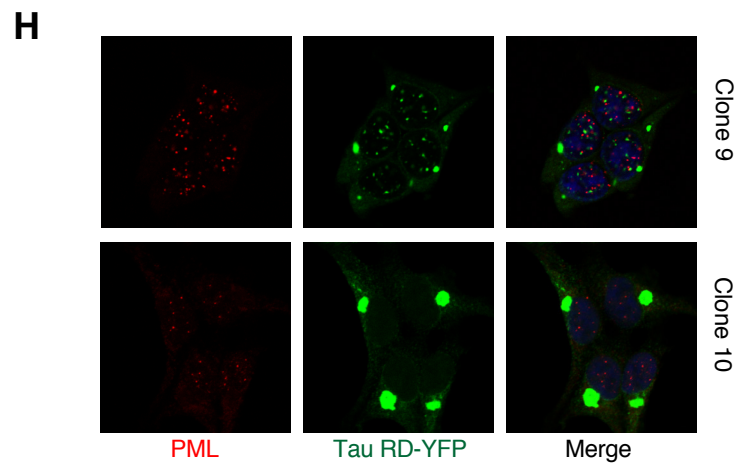
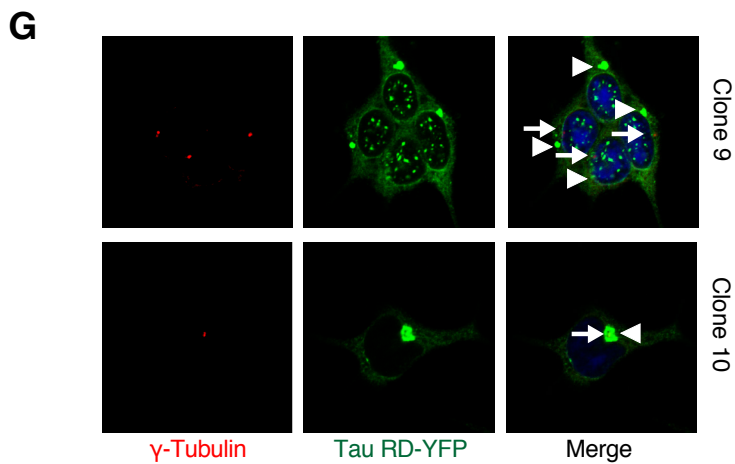
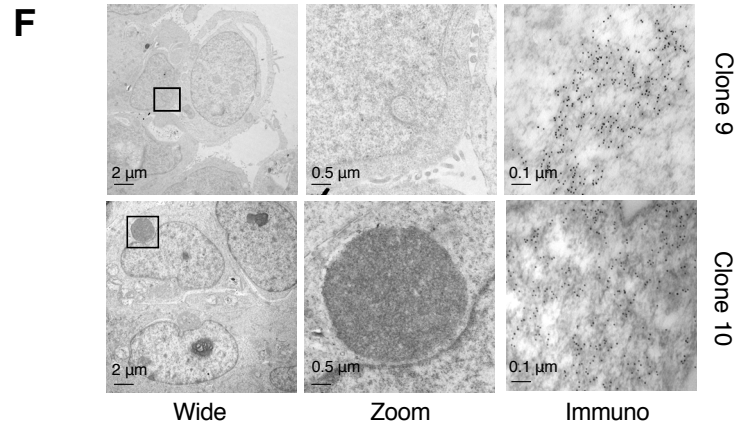
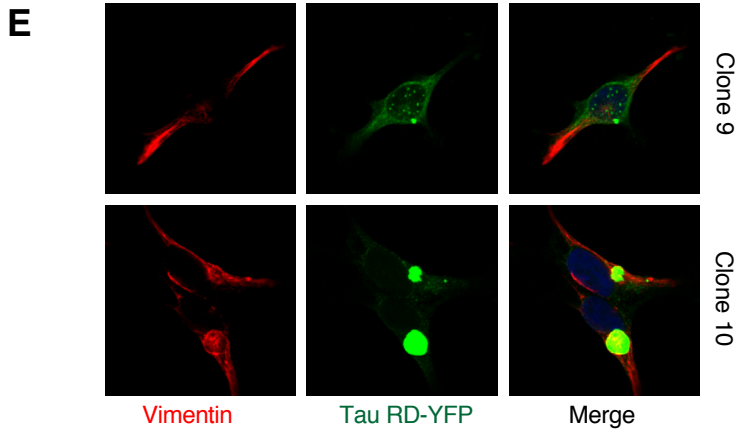
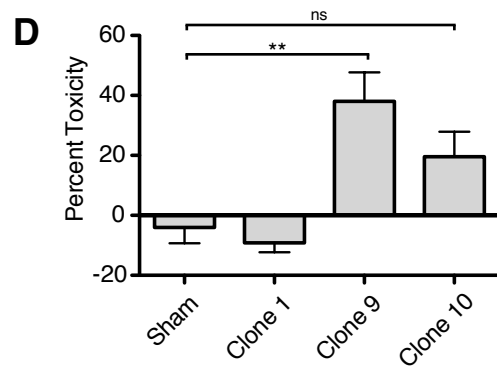
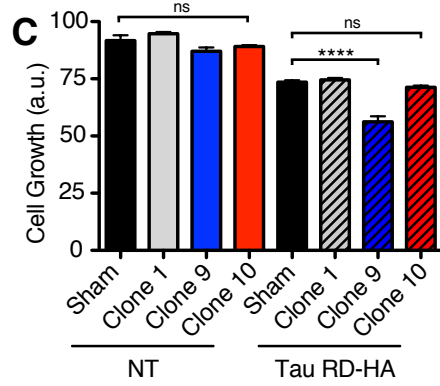
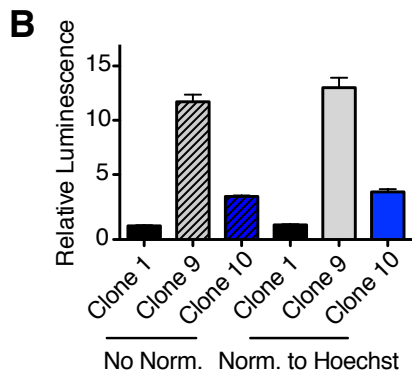
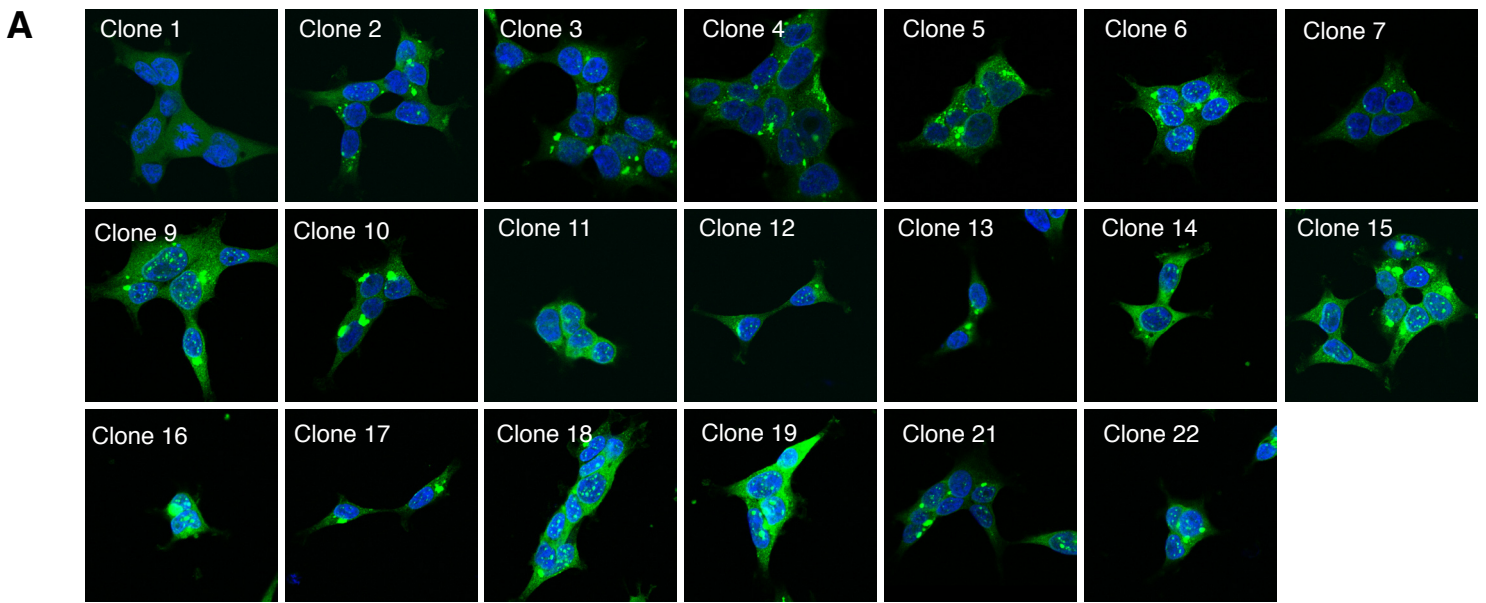


Figure S3, related to Figure 3. Templating in absence of liposomes, reversibility of aggregated phenotype, and seeding barriers between tau with different point mutations

(A) Tau RD prion strains template themselves into the inside of the cell without the use of liposomes. 30 µg of clarified Clone 9 and Clone 10 lysate were passively added to separate populations of naïve tau RD-YFP cells. Three monoclonal cell lines were isolated for each, following the protocol illustrated in **Figure 3A**. Morphologies of primary clones were recapitulated in these lines (P = passive origin).

(B) Three blots were used to construct panels in **Figure 3D** (T=total, S=supernatant, P=pellet).

(C) Clone 10 was transduced into a new monoclonal Tet Off-tau RD-YFP HEK293 cell line, and monoclonal derivatives were isolated as described in **Figure 3A**. Tau RD expression was turned off for the indicated period of time (T=days), prior to re-plating in normal media for 48 hours.

(D) Quantification of inclusion clearance (n=10 fields, each with 150+ cells, per time point). Repression of tau RD-YFP transcription for 7 days is required to revert all cells to the soluble state (error bars represent S.E.M.).

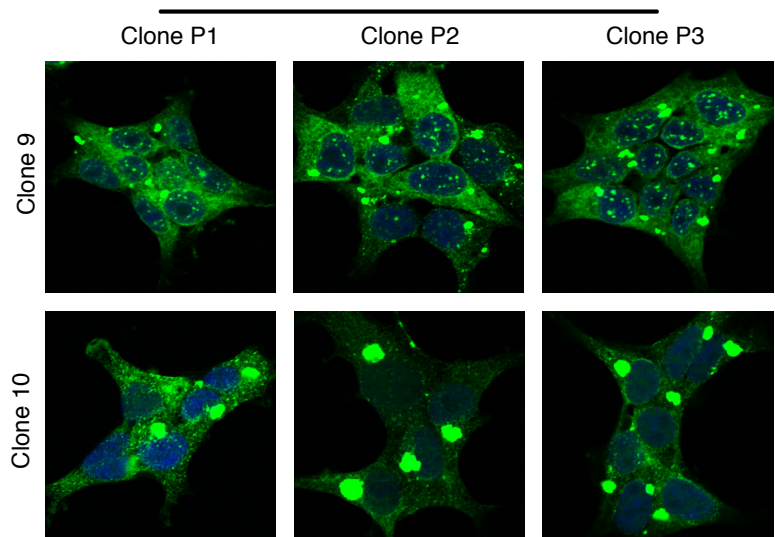
(E) Zoomed-out views of fixed and Triton X-extracted primary neurons expressing either FL tau P301S-YFP or FL tau WT-YFP reveal that tau RD strains seed mutant but not WT tau aggregation (green=YFP, red=AT8). Furthermore, Clone 9 seeds FL tau P301S more robustly than Clone 10, consistent with split-luciferase complementation data (Figure 2G).

(F) Clone 9 and 10 lysates seed the formation of phosphorylated (AT8-positive, red), detergent-resistant, untagged FL tau P301S species in primary neurons. Similar to FL tau P301S-YFP, Clone 10 inoculation results in detergent-resistant species confined primarily to the soma; Clone 9, throughout the neuron.

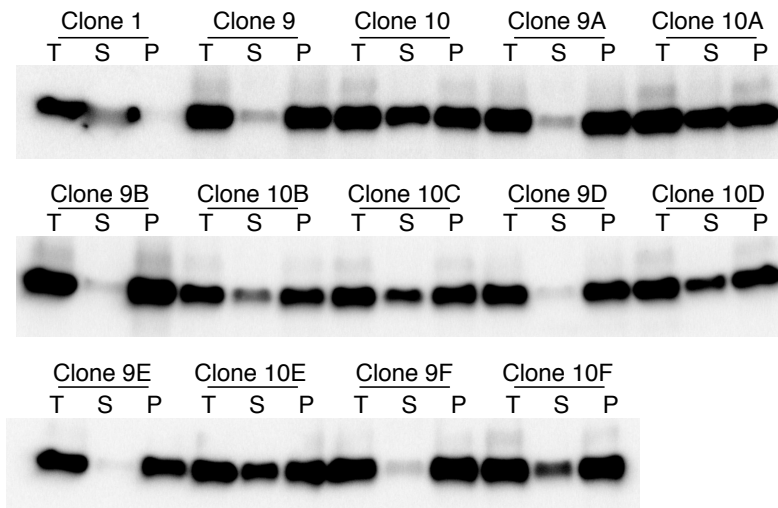
(G) Clone 9 lysate induces tangle-like insoluble tau inclusions in neuritic processes of both neurons expressing YFP-tagged and untagged versions of FL tau P301S. These structures are much less common in Clone 10-inoculated neurons (*data not shown*).

(H) Polyclonal HEK293 lines expressing different pairs of split-luciferase-tagged tau RD mutants were generated and transduced with lysate from Clones 1, 9, or 10; 1 µM recombinant tau RD fibrils; or 50 µg brain homogenate from aged tau P301S transgenic mice. Whereas all treatments besides Clone 1 seed tau RD featuring P301L, P301S, or P301L/V337M ("LM") mutations, only recombinant tau RD WT fibrils seed tau RD WT. This demonstrates that there is an asymmetric seeding barrier between tau containing and lacking P301 mutations. No treatment seeds tau RD 2P, consistent with this mutant's inability to form beta-sheet structure and amyloids. Averages of four separate experiments are shown, each read in quadruplicate 48-hours post-transduction of lysate (error bars = S.E.M).

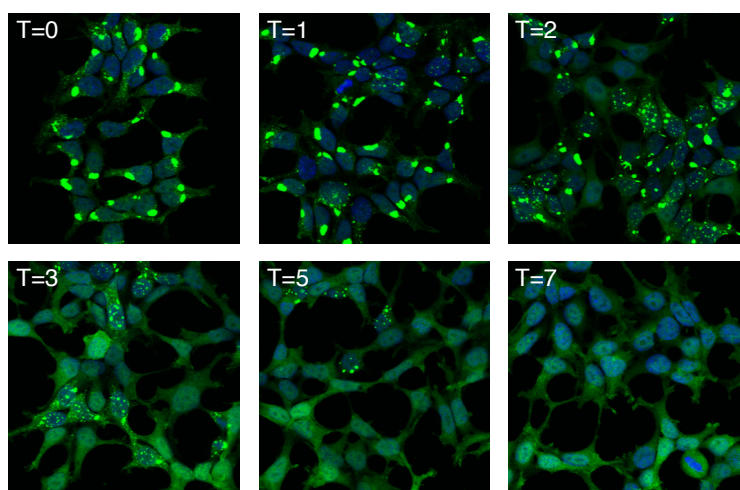
A Freshly Isolated Monoclonal Cell Line



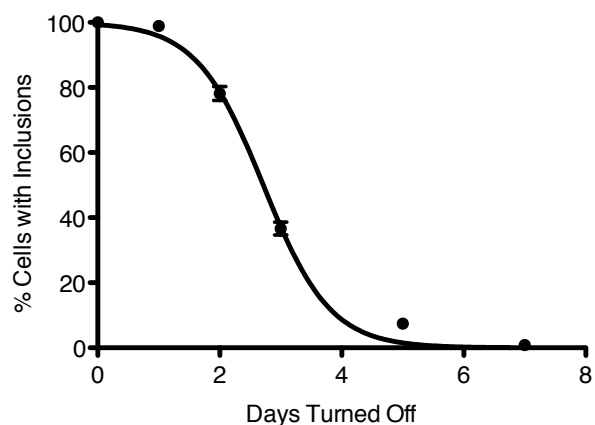
B



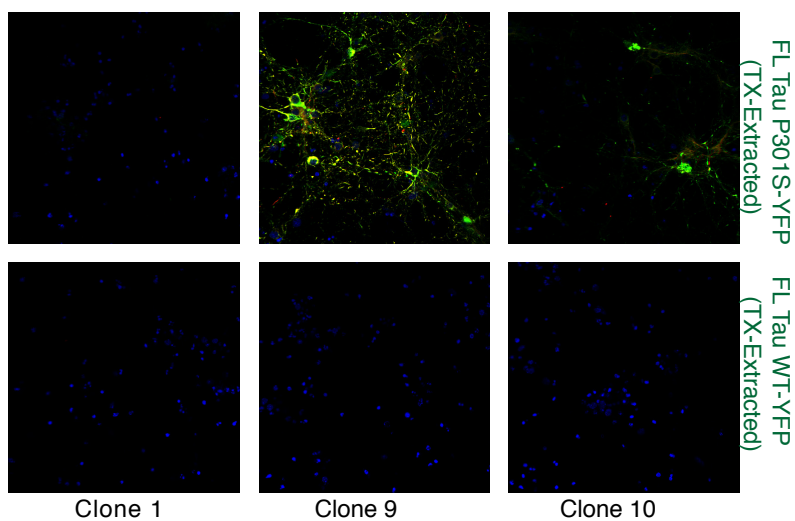
C



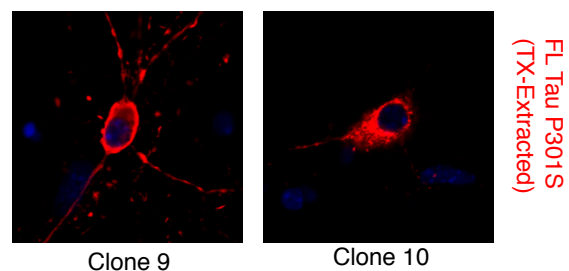
D



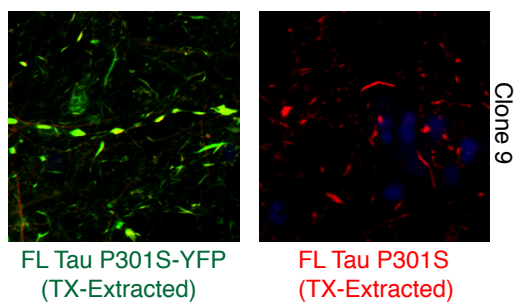
E



F



G



H

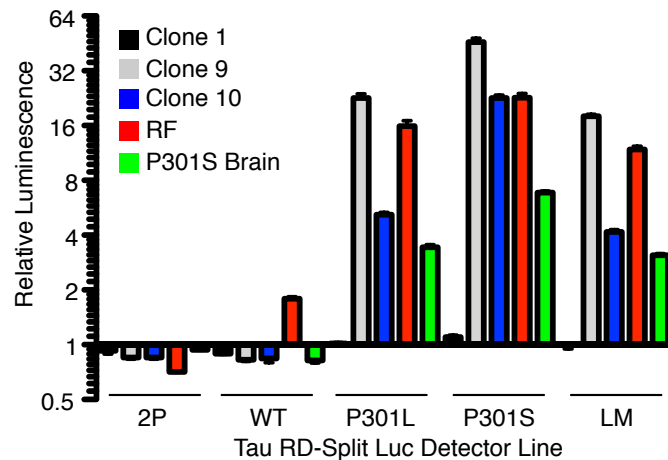


Figure S4, related to Figure 4. – Tau RD prion strains induce distinct pathologies in transgenic P301S but not WT mice

(A) Inoculated P301S mice were stained for conformationally-altered tau (MC1) or amyloid (X-34). MC1 staining corroborates morphologies of AT8-positive structures. Strong X-34 positivity is only seen in Clone 9-inoculated mice, although weak signal is seen in the CA1 region of Clone 10-inoculated animals.

(B) WT littermates were injected with Clone 1, Clone 9, or Clone 10 lysate. No induced AT8-positive pathology was evident. Representative examples are shown.

(C) Rod microglia, which are exclusive to Clone 10-inoculated P301S mice, form columns perpendicular to the cell layer of CA1.

(D) Rod microglia are absent in all cohorts of inoculated WT mice, indicating that their formation is dependent on seeding of intracellular FL tau P301S by Clone 10 aggregates.

(E) Amounts of insoluble Clone 9 and Clone 10 tau RD do not differ significantly (densitometric quantification, n=4 measurements, error bars = S.E.M.).

(F) Total tau RD does not differ between the three cell lines used to inoculate mice (densitometric quantification, n=4 measurements, error bars = S.E.M.).

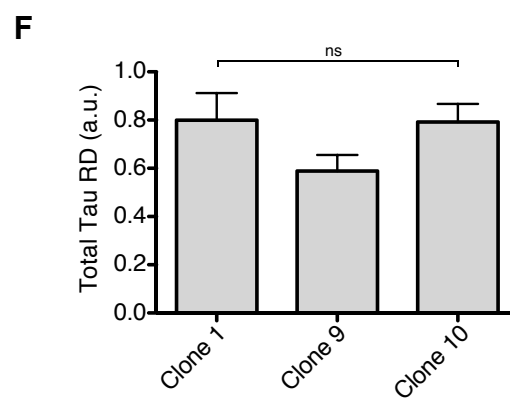
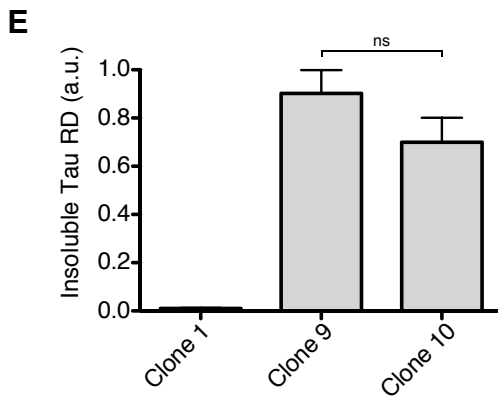
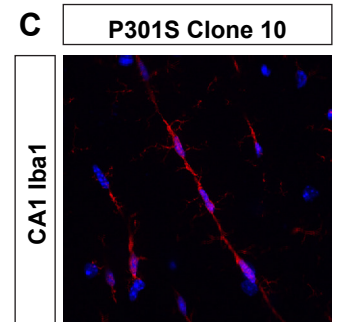
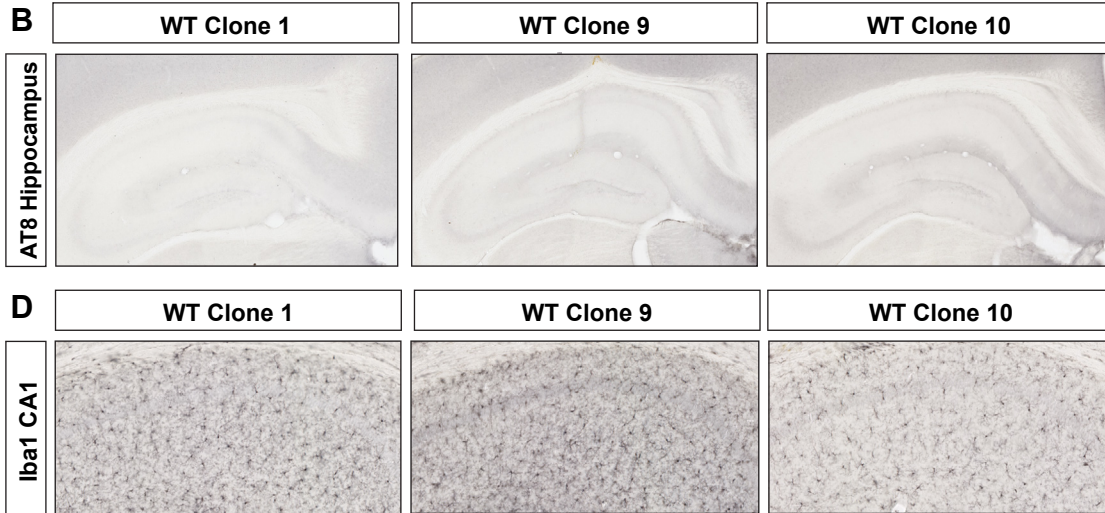
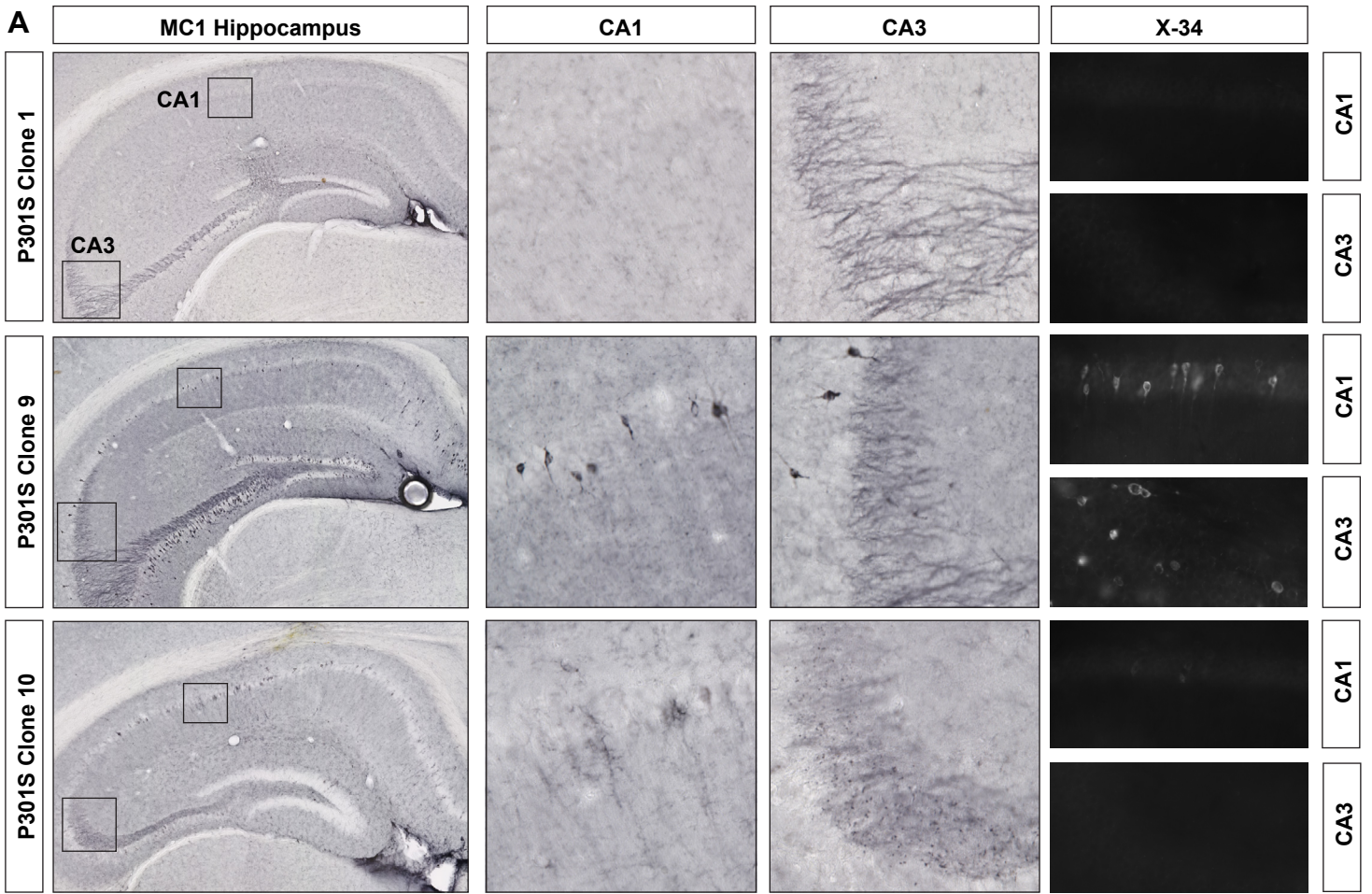


Figure S5 – Whole hippocampi used to generate images in Figure 5 and elimination of seeding following passage through non-transgenic mice

(A) Images of whole hippocampi for representative mice inoculated with indicated lysates/homogenates. Boxes indicate regions that were highlighted in **Figure 5**.

(B) AT8 immunofluorescence of CA1 and CA3 regions for serial inoculation of Clone 1.

(C) Residual tau RD-YFP seeds do not account for passage of strain phenotypes through multiple generations of mice as inoculated WT mice (Generation 0), which do not form insoluble FL tau, do not seed pathology when passaged into Generation 1 P301S mice.

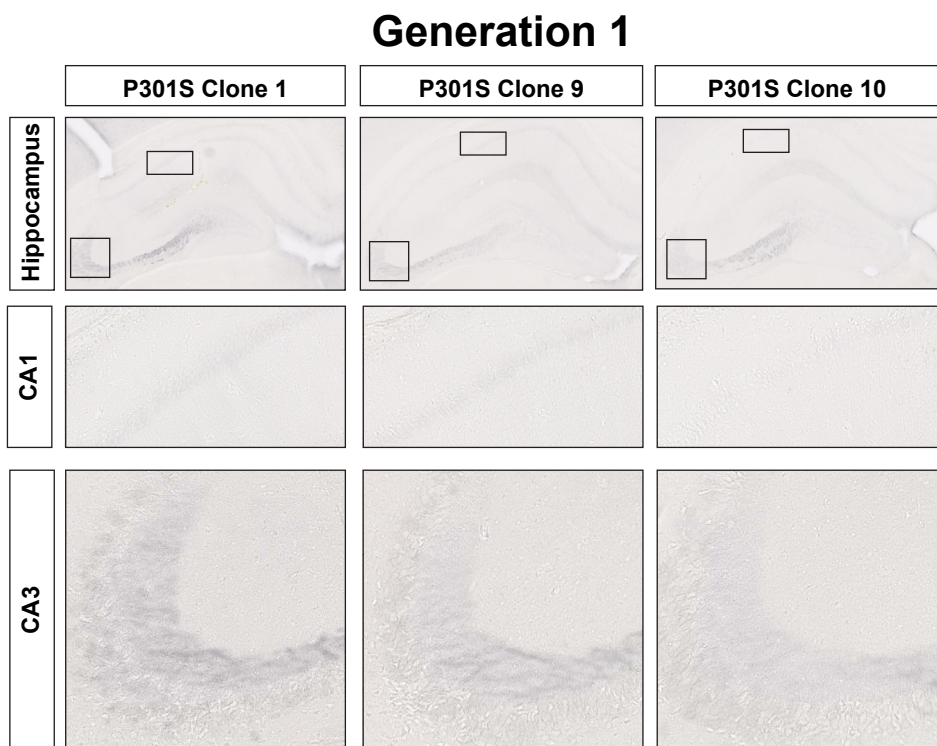
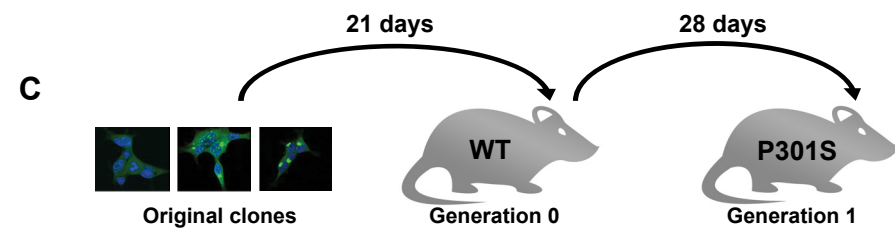
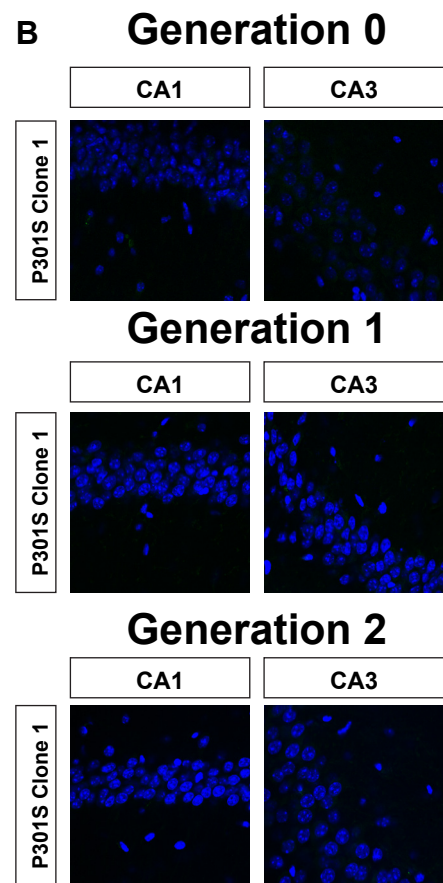
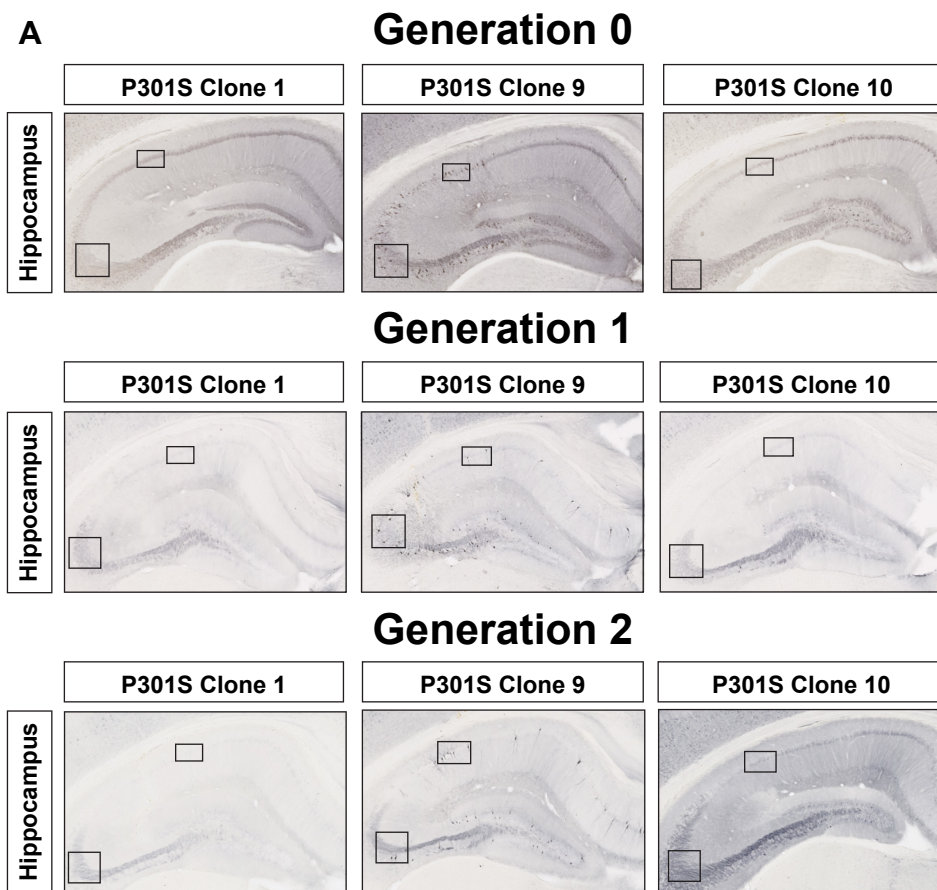


Figure S6, related to Figure 6. – Strain phenotypes are maintained in cell culture following passage through Generation 0 and Generation 2 mice

(A) Clone 9-inoculated hippocampi (G0) seed robustly relative to other homogenates based on split-luciferase complementation. FL tau was IPed from micro-dissected tau P301S and WT hippocampi inoculated 21 days prior with indicated cell lysate. IPed material from 60 µg total brain homogenate was transduced into split-luciferase cells, following the protocol outlined in **Figure 2G**. Four separate experiments were performed for each sample, each read in quadruplicate 48-hours post-transduction of lysate. Luminescence values were averaged within mouse cohorts (error bars = S.E.M., **** = $p < 0.0001$).

(B) Inclusion morphologies are maintained following passage through P301S mice. IPed FL tau from P301S mice inoculated with Clone 9 or Clone 10 was transduced into tau RD-YFP cells in a 12-well plate. 24 hours later, cells were re-plated into a 6-well plate. At confluency, cells were sparsely plated on coverslips and were given 8 days to amplify into discrete colonies. Colonies with inclusions were imaged. Representative examples are shown. Monoclonal strains were also isolated and examined with additional assays (see **Figure 6B-D**).

(C) Quantification of inclusion morphologies following passage through P301S mice. Inclusion-positive colonies were scored as either containing or lacking nuclear inclusions. 20+ colonies were scored per mouse, and percentage of each phenotype was calculated. These values were averaged within cohorts (error bars = S.E.M., **** = $p < 0.0001$).

(D) Quantification of total tau IPed from G0 mice inoculated with indicated cell lysates (densitometric quantification, $n=4$ measurements, error bars = S.E.M., * = $p < 0.05$).

(E) Split-luciferase complementation reveals that IPed tau from G2 brain seeds similarly to crude homogenate. IPed material from 60 µg brain homogenate or 60 µg crude homogenate was transduced into split-luciferase cells, following the protocol outlined in **Figure 2G**. Four separate experiments were performed for each sample, each read in quadruplicate 48-hours post-transduction of lysate (error bars = S.E.M.).

(F) Quantification of inclusion morphologies following passage from G2 mice. Inclusion-positive colonies were scored as either containing or lacking nuclear inclusions. Ten coverslips, each with 15+ inclusion-positive colonies per, were scored and averaged (error bars = S.E.M., **** = $p < 0.0001$, Student's t-test). Representative colonies are shown along with a rare instance of an inclusion-positive G2-Clone 1 colony. Monoclonal strains were also isolated and examined with additional assays (see **Figure 6F-H**).

(G) Confocal images of all 24 F2 colonies (G2-Clone 9 = 12, G2-Clone 10 = 12). All feature the same colony morphology as their parental counterpart, with the exception of 10D, which features nuclear speckles. Red boxes surround images of strains that feature a unique limited proteolysis digestion pattern and seeding ratio.

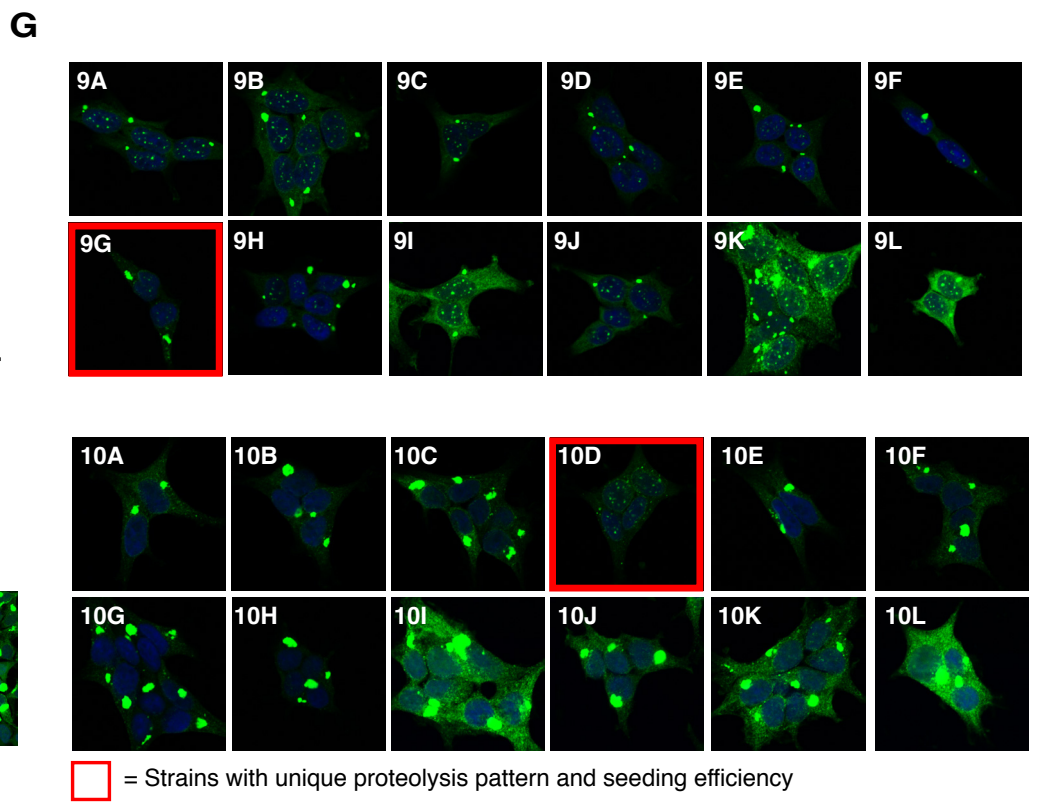
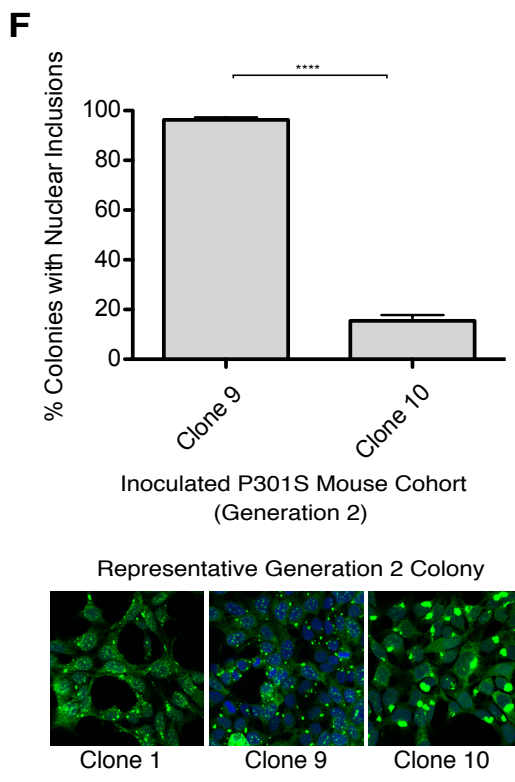
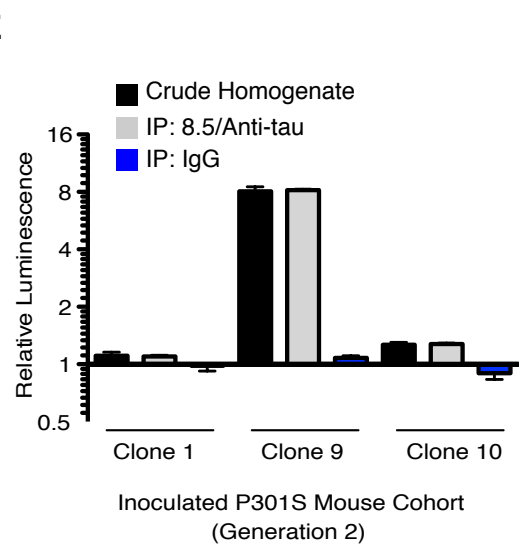
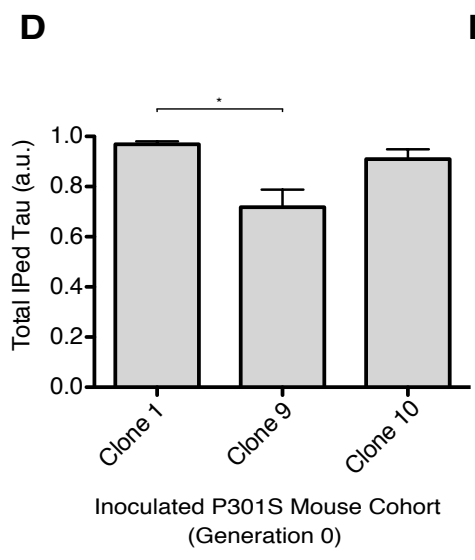
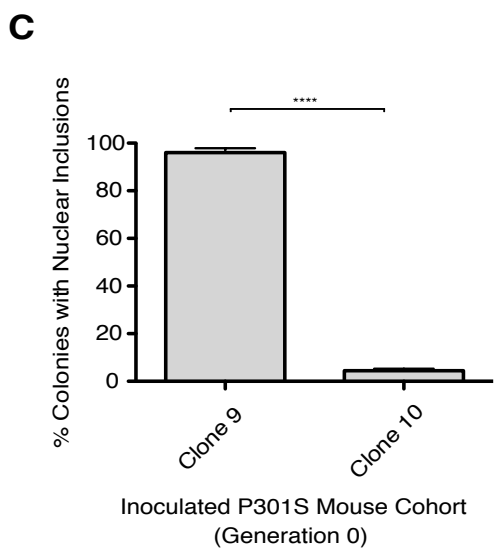
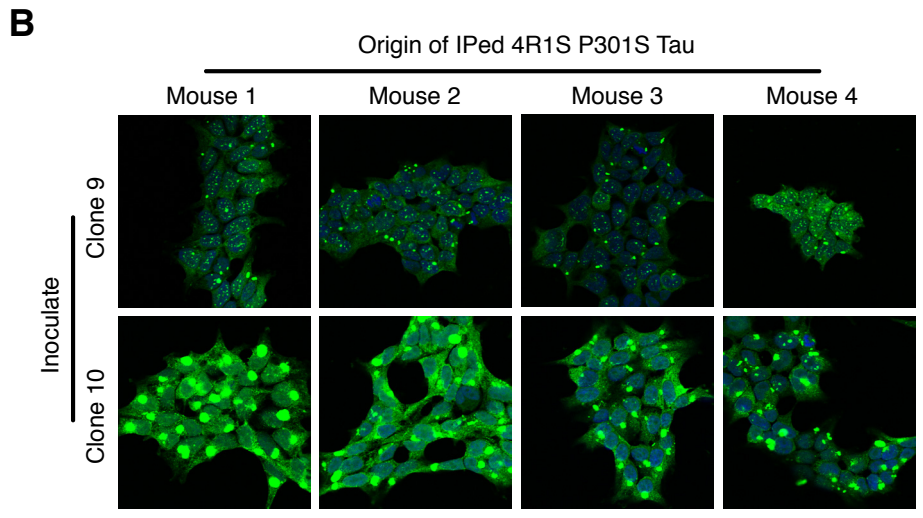
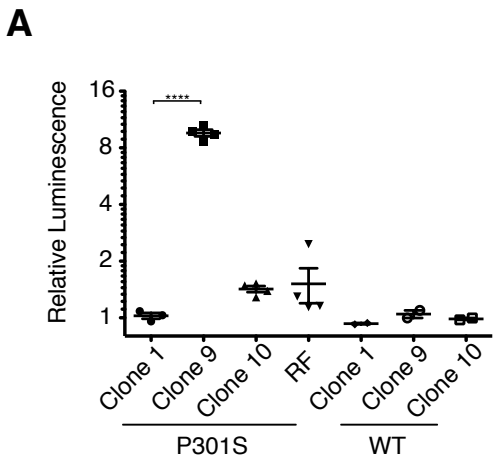
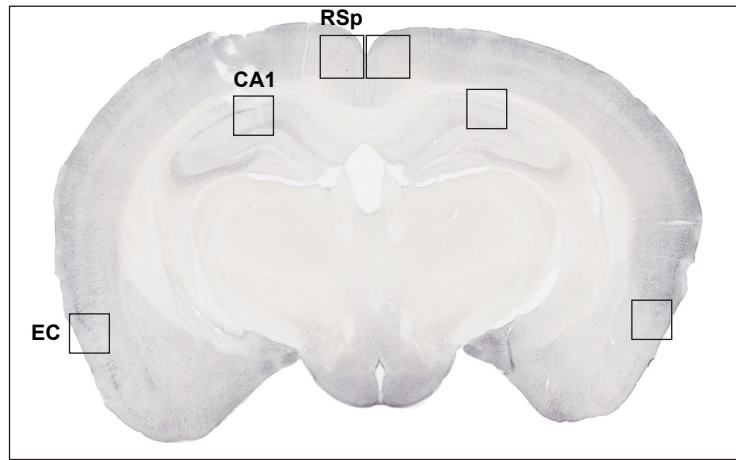


Figure S7 – Whole brain slices used in Figure 7 and additional sites of spread

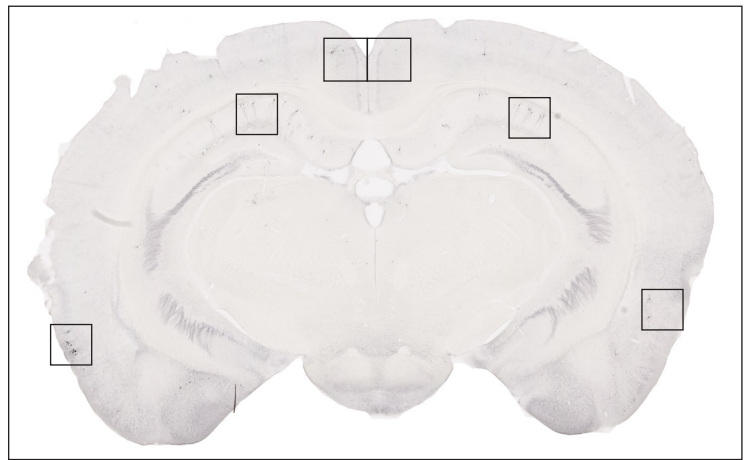
(A) Representative images of whole G3 brain slices stained with AT8. Black boxes indicate position of representative images found in **Figure 7D**; red boxes, images found in **Figure S7B**.

(B) Representative images of the subiculum and dentate gyrus (ipsilateral) of G3-Clone 1 and G3-Clone 9 mice.

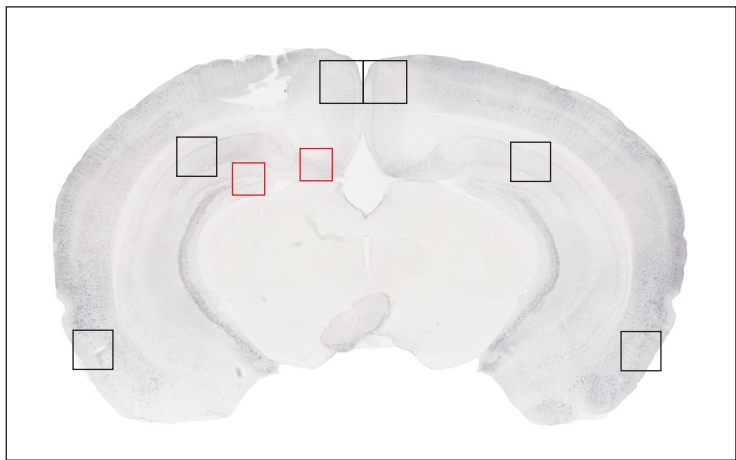
A P301S Clone 1 Rostral Hippocampus



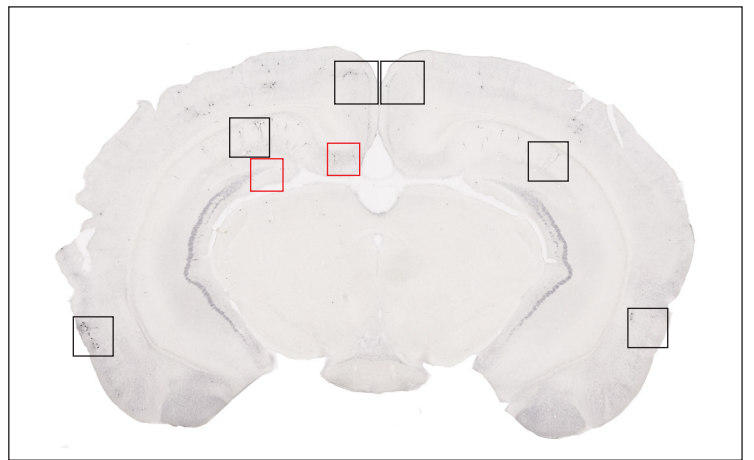
P301S Clone 9 Rostral Hippocampus



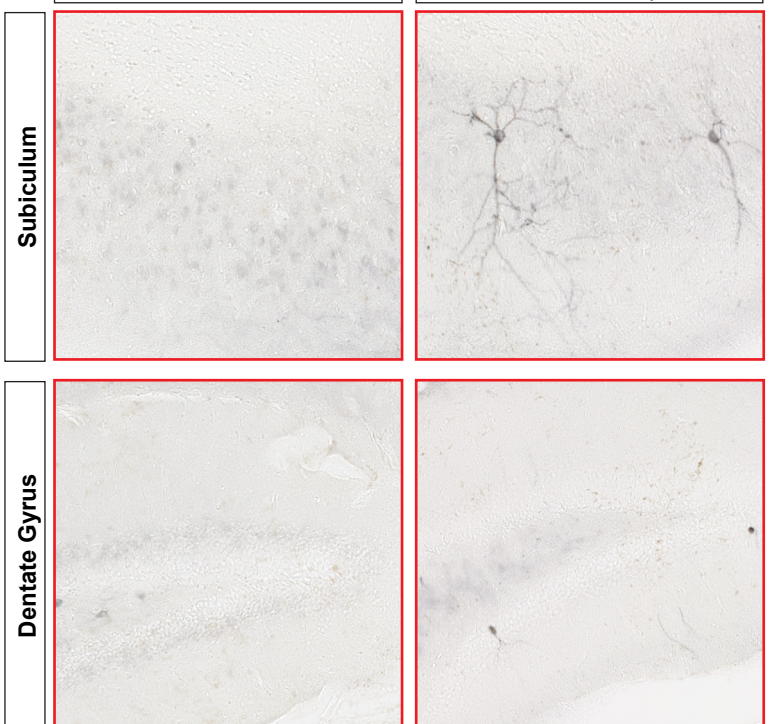
P301S Clone 1 Caudal Hippocampus



P301S Clone 9 Caudal Hippocampus



B P301S Clone 1 P301S Clone 9





 Image depicted in Figure 7
 Image depicted in Supplemental Figure 7

Figure S8, related to Figure 8. – Detailed analysis of strains derived from three human samples

- (A) 11 of 12 patient CBD clones isolated using both crude and IP induction (designated with a red *) feature the same phenotype (a wispy, disordered juxtannuclear deposition). CBD-2 is unique in having nuclear speckles.
- (B) All isolated patient AGD clones lost the aggregated state with time (arrow = inclusion-negative cells). Six representative clones are shown (crude=5, IP=1). An additional 41 clones (crude=30, immunoprecipitation=11) reverted to an inclusion-negative state at an early time point, thus having few cells with inclusions to image at Day 40 (*data not shown*). All sectoring colonies feature enormous juxtannuclear inclusions with occasional tangle-like aggregates (arrowhead).
- (C) All 3 Clone 10-derived lines in the Tet Off background feature large, juxtannuclear inclusions.
- (D) All 12 patient AD clones (8=crude, 4=IP) feature numerous speckles, both cytoplasmic and nuclear.
- (E) Sedimentation analysis was performed on three representative clones for each patient and average supernatant to total ratios (Sup/Total) were calculated for each using densitometric analysis (n=3 for each clone except Clone 1, n=6). CBD clones contain significantly more material in the pellet than AD clones as reflected by Sup/Total values averaged across clones (lower panel) (error bars represent S.E.M, * = p<0.05).
- (F) Representative AD clones seed significantly more than CBD clones. Averages of four separate experiments are shown, each read in quadruplicate 48-hours post-transduction of lysate. Seeding values were then averaged across clones (lower panel) (error bars = S.E.M, *** = p<0.001).
- (G) Lysates derived from all CBD and AD clones were separately transduced into the split-luciferase aggregation-sensor cell line and luminescence was read 48 hours later. Relative luminescence averages for all clones are shown, each measured in quadruplicate (error bars = S.E.M, **** = p<0.0001, Student's t-test).
- (H) Pronase digestion (100 µg/mL) of lysates from representative clones confirms that CBD, AD, and AGD clones are biochemically distinct from each other. AD2 is more sensitive than other clones to pronase, which suggests that its conformation might be slightly different than other AD clones.
- (I) Limited proteolysis digestion patterns are not affected by amount of insoluble tau in the digested sample. Various amounts of CBD-4 lysate were digested, spiking with non-transfected (NT) cell lysate to maintain a constant level of protein. Regardless of the quantity of CBD-4 lysate, all conditions feature a band around 8 kDa in size.

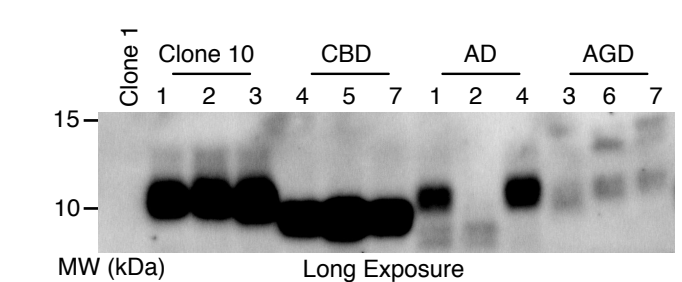
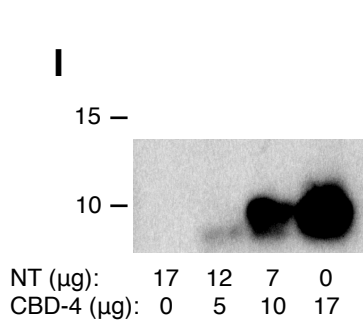
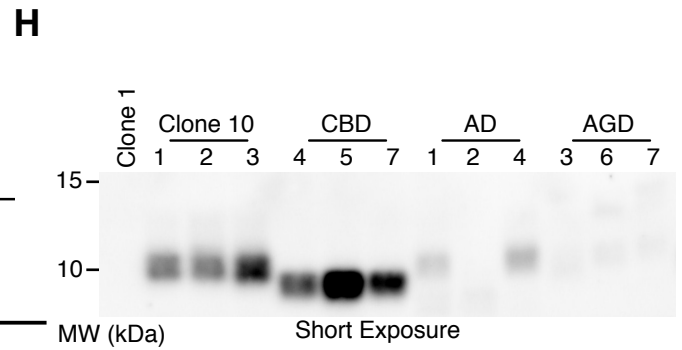
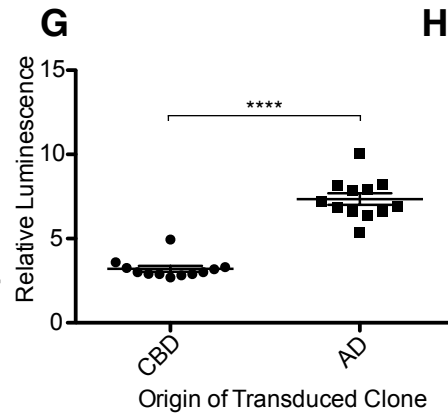
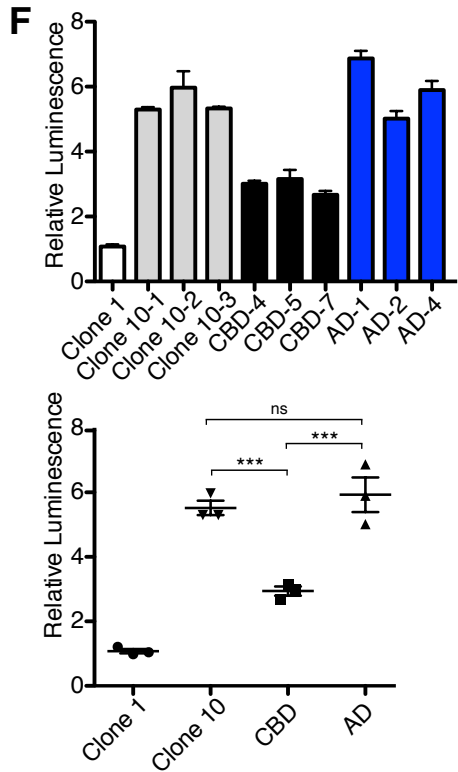
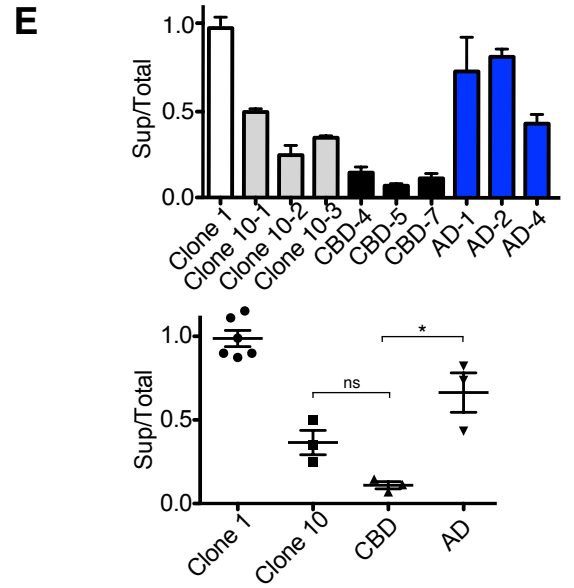
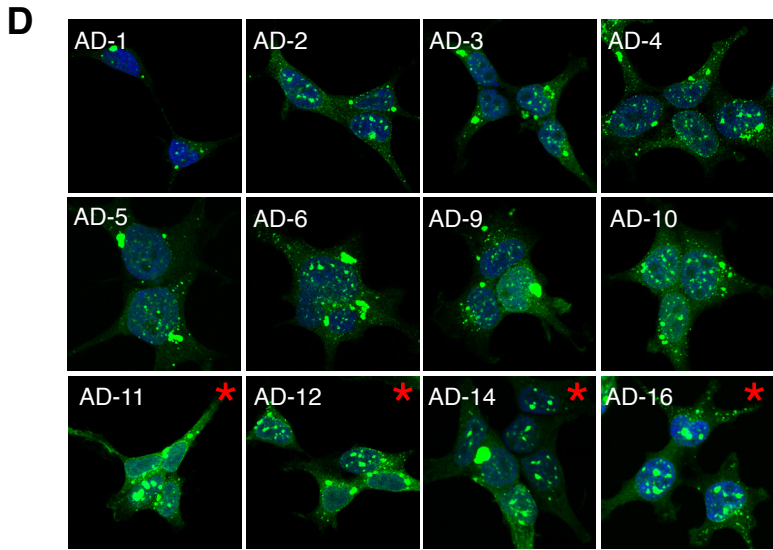
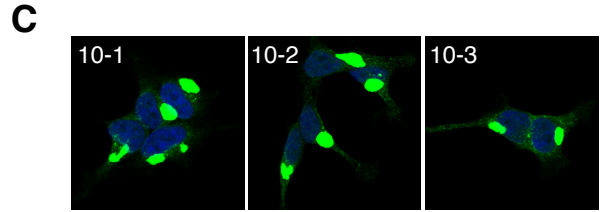
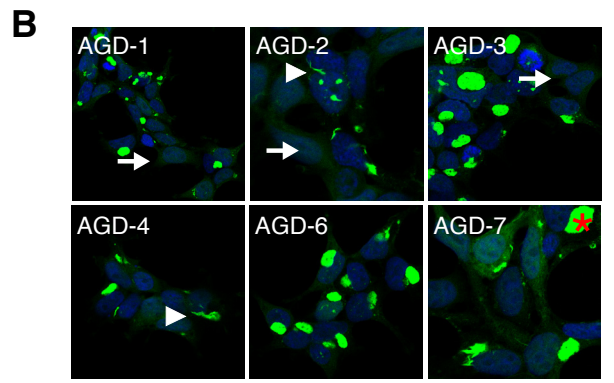
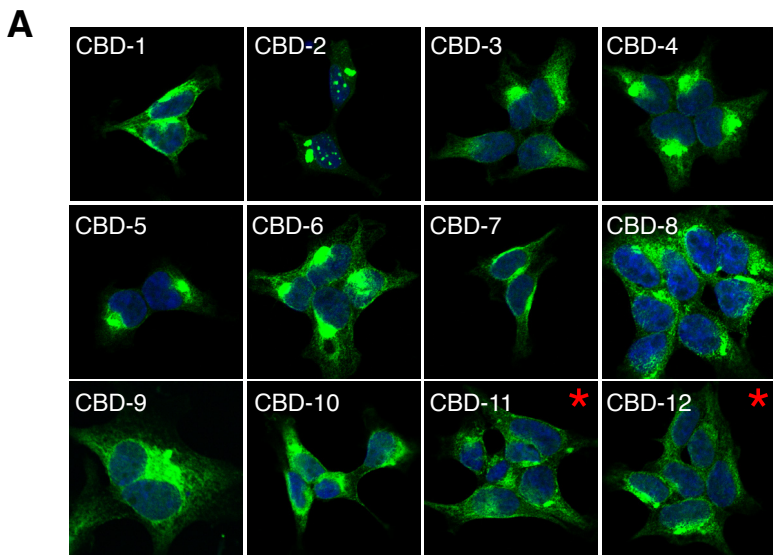


Table S1, related to Figure 4,5,7 – Characteristics of mice used in all in vivo experiments

Generation 0

Mouse	Genotype	Gender	Age (Days)	Condition
2133	P301S	m	95	Clone 1
2152	P301S	f	94	Clone 1
2153	P301S	f	94	Clone 1
2135	P301S	m	95	Clone 9
2143	P301S	m	94	Clone 9
2150	P301S	f	94	Clone 9
2170	P301S	f	90	Clone 9
2136	P301S	m	96	Clone 10
2144	P301S	m	95	Clone 10
2151	P301S	f	95	Clone 10
2171	P301S	f	91	Clone 10
2137	P301S	m	96	Recombinant fibrils
2145	P301S	m	95	Recombinant fibrils
2164	P301S	m	91	Recombinant fibrils
2138	P301S	f	96	Recombinant fibrils
2163	WT	m	90	Clone 1
2166	WT	m	90	Clone 1
2167	WT	m	90	Clone 9
2168	WT	f	90	Clone 9
2134	WT	m	95	Clone 10
2169	WT	f	90	Clone 10

Generation 1

Mouse	Genotype	Gender	Age (Days)	Condition
2535	P301S	f	66	P301S G0 Clone 1 BH
2536	P301S	f	66	P301S G0 Clone 1 BH
2537	P301S	f	66	P301S G0 Clone 1 BH
2581	P301S	f	64	P301S G0 Clone 9 BH
2580	P301S	f	64	P301S G0 Clone 9 BH
2583	P301S	f	64	P301S G0 Clone 9 BH
2584	P301S	f	64	P301S G0 Clone 9 BH
2582	P301S	f	65	P301S G0 Clone 10 BH
2558	P301S	f	65	P301S G0 Clone 10 BH
2579-2	P301S	f	64	P301S G0 Clone 10 BH
2985	P301S	f	80	WT G0 Clone 1 BH
2992	P301S	f	80	WT G0 Clone 9 BH
2993	P301S	f	80	WT G0 Clone 9 BH
2986	P301S	f	80	WT G0 Clone 10 BH
2991	P301S	f	80	WT G0 Clone 10 BH

Generation 2

Mouse	Genotype	Gender	Age (Days)	Condition
2667	P301S	f	61	P301S G1 Clone 1 BH
2668	P301S	f	61	P301S G1 Clone 1 BH
2720-5	P301S	f	55	P301S G1 Clone 1 BH
2675	P301S	f	61	P301S G1 Clone 9 BH
2678	P301S	f	61	P301S G1 Clone 9 BH
2794	P301S	f	48	P301S G1 Clone 9 BH
2767	P301S	f	51	P301S G1 Clone 9 BH
2669	P301S	f	61	P301S G1 Clone 10 BH
2670	P301S	f	61	P301S G1 Clone 10 BH
2764	P301S	f	48	P301S G1 Clone 10 BH
2795	P301S	f	51	P301S G1 Clone 10 BH

**Generation 3
(Unilateral inoculation)**

Mouse	Genotype	Gender	Age (Days)	Condition
3253	P301S	m	52	P301S G2 Clone 1 BH
3209	P301S	f	56	P301S G2 Clone 1 BH
3255	P301S	m	52	P301S G2 Clone 9 BH
3212	P301S	f	56	P301S G2 Clone 9 BH

Table S2, related to Figure 8 – Characteristics of patient material and morphological analysis of all clones isolated from patient samples

Pathology/ Brain #	Age	Sex	Location (Gyrus)	Clones Isolated	No Seeding?	Toxic?	Mosaic	Ordered	Disordered	Speckles
AD1	61	M	Mid frontal	12			0	0	0	12
AD2	93	F	Mid frontal	1			0	0	0	1
AD3	64	F	Mid frontal	10			0	0	0	10
AD4	75	F	Mid frontal	11			0	0	0	11
AD5	72	M	Mid frontal	10			0	0	1	9
AD6	80	M	Mid frontal	11			0	1	0	11
AGD1*	77	M	Inf temporal	0	x		0	0	0	0
AGD2*	82	M	Inf temporal	47			47	0	0	0
AGD3^	65	F	Inf temporal	0		x	0	0	0	0
AGD4^	72	M	Inf temporal	5			2	0	3	0
AGD5^	58	M	Inf temporal	0	x		0	0	0	0
AGD6^	66	M	Inf temporal	8			4	0	4	0
CBD1	64	M	Mid frontal	12			0	0	11	1
CBD2	69	F	Mid frontal	15			0	0	12	3
CBD3	61	M	Mid frontal	11			0	0	9	2
CBD4	57	F	Mid frontal	0		x	0	0	0	0
CBD5	63	M	Mid frontal	10			0	0	10	0
CBD6	60	M	Mid frontal	9			0	0	8	1
PiD1	57	M	Ant orbital	1			1	0	0	0
PiD2	70	M	Ant orbital	4			1	3	0	0
PiD3	58	F	Ant orbital	12			12	0	0	0
PiD4	60	F	Ant orbital	3			2	0	1	0
PiD5	71	M	Ant orbital	9			6	0	1	2
PSP1	66	M	Mid frontal	5			3	0	2	0
PSP2	84	F	Mid frontal	19			16	1	2	0
PSP3	69	M	Mid frontal	0	x		0	0	0	0
PSP4	56	F	Mid frontal	0	x		0	0	0	0
PSP5	69	F	Mid frontal	0		x	0	0	0	0
PSP6	74	M	Mid frontal	0		x	0	0	0	0
Clone1	n/a	n/a	n/a	0	x		0	0	0	0
Clone 9	n/a	n/a	n/a	0		x	0	0	0	0
Clone 10	n/a	n/a	n/a	3			0	3	0	0
Tau KO	12 mos	M	Whole brain	0	x		0	0	0	0

Bold = most common phenotype associated with tissue sample

* = patient carried a primary diagnosis of AGD

^ = patient carried a primary diagnosis of FTLD-TDP but had incidental AGD

Supplemental Experimental Procedures

Molecular cloning

The restriction endonucleases BamHI (5') and NotI (3') were used to remove YFP from the pEYFP-N1 vector (Clontech) and separately insert CBG-Cluc and CBG-Nluc, both derived from the pFRB vector (kind gift from the David Piwnica-Worms lab) (Naik and Piwnica-Worms, 2007). Tau RD (aa 244-372 of the 441 aa full-length tau 4R2N with the following variants: I277P/ Δ K280/I308P or 2P, WT, P301L, P301S, P301L/V337M or LM) was PCRed out of the pEYFP vector and placed upstream of each of the split-luciferase constructs using EcoRI (5') and KpnI (3'), thus generating p-tau RD-Cluc and p-tau RD-Nluc.

For lentiviral constructs, a backbone containing the ubiquitin C promoter IRES-Venus (FCIV FM5) (generously provided by the Jeffrey Milbrandt laboratory) (Araki et al., 2004) was modified to remove IRES-Venus by digestion with BsrGI (5') and BamHI (3'). DNA was extracted from agarose gel using Qiagen Gel Extraction Kit. Ends were blunted using DNATerminator End Repair Kit (Lucigen) and the resulting product was purified using Qiagen PCR purification Kit. The blunted product was re-ligated using T4 DNA ligase (New England Biolabs) to create a new plasmid called FM5. The following constructs were then subcloned from the pEYFP vector using NheI (5') and AscI (3'): tau RD(Δ K280/I277P/I308P) (2P)-YFP, tau RD(WT)-YFP, tau RD(Δ K280)-YFP, tau RD(P301L/V337M) (LM)-YFP, alpha synuclein(WT)-YFP, huntingtin Exon 1(Q25)-YFP, tau RD-Cluc (various mutants), tau RD-Nluc (various mutants), tau RD P301L/V337M (LM)-HA, full-length tau 4R1N P301S, full-length tau 4R1N P301S-YFP, full-length tau 4R1N WT, full-length tau 4R1N WT-YFP.

To create a plasmid expressing tau RD(LM)-YFP under the TRE (tetracycline response elements) promoter, tTA was subcloned into FM5 using AgeI (5') and EcoRI (3') to generate FM5-Ub-tTA. The TRE-Tight promoter was then PCRed using PacI (5') and NheI/BsrGI/PacI (3'). PacI digestion was then used to subclone the PCR product into FM5-tTA and sequencing confirmed proper orientation, thus generating the FM5-TRE-Ub-tTA plasmid (FM5 Tet Off).

Finally, NheI (5') and BsrGI (3') were used to subclone tau RD(LM)-YFP into FM5-TRE-Ub-tTA to generate FM5 Tet Off-tau RD(LM)-YFP. All restriction endonucleases were obtained from New England Biolabs.

Protein purification and fibrillization

Amyloid beta (1-42) fibrils were a generous gift from the John Cirrito laboratory: peptide was synthesized by Pepnome and monomer was re-suspended in HFIP, which was subsequently evaporated away under nitrogen gas. The resulting monomer was resuspended at 5 mM in DMSO prior to dilution to 100 μ M in 10 mM HCl/150 mM NaCl. Fibrils were prepared by incubating at 37°C for 24 hours. They were then stored at -20°C until use.

Synthetic huntingtin exon1 N17-Q35 peptide was synthesized at the Keck Biotechnology Resource Laboratory of Yale University. Peptide was solubilized in formic acid prior to being dialyzed into phosphate buffer solution. Re-solubilized monomer was fibrillized at room temperature at a concentration of 100 μ M for 24 hours. Resulting fibrils were stored at -20°C until use.

α -synuclein fibrils were a generous gift from the Paul Kotzbauer laboratory. Recombinant α -synuclein WT protein was produced in *E. coli* using previously published methods (Giasson et al., 2003; Huang et al., 2005): the purified protein was then dialyzed overnight in 10 mM Tris-HCl (pH=7.6)/1 mM DTT/50 mM NaCl. Recombinant monomer at a concentration of 2 mg/mL was then incubated with 100 mM NaCl and 20 mM Tris-HCl (pH=8.0) at 37°C for 72 hours with shaking (Eppendorf Thermomixer, 1000 rpm) to induce fibrillization. The fibril mixture was then centrifuged at 15,000xg for 15 minutes to separate fibrils (pellet) from monomer (supernatant). Following manufacturer's protocol, the concentration of α -synuclein in the supernatant was calculated using a BCA protein assay. The decrease in protein in the supernatant following centrifugation was used to calculate the monomer-equivalent concentration of α -synuclein in the pellet (fibrils). Fibrils were stored at a concentration of 80 μ M at -20°C until use.

Recombinant tau RD-HA monomer was prepared as previously described (Frost et al., 2009; Goedert and Jakes, 1990) by expressing pRK172-Tau RD-HA in Rosetta (DE3)pLacI competent cells (Novagen). Monomer was lyophilized and stored at -80°C as single-use aliquots. Monomer was re-suspended in 25 mM DTT for one hour. The reduced protein was then fibrillized at a final concentration of 8 µM in 2.5 mM DTT/10 mM HEPES (pH=7.4)/100 mM NaCl/8 µM heparin (tau buffer) at 37°C without agitation. Fibrils were stored at a concentration of 8 µM at -20°C until use.

Cell culture

HEK293 and HEK293T cell lines were all grown in Dulbecco's modified Eagle's medium (Gibco) supplemented with 10% fetal bovine serum (HyClone), 1% penicillin/streptomycin (Gibco), and 1% glutamax (Gibco). Cell lines were maintained and passaged in 10 cm dishes at 37°C, 5% CO₂, in a humidified incubator.

Lentivirus production

Lentivirus was prepared as described previously (Araki et al., 2004): HEK293T cells were plated at a concentration of 1×10^6 cells/well in a 6-well plate. 18 hours later, cells were transiently co-transfected with PSP (1200 ng), VSV-G (400 ng), and FM5 (400 ng) plasmids using 6 µL FuGene HD (Promega). 72 hours later, conditioned media was harvested and centrifuged at 1000xg for 5 minutes to remove dead cells and debris. Supernatant was stored at -80°C until use. For primary neuron transduction, lentivirus was concentrated 10x using lenti-X concentrator (Clontech) with the concentrated pellet being re-suspended in PBS with 25 mM HEPES, pH 7.4.

Stable HEK293 cell line generation

HEK293 cells were plated at a concentration of 100,000 cells/well in wells of a 6-well plate. 18 hours later, 1 mL of media was removed and replaced with 1.5 mL conditioned media containing lentivirus. For the split-luciferase aggregation reporter line, cells were co-transduced with 750 μ L of tau RD-Cluc and 750 μ L tau RD-Nluc lentivirus. These amounts were used for all mutant tau RD split-luciferase pair lines with lentivirus being made in the same batch to ensure roughly equivalent viral titers. For all stable lines, cells were given 5 days to amplify to confluency in the presence of virus. At this point, cells were re-plated in a 10 cm dish and were grown to confluency. For cell lines featuring protein with a fluorescent tag, epifluorescence microscopy was used to confirm that all cells were expressing fluorescent protein. Polyclonal cell lines were then stored in liquid nitrogen until use.

To generate monoclonal lines, polyclonal cell populations were diluted sparsely in 10 cm dishes. Colonies were given 9 days to amplify, at which point cloning cylinders (Bel-Art Products) were used to isolate single colonies. Monoclonal cultures were serially amplified to confluency using 12-well then 6-well then 10 cm dishes. Resulting monoclonal lines were frozen in liquid nitrogen until use.

Liposome-mediated transduction of amyloids into HEK293 cells

A previously used fibril-transduction protocol (Nekooki-Machida et al., 2009) was used with minor modifications: polyclonal HEK293 cells stably expressing either tau RD Δ K280/I277P/I308P(2P)-YFP, tau RD(WT)-YFP, tau RD(Δ K280)-YFP, tau RD P301L/V337M(LM)-YFP, α -synuclein(WT)-YFP, huntingtin exon 1(Q25)-YFP, FL tau 4R1N P301S-YFP, or FL tau 4R1N P301S were plated at 250,000 cells/well in 12-well plates. Tau buffer (2.5 mM DTT/10 mM HEPES (pH=7.4)/100 mM NaCl/8 μ M heparin) or indicated fibrils were then combined with OptiMEM (Gibco) to a final volume of 100 μ L. 96 μ L OptiMEM and 4 μ L lipofectamine-2000 (Invitrogen) was then added to the OptiMEM mixture to a final volume of 200 μ L. After a 20-minute incubation, liposome preparations were added to cells so that fibrils

were at the following final concentrations: tau RD (400 nM), α -synuclein (400 nM), amyloid beta (1-42) (1 μ M), huntingtin exon 1 N17(Q35) (1 μ M), or tau buffer (400 nM tau fibril equivalent). 18 hours later, cells were washed, trypsinized, and re-plated in wells of a 6-well plate. Once confluent, cells were plated on coverslips (thickness = 0.09 to 0.12 mm; Carolina Biologicals) for imaging and quantification (time = Day 6). For transductions involving FL tau, fixed cells were stained with AT8 (see immunocytochemistry methods).

Quantification of percent cells positive for inclusions

For inclusion-elimination time course experiments, cells were passaged every two days for 50 days, plating cells for fixation on every other passage. Cells were fixed by incubating with 4% PFA in PBS for 15 minutes. Coverslips were washed twice and stained with DAPI (1:3000 dilution from 1 mg/mL stock) for 5 minutes. Coverslips were mounted on Prolong Gold Antifade Reagent (Invitrogen), sealed with nail polish, and placed at 4°C prior to analysis. To quantify percent cells positive for inclusions, a total of 10 fields, each with 150+ cells, were analyzed per condition. The number of cells per field was determined by counting the number of DAPI-positive nuclei. Then, cells with inclusions were counted and a percentage was calculated. Mean and standard error were subsequently determined and plotted.

Isolation of monoclonal tau prion strains induced by recombinant tau RD fibrils

A monoclonal HEK293 cell line stably expressing tau RD(LM)-YFP was generated. Cells were plated at 240,000 cells/well in a 12-well plate. 24 hours later, 400 nM tau RD-HA fibrils were transduced using lipofectamine-2000 (Invitrogen) as previously described. 18 hours later, cells were washed, trypsinized, and re-plated in a 6-well plate. At confluency (Day 3), cells were diluted sparsely in 10 cm dishes so that there were less than 100 cells per dish. Cells were given 9 days to amplify into colonies. At Day 12, epifluorescence microscopy was used to mark colonies featuring cells with inclusions. Cloning cylinders (Bel-Art Products) were used to

isolate single clones, which were subsequently serially amplified to confluency in 12-well, then 6-well, and 10 cm dishes. At Day 30, cells were either plated on coverslips for fixation and confocal analysis or were frozen down in single-use pellets at -80°C for later analysis.

Confocal analysis

All confocal microscopy was performed using a Zeiss LSM 5 PASCAL system coupled to a Zeiss Axiovert 200M microscope. A pinhole size of 0.8 μm was used for the collection of all images. Images were processed minimally using ImageJ. When post-hoc processing was performed, the same modifications were made across all images collected for a single experiment.

Semi-denaturing detergent agarose gel electrophoresis (SDD-AGE)

SDD-AGE was performed as previously described (Kryndushkin et al., 2003) with minor modifications. Cell pellets were thawed on ice, lysed by triturating in PBS containing 0.05% Triton-X and a cOmplete mini protease inhibitor tablet (Roche), and clarified by 5-minute sequential centrifugations at 500xg and 1000xg. Low-SDS 1.5% agarose gels were prepared by dissolving agarose in buffer G (20 mM Tris-Base, 200 mM glycine, in ddH₂O) with 0.02% SDS. For each condition, 5 μg of clarified cell lysate was incubated with 0.02% SDS sample buffer for 7 minutes prior to loading. SDD-AGE was ran in Laemmli buffer (Buffer G with 0.1% SDS) at 125 V for 90 minutes or until dye front reached the bottom of the gel. Protein was transferred at 100 V for 90 minutes at 4°C to Immobilon P (Millipore) using a custom-modified SDS-PAGE transfer cassette (Bio-Rad) for accommodation of the thick agarose gel. Membranes were probed for tau RD using rabbit polyclonal anti-tau ab64193 (1:4000, AbCam) overnight, washed four times with TBS-T, counter-probed with goat anti-rabbit HRP (1:4000, Jackson Immunotherapy) for 1.5 hours, and were washed an additional 4 times. Finally, membranes

were imaged by exposure to ECL Prime Western Blotting Detection System (Fisher Scientific) for 3 minutes and development using a digital Syngene imager.

Sedimentation analysis and densitometry

Clarified cell lysate was prepared as described above (see SDD-AGE). 10% of the lysate was set aside as the total fraction; the rest was centrifuged at 100,000xg for 1 hour. The supernatant was placed aside and the pellet was washed with 1.5 mL PBS prior to ultracentrifugation at 100,000xg for 30 minutes. The supernatant/wash was aspirated and the pellet was re-suspended in RIPA buffer with 4% SDS and 100 mM DTT with the aid of boiling. Bradford assay (Bio-Rad) with BSA standard curve was used to normalize all protein concentrations with additional 0.05% Triton-X in PBS being used for dilution. 1 µg of total protein was loaded per well on a 4-15% SDS-PAGE gel (Bio-Rad). For all samples besides the negative control (Clone 1), supernatant was loaded at a 3:1 ratio relative to pellet and total fractions; for Clone 1, a 1:1 ratio was used. Gels were ran at 120 V for 60 minutes and protein was transferred to Immobilon P (Millipore) using a semi-dry transfer apparatus (Bio-Rad). Membranes were blocked for an hour with 5% milk, probed with rabbit polyclonal anti-tau ab64193 (1:4000, AbCam) overnight, washed four times with TBS-T, counter-probed with goat anti-rabbit HRP (1:4000, Jackson Immunotherapy) for 1.5 hours, and were washed an additional 4 times. Finally, membranes were imaged by exposure to ECL Prime Western Blotting Detection System (Fisher Scientific) for 3 minutes and development using a digital Syngene imager. Densitometric units were calculated using Syngene GeneTools software with manual band quantification, normalizing against background. Units were then corrected for loading ratios. For calculating densitometric ratios, blots were performed in triplicate and statistical analysis was performed using one-way analysis of variance with Bonferroni's multiple comparison test.

Split-luciferase complementation assay

Polyclonal HEK293 cells stably expressing tau RD(LM)-Cluc and tau RD(LM)-Nluc were plated at 240,000 cells/well in 12-well plates 24-hours prior to cell lysate transduction. Clarified cell lysate was prepared as previously described (see SDD-AGE) and was normalized to final protein concentrations of 2 $\mu\text{g}/\mu\text{L}$ using PBS with 0.05% Triton-X to dilute. 20 μg (10 μL) of each cell lysate was diluted with 90 μL OptiMEM (Gibco) and incubated with 96 μL OptiMEM and 4 μL lipofectamine-2000 (Invitrogen) for 20 minutes. Liposome preparations were then added to cells (each condition performed in quadruplicate) and 18 hours later, cells were washed, trypsinized, and re-plated in quadruplicate in a 96-well plate. 24 hours later, media was aspirated from wells and replaced with luciferin solution (150 $\mu\text{g}/\text{mL}$ D-luciferin potassium salt, Gold Biosciences, in Dulbecco's phosphate-buffer saline, Gibco). Cells were incubated with luciferin solution for 3 minutes at 37°C prior to reading luminescence with a TecanM1000 fluorescence plate reader. Luminescence reads were first averaged across technical replicates (n=4) and subsequently averaged across biological replicates (n=4 experiments unless otherwise noted) to determine standard errors of the mean. One-way analysis of variance with Bonferroni's multiple comparison test was used for statistical analysis. For cross-seeding experiments, the same protocol was used with minor exceptions: different stable split-luciferase cell lines were used; recombinant tau RD-HA fibrils were transduced at a concentration of 1 μM ; 50 μg of aged transgenic P301S brain (age=12 months) was transduced .

Protease digestion

Pronase (Roche) was diluted in PBS to a final concentration of 1 mg/mL and single-use aliquots were stored at -80°C. Clarified cell lysate was prepared as previously described (see SDD-AGE) and protein concentrations were normalized to 1.7 $\mu\text{g}/\mu\text{L}$, unless otherwise noted. 17 μg (10 μL) of cell lysate was added to 10 μL of pronase at a concentration of 100 $\mu\text{g}/\text{mL}$ (diluted in PBS) for a final volume of 20 μL and a final pronase concentration of 50 $\mu\text{g}/\text{mL}$. Cell

lysates were digested at 37°C for one hour. Reactions were quenched by addition of 20 µL 2x sample buffer (final SDS concentration of 1%) and boiling for 5 minutes. 15 µL of each sample was loaded onto a 10% Bis-Tris NuPAGE gel (Novex by Life Technologies) and were ran at 150 V for 65 minutes. Protein was transferred to Immobilon P (Millipore) using a semi-dry transfer apparatus (Bio-Rad) and membranes were probed for tau RD as described above.

X-34 staining of amyloids

To visualize amyloids, cells were stained with X-34, a derivative of Congo Red (Styren et al., 2000): Cells were fixed with 4% PFA in PBS for 15 minutes, washed twice with PBS, and permeabilized with 0.25% Triton-X/PBS for 30 minutes. They were then incubated with 1 µM X-34 (generous gift from the John Cirrito lab) in X-34 staining buffer (60% PBS/39% ethanol/0.02 M NaOH) for 15 minutes. Stained cells were rinsed briefly with staining buffer 3x followed by two 5-minute washes with PBS. Coverslips were mounted on Prolong Gold Antifade Reagent (Invitrogen), sealed with nail polish, and placed at 4°C prior to analysis.

Toxicity assays

To assess relative toxicity of Clone 9 and Clone 10 amyloids, cell growth propensity when lacking or containing tau RD inclusions was examined. Monoclonal HEK293 cells stably expressing tau RD(LM)-YFP were plated at 240,000 cells/well in a 12-well plate. 24 hours later, cells were transduced with 20 µg clarified cell lysate (Clone 9, Clone 10). 18 hours later, transduced cells were re-plated in a 6-well dish and grown to confluency. On Day 3, cells were plated sparsely on coverslips and were given 6 days to amplify into colonies. On Day 9, cells were fixed with 4% PFA and DAPI stained. For each condition, 80 inclusion-positive and 80 inclusion-negative colonies were quantified by size (number of DAPI-stained nuclei per colony). Average colony size was plotted and one-way analysis of variance with Bonferroni's multiple comparison test was used to assess statistical significance.

Concurrently, at Day 3, Clone 1-, Clone 9- and Clone 10-transduced cells were passaged onto either coverslips or into a new 6-well plate. Every three days, cells were passaged, with cells being fixed and DAPI-stained at Days 4, 17, and 30. Percent cells positive for inclusions at each time point were quantified and plotted as previously described. One-way analysis of variance with Bonferroni's multiple comparison test was used to assess statistical significance.

For LDH and cell growth toxicity experiments, a polyclonal HEK293 cell line stably expressing tau RD(LM)-HA was generated and transduced with 20 µg clarified cell lysate (Clone 1, Clone 9, Clone 10) or sham treatment in 12-well plates (quadruplicate). 18 hours later, each biological replicate was re-plated at 1:100 dilution in 100 µL total volume in technical quadruplicates in 96-well plates. 72 hours later, confluency was assessed with a Hoechst stain. Media was removed and transferred to new 96-well plates and LDH assay (Roche) was performed according to manufacturer's protocol. One-way analysis of variance with Bonferroni's multiple comparison test was used to assess statistical significance.

Preparation of cells for ultrastructural analysis by transmission electron microscopy

Cells were pelleted at 15,000 rpm for 5 minutes and fixed in 2.5% glutaraldehyde in 0.1 M mono/disodium phosphate buffer, pH 7.4, for 1 hour at room temperature and then at 4°C on a rotator overnight. After buffer rinsing, the pellets were then post-fixed in 1% (w/v) osmium tetroxide in 0.1 M mono/disodium phosphate buffer, pH 7.4, for 2 hours at room temperature before being rinsed in distilled water and then dehydrated in an ethanol series. After 2x20 min in propylene oxide and infiltrating overnight in 1:1 propylene oxide:TAAB low viscosity resin (TAAB Laboratories Ltd., Aldermaston, UK), the pellets were further infiltrated in resin over several days, with several resin changes, before polymerizing at 60°C for 16 hours. The pellets were then sectioned and stained with 0.5% (w/v) aqueous, 0.22 mm-filtered uranyl acetate at room temperature for 1 hour.

Preparation of cells for immunogold labelling

Cells were spun at 15,000 rpm and pellets were fixed in fixed in 4% formaldehyde/0.1% glutaraldehyde in 0.1 M mono/disodium phosphate, pH 7.4, for one hour at room temperature and then at 4°C on a rotator overnight. The following procedures were all carried out at 4°C: the fixed pellets were washed in 0.1 M mono/disodium phosphate and dehydrated in an ethanol series, followed by 2:1, then 1:2 100% ethanol/Unicryl resin (British BioCell International, Cardiff, UK) for 30 minutes each. Finally, the pellets were infiltrated in complete Unicryl resin, with several changes over a few days, and light-polymerized as previously described (Thorpe, 1999).

Immunogold labelling

Thin sections were cut and collected upon TEM support grids and then blocked for 30 minutes at room temperature in normal goat serum (1:10 dilution in PBS+ (PBS, pH 8.2, modified by the addition of 1% BSA, 500 µL/L Tween-20, 10 mM Na-EDTA, and 0.2 g/L sodium azide)). They were then left in the primary antibody, HJ 9.3 mouse monoclonal (10 mg/ml), overnight at 4°C. The following day, the grids were given three rinses in 1 mL PBS+ for 2 minutes each and then placed into the secondary antibody, 10 nm gold particle-conjugated goat anti-mouse IgG (1:10 dilution in PBS+) for one hour and then rinsed in PBS+ three times for 10 minutes each, followed by four rinses in distilled water for 5 minutes each. Finally, subsequent to drying, the grids were stained in 0.5% (w/v) aqueous, 0.22 µm-filtered uranyl acetate for 1 hour.

Imaging by transmission electron microscopy

Grids were examined using a Hitachi-7100 transmission electron microscope operated at 100 kV. Digital images were captured via an axially mounted (2000x2000 pixel) Gatan

Ultrascan 1000 charge-coupled device camera (Gatan, Abingdon, UK) and subsequently examined using ImageJ software.

Immunocytochemistry

HEK293 cells were fixed in 4% PFA (Vimentin and AT8 stains) or 100% ice-cold methanol (γ -tubulin and PML stains) for 15 minutes followed by permeabilization with 0.25% Triton X-100 for 30 minutes. Coverslips were then blocked in blocking solution (10% fetal goat serum, 25 mg/mL BSA, 0.25% Triton X-100, PBS) for one hour at room temperature. For primary stains, coverslips were exposed to one of the following in blocking buffer overnight at 4°C: mouse monoclonal anti-vimentin V9 (1:50, Santa Cruz), mouse monoclonal anti-phospho-tau AT8 (1:400, ThermoScientific), mouse monoclonal anti- γ -tubulin GTU-88 (1:2500, Sigma Aldrich), or mouse monoclonal anti-PML PG-M3 (1:100, Santa Cruz). Following washes, stained coverslips were counterstained with either Alexa Fluor 488-tagged goat anti-mouse antibody (1:400 in blocking buffer, Life Technologies) or Alexa Fluor 546-tagged goat anti-mouse antibody (1:400 in blocking buffer; Life Technologies) for 1 hour at room temperature. Coverslips were then washed, DAPI-stained, mounted using Prolong Gold Antifade Reagent (Invitrogen), sealed with nail polish, and placed at 4°C prior to analysis by confocal microscopy.

Primary cortical neuron culture and Triton X-100 extraction

For primary cortical neuron culture, the cortex of embryonic day 18.5 mouse embryos was isolated and digested with 2 mg/mL papain (Worthington Biochemistry) and 0.1% DNase I (Invitrogen). Neurons in Neurobasal media (Gibco) containing serum-free B-27 (Invitrogen) and GlutaMAX (Invitrogen) were plated in 24-well dishes with coverslips pre-treated with 10 μ g/mL poly-D-lysine (Sigma Aldrich). Day 1 post-plating (DIV1), 20 μ L of indicated 10x concentrated lentivirus was added per well. On DIV3, 25 μ g cell lysate (10 μ g/ μ L sonicated in PBS, clarified

and sterilized with 0.22 micron filter) or equivalent amount of PBS, was added to wells. On DIV17, 14 days after inoculation with clarified lysates, neurons were fixed with 4% PFA/4% sucrose/PBS containing or lacking 1% Triton X-100 for 30 minutes, a slight modification from a previously described protocol for extracting soluble cytoplasmic proteins for easy visualization of insoluble inclusions (Volpicelli-Daley et al., 2011). After 30 minute permeabilization with 0.25% Triton X-100 in PBS for 30 minutes, coverslips were placed in blocking solution (10% fetal goat serum, 25 mg/mL BSA, 0.25% Triton X-100, PBS) for one hour at room temperature. Coverslips were then exposed to mouse monoclonal anti-phospho-tau AT8 (1:400, ThermoScientific) overnight at 4°C in blocking solution. Following washes, stained coverslips were counterstained with Alexa Fluor 546-tagged goat anti-mouse secondary (1:400 in blocking buffer; Life Technologies) for 1 hour in blocking solution at room temperature. Coverslips were then washed, DAPI-stained, mounted using Prolong Gold Antifade Reagent (Invitrogen), sealed with nail polish, and placed at 4°C prior to analysis by confocal microscopy.

Reversing aggregated state using doxycycline in Tet off background

A monoclonal HEK293 cell line stably expressing tau RD(LM)-YFP under the TRE repressor (Tet Off) was generated and plated at 240,000 cells/well in wells of a 12-well plate. 24 hours later, 20 µg clarified lysate from Clone 10 cells was transduced using lipofectamine-2000 (Invitrogen). 18 hours later, cells were re-plated into a 6-well plate. On Day 3, cells were plated sparsely in a 10 cm dish and on Day 12, cloning cylinders (Bel-Art Products) were used to select three clones containing inclusions (these clones were picked in order of identification using an epifluorescence microscope). The three clones, annotated Clone 10-1, Clone 10-2, and Clone 10-3, were amplified to confluency in 12-well then 6-well then 10 cm plates and were frozen down in liquid nitrogen. All featured a similar morphology (large juxtannuclear inclusion, no nuclear inclusions) to the original Clone 10. Clone 10-1 was plated in a 6-well plate and media

containing 30 ng/mL doxycycline was used to turn off expression for 0, 1, 2, 3, 5, or 7 days. At this point, all cells were re-plated on coverslips, and were given two days to recover in media lacking doxycycline, thus turning tau RD(LM)-YFP expression back on. At this point, cells were fixed with 4% PFA in PBS and DAPI stained, analyzing percent cells positive with confocal microscopy as described above (n=10 fields, each with >150 cells).

Animals

Transgenic mice expressing human 4R1N P301S tau under the murine prion promoter (Yoshiyama et al., 2007) were obtained from The Jackson Laboratory and maintained on a B6C3 background. Mice had food and water *ad libitum* and were housed with a 12 hour light/dark cycle. All protocols involving animal use were approved by the institutional animal care and use committee at Washington University in St. Louis. For all experiments, conditions were gender-matched (Table S1).

Murine hippocampal injections

P301S and non-transgenic littermates were anesthetized with isoflurane as previously described (Devos and Miller, 2013). Mice were bilaterally injected into the hippocampus (from bregma: -2.5 mm posterior, +/-2 mm lateral, -1.8 mm ventral) with either 2 μ L of 5 μ g/ μ L lysate/homogenate or 2 μ L of 2.5 μ g/ μ L recombinant tau RD fibrils at an infusion rate of 0.2 μ L/minute. 10 μ L gas-tight syringes (Hamilton) and 30 gauge needles with a 60° bevel from the vertical (Hamilton) were used for all injections.

Tissue collection

Mice were anesthetized with isoflurane and perfused with chilled 1x PBS with 0.03% heparin. Brains were rapidly removed and for Generations 0-2 transected mid-sagittally. The right hemisphere was micro-dissected into hippocampus, brainstem, cortex, and frontal sections

and subsequently snap-frozen and stored at -80°C until further use. The left hemisphere was post-fixed in 4% paraformaldehyde at 4°C for 24 hours and then transferred to 30% sucrose. For Generation 3 mice, whole brains were post-fixed as described above.

Serial Inoculations

Hippocampi (right hemisphere) from all Generation 0 mice were micro-dissected and homogenized: while still frozen, samples were sonicated in 1:4 w/v TBS with cOmplete protease inhibitors (Roche) and phosSTOP (Roche) using an Omni-Ruptor 250 probe sonicator at 30% power for 20, 10-second cycles. Crude homogenates were then clarified by centrifugation at $15,000\times g$ for 15 minutes and supernatants were frozen down at -80°C until use. Homogenates were standardized by Bradford assay to final protein concentrations of $5\ \mu\text{g}/\mu\text{L}$. Hippocampi from the same cohort (e.g. Clone 1) were pooled and $2\ \mu\text{L}$ (i.e. $10\ \mu\text{g}$) was bilaterally injected into the hippocampi of transgenic P301S mice (Generation 1) as per before ($n=3-4$ for all inoculation cohorts). Four weeks later, generation 1 mice were sacrificed and the procedure was repeated for generation 2 mice ($n=3-4$ for all cohorts). For generation 3 mice, $10\ \mu\text{g}$ total protein was unilaterally injected into the right hippocampus so that both ipsilateral and contralateral spread could be examined 5-weeks later ($n=2$ per cohort).

Histology and Immunohistochemistry

$50\ \mu\text{m}$ sections were taken through the entire left hemisphere using a freezing microtome. Slices were first blocked for one hour with 10% goat serum and 3% milk in TBS with 0.25% Triton X-100 (blocking buffer). For DAB stains, brain slices were incubated with either biotinylated AT8 antibody (1:500, ThermoScientific); MC1 antibody (1:500, kind gift from Peter Davies laboratory); or rabbit anti-Iba1 (1:500, Wako Chemicals USA), all overnight in blocking buffer at 4°C . For secondary staining of MC1, slices were incubated with biotinylated goat anti-mouse $\text{F}(\text{ab}')_2$ fragment (1:1000 in blocking buffer, Jackson ImmunoResearch). For secondary

staining of Iba1, slices were subsequently incubated in biotinylated goat anti-rabbit IgG (1:500 in blocking buffer, Sigma) for one hour at room temperature. Using the VECTASTAIN Elite ABC Kit (Vector Labs), all stained slices were then incubated at room temperature for 30 minutes, followed by DAB development using the DAB Peroxidase Substrate Kit with the optional nickel addition (Vector Labs). Histological images and z-stacks were captured using the Olympus Nanozoomer 2.0-HT (Hamamatsu) and analyzed with the NDP viewer software (Hamamatsu). Counts of neurons with AT8-positive tangle-like structures in CA1/CA3 of the hippocampus were performed by a blinded individual. One-way analysis of variance with Bonferroni's multiple comparison test was used to assess statistical significance.

For immunofluorescence stains, slices were placed in blocking solution for one hour and were then incubated in blocking solution with either AT8 antibody (1:500, ThermoScientific) or rabbit anti-Iba1 (1:500, Wako Chemicals USA) overnight at 4°C. Slices were then incubated with either Alexa Fluor 488-tagged goat anti-mouse antibody (1:2000, Life Technologies) in the case of AT8 or Alexa Fluor 546-tagged goat anti-rabbit antibody (1:2000, Life Technologies) for one hour at room temperature in blocking solution. Slices were subsequently stained with DAPI as described above and mounted onto coverslips with Fluoromount G (Sigma Aldrich). Slices were imaged by confocal microscopy.

For X-34 staining, sections were incubated in PBS with 0.25% Triton X-100 for 30 minutes, followed by a 20 minute incubation with X-34 (10 µM final concentration) in 40% ethanol, 60% PBS and 1/500 volume of 10 N NaOH. Slices were subsequently rinsed in 40% Ethanol/60% PBS at 3 x 2 minutes followed by rinse for 2 x 5 minutes in PBS. Slices were finally mounted with Fluoromount-G (Sigma Aldrich). Slices were imaged with a Nikon Instruments Eclipse E800 microscope.

Immunoprecipitation of full-length tau from strain-inoculated mice

1:50 HJ8.5 (kind gift from the David Holtzman lab) was added to 120 μL (600 μg) hippocampal homogenates freshly thawed on ice. Homogenate and antibodies were incubated overnight at 4°C with rotation. 18 hours later, 50 μL of protein-G agarose beads (Pierce) were added and samples were again incubated overnight at 4°C with rotation. 24 hours later, samples were centrifuged at 2000 $\times\text{g}$ for 3 minutes at 4°C. Supernatant was discarded and replaced with 500 μL Ag/Ab gentle binding buffer (Pierce). This centrifugation/wash step was repeated three times. After the final aspiration, proteins bound to beads were eluted using 50 μL low pH elution buffer (Pierce) by incubating at room temperature for 5 minutes. Samples were centrifuged at 2000 $\times\text{g}$ for 3 minutes and supernatants were collected. This elution step was repeated to give a total volume of 100 μL . Finally, 10 μL 1 M Tris-Base pH 8.5 was added to the eluate to neutralize the elution buffer. When seeding of eluate and crude homogenate were compared, volumes were standardized. Eluted samples were stored at -80°C until use.

Analysis of seeding potential of immunoprecipitated tau from strain-inoculated mice

Seeding activity of immunoprecipitated full-length tau was examined using split-luciferase complementation and inclusion counts for both generation 0 (un-pooled) and generation 2 (pooled by cohort) mice. IPed material from 60 μg brain homogenate was transduced into split-luciferase cells, following the protocol previously described. Four separate experiments were performed for IPed samples from each brain, each read in quadruplicate 48-hours post-transduction of lysate. Average seeding ratios were calculated for each sample, comparing luminescence versus sham-inoculated cells (lipofectamine-2000 alone). Luminescence values were averaged within mouse cohorts and compared by one-way analysis of variance with Bonferroni's multiple comparison test was used to assess statistical significance.

For inclusion counts, IPed full-length tau from 60 μg brain homogenate-equivalent was transduced into tau RD(LM)-YFP cells in a 12-well plate. 24 hours later, cells were re-plated

onto coverslips. At 96 hours, cells were fixed. Six fields, each with 100+ cells, were analyzed per mouse and averages were calculated for each. These averages were then collapsed within cohorts and compared by one-way analysis of variance with Bonferroni's multiple comparison test to assess statistical significance.

Re-introduction of strains passaged through mice into naive tau RD-YFP cells

IPed FL tau from 60 µg brain homogenate from transgenic tau P301S mice (Generation 0 = un-pooled, Generation 2 = pooled) was transduced into tau RD(LM)-YFP cells in a 12-well plate. 24 hours later, cells were re-plated into a 6-well plate. At confluency, cells were sparsely plated on coverslips and were given 8 days to amplify into discrete colonies. Cells were then fixed with 4% PFA and DAPI-stained. Colonies with inclusions were imaged by confocal microscopy. Inclusion-positive colonies were scored as either containing or lacking nuclear inclusions. For generation 0 mice, 20+ colonies were scored per mouse and percentage with each phenotype was calculated. For generation 2 mice, 10 coverslips, each with 15+ inclusion-positive colonies, were scored per cohort. Values were averaged within cohorts and compared by student's t-test.

For isolation of monoclonal lines, this protocol was repeated except inoculated cells were re-plated sparsely into 10 cm dishes following confluency in the first 6-well plate. Monoclonal inclusion-positive lines were isolated as described previously. For Generation 0 mice, one representative colony was blindly picked and amplified per mouse. For Generation 2 mice, 12 colonies were blindly picked and amplified per cohort. Each monoclonal line was examined by inclusion morphology/confocal, pronase digestion, and split-luciferase complementation as described previously.

Human patient case selection and neuropathological methods

Cases were selected from the Neurodegenerative Disease Brain Bank (NDBB) at the University of California, San Francisco (UCSF). The NDBB receives brain and spinal cord materials from patients enrolled in UCSF Memory and Aging Center longitudinal clinical research programs. The fresh brains were cut into ~1 cm coronal slabs, which were alternately fixed in 10% neutral buffered formalin for 72 hours or rapidly frozen, providing tissues preserved with both methods bilaterally for every cut surface. Neuropathological diagnoses were made in accordance with consensus diagnostic criteria (Hyman et al., 2012; Mackenzie et al., 2010) using previously described histological and immunohistochemical methods (Kim et al., 2012). Cases were selected based on neuropathological diagnosis. Blocks (~0.5 g) were dissected from frozen brain slabs, targeting regions for each diagnostic group in which all patients showed no less than a mild-to-moderate tau inclusion burden in the apposed fixed tissue block: middle frontal gyrus (6 AD, 6 PSP, and 6 CBD); inferior temporal cortex (6 AGD) and anterior orbital gyrus (5 PiD). Among the six AGD cases, 2 carried a primary diagnosis of AGD (AGD1 and AGD2) whereas the others carried a primary diagnosis of FTLD-TDP but had incidental AGD (AGD3, AGD4, AGD5, AGD6). The inferior temporal gyrus was chosen for AGD to capture AGD tau while avoiding comorbid AD-related tau as much as possible. See Table S2 for patient characteristics and scoring of morphologies.

Brain homogenate preparation and clarification

Human brain samples were shipped from UCSF to Washington University on dry ice. Tau knock-out mouse (Jackson Labs, STOCK Maptm1(EGFP)Klt/J) brain (male, 12 months of age) was harvested and stored at -80°C. While still frozen, 0.5 gram sections were sonicated in 5 mL TBS with cOmplete protease inhibitors (Roche) and phosSTOP (Roche) using an Omni-Ruptor 250 probe sonicator at 30% power for 20, 10-second cycles. Crude brain homogenates were then clarified by centrifugation at 15,000xg for 15 minutes and supernatants were frozen down at -80°C until use.

Immunoprecipitation of tau from human samples and mouse tau knock-out brain

1:100 HJ9.3 and 1:100 HJ8.5 (kind gifts from the David Holtzman lab) were added to 1 mL 10% weight/volume brain homogenates freshly thawed on ice. Homogenate and antibodies were incubated overnight at 4°C with rotation. 18 hours later, 50 µL of protein-G agarose beads (Pierce) were added and samples were again incubated overnight at 4°C with rotation. 24 hours later, samples were centrifuged at 2000xg for 3 minutes at 4°C. Supernatant was discarded and replaced with 500 µL Ag/Ab gentle binding buffer (Pierce). This centrifugation/wash step was repeated three times. After the final aspiration, proteins bound to beads were eluted using 50 µL low pH elution buffer (Pierce) by incubating at room temperature for 5 minutes. Samples were centrifuged at 2000xg for 3 minutes and supernatants were collected. This elution step was repeated to give a total volume of 100 µL. Finally, 10 µL 1 M Tris-Base pH 8.5 was added to the eluate to neutralize the elution buffer. Eluted samples were stored at -80°C until use.

Isolation of brain homogenate-derived tau RD prion strains

Monoclonal Tet Off-tau RD(LM)-YFP cells were plated at 240,000 cells/well in 12-well plates. 24 hours later, 30 µL clarified brain homogenate/70 µL OptiMEM (crude approach) or 100 µL eluted tau (IP approach) was incubated with 96 µL OptiMEM/4 µL lipofectamine-2000 for 20 minutes prior to addition to wells. 18 hours later, transduced cells were re-plated in 6-well plates. On Day 3, cells were plated sparsely in 10 cm plates (<100 cells/plate). Conditions with rounded, dying cells were noted at this time as “toxic.” On Day 12, clones containing inclusions were isolated for each condition. As many positive/mosaic clones as could be identified were picked. Differences in sample size between conditions reflect efficiency of seeding and amplification. Clones were serially passaged to confluency in 12-well, then 6-well, then 10 cm plates. At Day 30, cells were frozen down in liquid nitrogen or plated on cover slips for assessment of morphology by confocal.

Supplemental References

- Araki, T., Sasaki, Y., and Milbrandt, J. (2004). Increased nuclear NAD biosynthesis and SIRT1 activation prevent axonal degeneration. *Science* 305, 1010–1013.
- Devos, S.L., and Miller, T.M. (2013). Direct intraventricular delivery of drugs to the rodent central nervous system. *J Vis Exp*. 75.
- Frost, B., Ollesch, J., Wille, H., and Diamond, M.I. (2009). Conformational diversity of wild-type Tau fibrils specified by templated conformation change. *J. Biol. Chem.* 284, 3546–3551.
- Giasson, B.I., Forman, M.S., Higuchi, M., Golbe, L.I., Graves, C.L., Kotzbauer, P.T., Trojanowski, J.Q., and Lee, V.M.-Y. (2003). Initiation and synergistic fibrillization of tau and alpha-synuclein. *Science* 300, 636–640.
- Goedert, M., and Jakes, R. (1990). Expression of separate isoforms of human tau protein: correlation with the tau pattern in brain and effects on tubulin polymerization. *Embo J.* 9, 4225–4230.
- Huang, C., Ren, G., Zhou, H., and Wang, C.-C. (2005). A new method for purification of recombinant human alpha-synuclein in *Escherichia coli*. *Protein Expr. Purif.* 42, 173–177.
- Hyman, B.T., Phelps, C.H., Beach, T.G., Bigio, E.H., Cairns, N.J., Carrillo, M.C., Dickson, D.W., Duyckaerts, C., Frosch, M.P., Masliah, E., et al. (2012). National Institute on Aging-Alzheimer's Association guidelines for the neuropathologic assessment of Alzheimer's disease. *Alzheimers Dement* 8, 1–13.
- Kim, E.-J., Sidhu, M., Gaus, S.E., Huang, E.J., Hof, P.R., Miller, B.L., DeArmond, S.J., and Seeley, W.W. (2012). Selective fronto-insular von Economo neuron and fork cell loss in early behavioral variant frontotemporal dementia. *Cereb. Cortex* 22, 251–259.
- Kryndushkin, D.S., Alexandrov, I.M., Ter-Avanesyan, M.D., and Kushnirov, V.V. (2003). Yeast [PSI⁺] prion aggregates are formed by small Sup35 polymers fragmented by Hsp104. *J. Biol. Chem.* 278, 49636–49643.
- Mackenzie, I.R.A., Neumann, M., Bigio, E.H., Cairns, N.J., Alafuzoff, I., Kril, J., Kovacs, G.G., Ghetti, B., Halliday, G., Holm, I.E., et al. (2010). Nomenclature and nosology for neuropathologic subtypes of frontotemporal lobar degeneration: an update. *Acta Neuropathol.* 119, 1–4.
- Naik, S., and Piwnica-Worms, D. (2007). Real-time imaging of beta-catenin dynamics in cells and living mice. *Proc. Natl. Acad. Sci. U.S.A.* 104, 17465–17470.
- Nekooki-Machida, Y., Kurosawa, M., Nukina, N., Ito, K., Oda, T., and Tanaka, M. (2009). Distinct conformations of in vitro and in vivo amyloids of huntingtin-exon1 show different cytotoxicity. *Proc. Natl. Acad. Sci. U.S.A.* 106, 9679–9684.
- Styren, S.D., Hamilton, R.L., Styren, G.C., and Klunk, W.E. (2000). X-34, a fluorescent derivative of Congo red: a novel histochemical stain for Alzheimer's disease pathology. *J. Histochem. Cytochem.* 48, 1223–1232.

- Thorpe, J.R. (1999). The application of LR gold resin for immunogold labeling. *Methods Mol. Biol.* 117, 99–110.
- Volpicelli-Daley, L.A., Luk, K.C., Patel, T.P., Tanik, S.A., Riddle, D.M., Stieber, A., Meaney, D.F., Trojanowski, J.Q., and Lee, V.M.-Y. (2011). Exogenous α -synuclein fibrils induce Lewy body pathology leading to synaptic dysfunction and neuron death. *Neuron* 72, 57–71.
- Yoshiyama, Y., Higuchi, M., Zhang, B., Huang, S.-M., Iwata, N., Saido, T.C., Maeda, J., Suhara, T., Trojanowski, J.Q., and Lee, V.M.-Y. (2007). Synapse loss and microglial activation precede tangles in a P301S tauopathy mouse model. *Neuron* 53, 337–351.